

# The Simultaneous Optical-to-X-ray Spectral Energy Distribution of Soft X-ray Selected AGN observed by *Swift*

Dirk Grupe<sup>1</sup>,  
 grupe@astro.psu.edu  
 S. Komossa<sup>2</sup>, Karen M. Leighly<sup>3</sup>, & Kim L. Page<sup>4</sup>

## ABSTRACT

We report *Swift* observations of a sample of 92 bright soft X-ray selected active galactic nuclei (AGN). This sample represents the largest number of AGN observed to study the spectral energy distribution (SED) of AGN with simultaneous optical/UV and X-ray data. The principal motivation of this study is to understand the SEDs of AGN in the optical/UV to X-ray regime and to provide bolometric corrections which are important in determining the Eddington ratio  $L/L_{\text{Edd}}$ . In particular, we rigorously explore the dependence of the UV-EUV contribution to the bolometric correction on the assumed EUV spectral shape. We find strong correlations of the spectral slopes  $\alpha_X$  and  $\alpha_{\text{UV}}$  with  $L/L_{\text{Edd}}$ . Although Narrow-Line Seyfert 1 galaxies (NLS1s) have steeper  $\alpha_X$  and higher  $L/L_{\text{Edd}}$  than Broad-Line Seyfert 1 galaxies (BLS1s), their optical/UV to X-ray spectral slopes  $\alpha_{\text{ox}}$  and optical/UV slopes  $\alpha_{\text{UV}}$  are very similar. The mean SED of NLS1s shows that in general this type of AGN appears to be fainter in the UV and at hard X-ray energies than BLS1s. We find a strong correlation between  $\alpha_X$  and  $\alpha_{\text{UV}}$  for AGN with X-ray spectral slopes  $\alpha_X < 1.6$ . For AGN with steeper X-ray spectra, both this relation and the relation between  $\alpha_X$  and  $L/L_{\text{Edd}}$  break down. At  $\alpha_X \approx 1.6$ ,  $L/L_{\text{Edd}}$  reaches unity. We note an offset in the  $\alpha_{\text{UV}}-L/L_{\text{Edd}}$  relation between NLS1s and BLS1s. We argue that  $\alpha_{\text{UV}}$  is a good estimator of  $L/L_{\text{Edd}}$  and suggest that  $\alpha_{\text{UV}}$  can be used to estimate  $L/L_{\text{Edd}}$  in high-redshift QSOs. Although NLS1s appear to be highly variable in X-rays they only vary marginally in the UV.

*Subject headings:* galaxies: active

## 1. Introduction

Two of the key parameters of Active Galactic Nuclei (AGN) are their bolometric luminosity  $L$  and their Eddington ratio  $L/L_{\text{Edd}}$ . Besides the mass of the central black hole,  $L/L_{\text{Edd}}$  is the parameter that is likely to control a va-

riety of observed AGN properties such as spectral slopes and some emission-line properties (e.g. Boroson & Green 1992; Sulentic et al. 2000; Boroson 2002; Grupe 2004; Shemmer et al. 2008). The Eddington ratio  $L/L_{\text{Edd}}$  may also be seen as an indicator of the evolutionary stage of an AGN. In this picture, Narrow Line Seyfert 1 galaxies (NLS1s) with their high  $L/L_{\text{Edd}}$  are young members of the AGN family (Grupe et al. 1999; Mathur 2000; Grupe 2004). The knowledge of the shape of the Spectral Energy Distribution (SED) of an AGN is critical for measuring the bolometric luminosity and  $L/L_{\text{Edd}}$ .

In this paper we study the SEDs of a sample of 92 AGN with *simultaneous* optical/UV and X-ray observations obtained by *Swift*. The main goal of our study is to estimate the UV-EUV contri-

<sup>1</sup>Department of Astronomy and Astrophysics, Pennsylvania State University, 525 Davey Lab, University Park, PA 16802

<sup>2</sup>Max-Planck-Institut für extraterrestrische Physik, Giessenbachstr., D-85748 Garching, Germany; email: skomossa@mpe.mpg.de

<sup>3</sup>Homer L. Dodge Department of Physics and Astronomy, University of Oklahoma, 440 West Brooks Street, Norman, OK 73019; email: leighly@nhn.ou.edu

<sup>4</sup>Department of Astronomy, University of Leicester, Leicester, U.K.

bution to the SED based on these simultaneous multi-wavelength data. Another goal is to look for relations between properties of the SED such as the optical/UV and X-ray spectral slopes  $\alpha_{UV}$  and  $\alpha_X$  and other observed properties, and determine how they are related to the Eddington ratio  $L/L_{Edd}$ . The aim is to find properties such as e.g.  $\alpha_{UV}$  that can be used to estimate  $L/L_{Edd}$  in a similar way as it has already been done for  $\alpha_X$  and  $L/L_{Edd}$  (Grupe 2004; Shemmer et al. 2008). If there is such a relation, it could be applied to high-redshift quasars where the soft X-ray band is shifted out of the observing window, and which are typically X-ray faint making a robust X-ray spectral analysis challenging or impossible. Bolometric corrections, and their dependence on AGN type, luminosity, Eddington ratio and redshift are also a key ingredient in determining black hole mass functions from (single-band) luminosity functions (e.g., Hopkins et al. 2007). Since the bolometric AGN luminosity is usually dominated by the UV to soft-X-ray part of the SED, its careful measurement, and an evaluation of its uncertainties, in nearby, well-studied AGN is important.

The presence of a soft X-ray excess over a flatter hard X-ray component was first reported by Arnaud et al. (1985) in *EXOSAT* spectra from the Seyfert 1 galaxy Mkn 841. It is commonly thought that this soft X-ray excess is the high-energy tail of the Big-Blue-Bump emission (BBB). In Seyferts, this part of the SED is the most energetic part of the entire electromagnetic spectrum. A popular interpretation of the BBB is thermal emission from the accretion disk around the central black hole (e.g., Shields 1978). The thermal UV photons which originate from the center of the accretion disk are then thought to be modified by Comptonization by hot electrons in the corona above the disk. Some of the UV photons may end up in the soft X-ray band (e.g., Czerny & Elvis 1987; Ross et al. 1992; Mannheim et al 1995; Pounds et al. 1995).

However, as pointed out by Gierlinski & Done (e.g., 2004) this simple picture of the SED may be far more complicated. Given recent findings of spectral complexity of AGN soft X-ray spectra, including the presence of power law or black body-like soft excesses, ionized reflection, ionized absorption, or partial covering (e.g., Fabian et al. 2004; Done et al. 2007; Gallo

2006; Crummy et al. 2006; Grupe et al. 2008a; Turner & Miller 2009), it is especially important to consider broad-band SEDs in efforts to constrain the AGN continuum emission mechanisms. This is the approach that we followed in our study. Since the *Swift* X-ray telescope spectra do not allow complex multi-component X-ray spectral fitting due to the relatively small number of counts typically obtained during an observation, we instead focus on power laws to assess the global spectral steepness in the 0.3-10 keV band, and concentrate on the UV/X-ray relationships.

A number of previous studies have focused on the measurements of SEDs, and the determination of bolometric corrections in different wave-bands. In order to determine the bolometric luminosity it is quite common to use a linear relation between an observed monochromatic luminosity and  $L_{bol}$ . For example, Elvis et al. (1994) gave a relation with  $L_{bol} = 5.6 \times L_{2500\text{\AA}}$  and  $13.2 \times L_V$ . On the other hand, Marconi et al. (2004) suggested that the conversion from a monochromatic luminosity to  $L_{bol}$  is actually luminosity dependent (see also Hopkins et al. 2007). By using *XMM-Newton* with simultaneous optical/UV and X-ray data, Vasudevan & Fabian (2009a) recently concluded that the bolometric correction for the conversion between  $L_{2-10\text{keV}}$  is larger for high  $L/L_{Edd}$  objects than for AGN which operate at lower  $L/L_{Edd}$ . Walter & Fink (1993) studied the UV and X-ray properties of a sample of 58 Seyfert 1 galaxies and found that the soft X-ray excess found from ROSAT observations is well-correlated with the strength of the BBB observed by IUE. Based on a sample of 76 bright soft X-ray selected ROSAT AGN, Grupe et al. (1998a) showed that the BBB extends as far as the optical band and that sources with steeper X-ray spectra tend to have bluer optical spectra, suggesting that Narrow Line Seyfert 1 galaxies (NLS1s) are the AGN with the strongest BBB component. However, from a study of the IUE spectra of NLS1s, Rodríguez-Pascual et al. (1997) came to the conclusion that NLS1s have weaker UV emission than Broad Line Seyfert 1s (BLS1s). Grupe (2004) found that there is a strong correlation between the ROSAT X-ray spectral slope  $\alpha_X$  and the Eddington ratio  $L/L_{Edd}$ . This result was confirmed by Williams et al. (2004) who showed a correlation between the soft X-ray photon index  $\Gamma_X$  and

the ratio of the luminosity density at 1 keV to the Eddington luminosity. Shemmer et al. (2008) extended this relation into the hard X-ray regime. Atlee & Mathur (2009) recently presented a sample of AGN based on our soft X-ray selected AGN sample (Grupe et al. 1998a; Grupe et al. 2001a) using *GALEX* Far-UV low-resolution spectra and *ROSAT* All Sky Survey (RASS) data. They found that the strength of the BBB is correlated with the X-ray spectral slope, but that there is no correlation with the shape of the UV continuum. They concluded that the properties of the accretion disk are independent of the mass of the central black hole and the Eddington ratio.

In the past, however, this type of SED studies were hampered by the lack of simultaneous observations in the optical/UV and X-ray bands; the observations available frequently had been performed years apart. Since AGN are known to be variable in both the X-ray and the UV, the lack of simultaneity adds considerable scatter to the data. For a long time, the only sample study with simultaneous UV and X-ray observations was the one performed by Walter et al. (1994), who obtained simultaneous *IUE* and *ROSAT* observations of a sample of 8 AGN and found no difference to their results presented in Walter & Fink (1993). This situation has changed with the availability of the multi-wavelength observatories *XMM-Newton* and *Swift*. Based on *XMM-Newton* observations with the Optical Monitor (OM, Mason et al. 2001), Brocksopp et al. (2006) presented a multi-wavelength analysis of a sample of 23 Palomar-Green quasars and correlated X-ray continuum with optical line properties. Recently, Vasudevan & Fabian (2009a) presented the bolometric corrections for 29 AGN with simultaneous optical/UV and X-ray observations from the *XMM-Newton* OM and EPIC pn and Vasudevan et al. (2009b) presented a sample of 26 AGN selected from the 9 months *Swift* BAT survey (Markwardt et al. 2005; Winter et al 2009) with *Swift* UVOT and XRT data. In our paper, we present a sample of 92 bright soft X-ray selected AGN with simultaneous optical/UV and X-ray data obtained with *Swift*.

The *Swift* mission (Gehrels et al. 2004) was launched on 2004 November 20. While its main purpose is to hunt and observe Gamma-Ray Bursts (GRBs), a significant part of *Swift*'s observ-

ing time is used for fill-in targets and targets-of-opportunity when no GRBs or guest investigator targets are observed. Due to its multi-wavelength capacities and its flexible scheduling, *Swift* is the ideal observatory for multi-wavelength and/or monitoring observations of AGN, as demonstrated by e.g. Grupe et al. (2006a) on the NLS1s RX J0148.3–2758, WPVS 007 (Grupe et al. 2007a; Grupe et al 2008b), PHL 1811 (Leighly et al. 2007), PG 1211+143 (Bachev et al. 2009), and Mkn 335 (Grupe et al 2007b). *Swift* is equipped with three telescopes: at the high energy end the Burst Alert Telescope (BAT, Barthelmy 2005) operating in the 15-150 keV energy range, the X-Ray Telescope (XRT, Burrows et al. 2005), which covers the soft X-ray range between 0.3-10.0 keV, and at the long wavelength end, the UV-optical Telescope (UVOT, Roming et al. 2005). The XRT uses a CCD detector identical to the EPIC MOS on-board XMM (Turner et al. 2001). The UVOT covers the range between 1700-6500Å and is a sister instrument of *XMM-Newton*'s OM. The UVOT has a similar set of filters to the OM (Mason et al. 2001; Roming et al. 2005). However, the UVOT UV throughput is a factor of about 10 higher than that of the OM.

Although the BAT is performing a hard X-ray survey and has found several hundreds of AGN so far (Markwardt et al. 2005; Tueller et al. 2009; Winter et al 2009; Fabian et al. 2009), here we only use the *Swift* XRT and UVOT data and the majority of the AGN in our sample are not detected (so far) in the BAT survey. We have started our project in 2005 and the data in this paper represent the status of our study by the beginning of January 2010. We focus on presenting the data and some simple statistical analyses. A more detailed statistical analysis, a study of the relationships with the optical emission-line properties, and a rigorous discussion of the implications for models of NLS1 galaxies will be presented in a separate paper. The outline of the present paper is as follows: In §2 we describe the sample selection, the *Swift* observations, and the data reduction. In §3 we present the results of the *Swift* XRT and UVOT data analysis, and these are then discussed in §4. Throughout this paper spectral indices are denoted as energy spectral indices with  $F_\nu \propto \nu^{-\alpha}$ . Luminosities are calculated assuming a  $\Lambda$ CDM cosmology with  $\Omega_M=0.27$ ,  $\Omega_\Lambda=0.73$  and

a Hubble constant of  $H_0=75 \text{ km s}^{-1} \text{ Mpc}^{-1}$ . All errors are  $1\sigma$  unless stated otherwise.

## 2. Sample selection, observations and data reduction

The AGN in the sample presented here were selected from the bright soft X-ray selected AGN sample of Grupe et al. (2001a); Grupe et al. (2004a) which contains a total of 110 AGN. This sample contains all Seyferts of the bright, soft X-ray sources by Thomas et al. (1998) which were selected from the *ROSAT* All-Sky Survey (RASS; Voges et al. 1999) which was using a Position Sensitive Proportional Counter (PSPC; Pfeffermann et al. 1986). The X-ray sources in the Thomas et al. (1998) sample and consequently in the Grupe et al. (2001a) AGN sample had to be X-ray bright with a PSPC count rate  $\geq 0.5$  counts  $\text{s}^{-1}$ , X-ray soft with a PSPC hardness ratio  $\text{HR}^1 < 0.0$ , and a position at a high Galactic latitude with  $|b| > 20^\circ$ . In addition to the AGN from the Grupe et al. (2001a) AGN sample, we added the NLS1s RX J0134.2–4258 and RX J0136.9–3510 to our sample. These AGN had been members of the original bright soft X-ray AGN *ROSAT* sample (Grupe et al. 1998a; Grupe et al. 1999) but were excluded from the final sample of 110 AGN because after reprocessing the RASS data their count rate dropped below the cut off at 0.5 counts  $\text{s}^{-1}$  in the *ROSAT* PSPC. The AGN of our sample were selected from the Grupe et al. (2001a) sample starting with the brightest sources first. There is some randomness in the sample selection for the sources which were observed during the last year due to the nature of the fillin program. We have still about 20 AGN which need to be observed in the next years. As always throughout this paper, we have used the  $\text{FWHM}(\text{H}\beta)=2000 \text{ km s}^{-1}$  criterion as defined by Osterbrock & Pogge (1985) to separate between the 43 NLS1s and 49 BLS1s.

Table 1 lists all AGN presented here with their optical position, redshift, Galactic absorption column density derived from the Dickey & Lockman (1990) HI maps, RASS 0.2-2.0 keV spectral slope and rest-frame 0.2-2.0 keV flux (Grupe et al.

2001a),  $E_{B-V}$  given by Schlegel et al. (1998), and black hole mass estimated from  $\text{FWHM}(\text{H}\beta)$  and  $L_{5100\text{\AA}}$  using the Kaspi et al. (2000) relation<sup>2</sup>.

The table also contains the Balmer decrement of the broad hydrogen lines and the  $E_{B-V}$  derived from  $\text{H}\alpha/\text{H}\beta$ . While the majority of soft X-ray selected AGN do not show strong intrinsic reddening, some do (e.g. Goodrich 1989; Grupe et al. 1998b). In order to correct for intrinsic reddening, we used the Balmer decrements  $\text{H}\alpha/\text{H}\beta$  of the broad-line components measured by re-analyzing the optical spectra published in Grupe et al. (1999) and Grupe et al. (2004a). In order to subtract the contributions by narrow lines we first used the MIDAS<sup>3</sup> command *deblend/line* to separate the broad and narrow line components. While this works quite well for most BLS1s, it becomes unreliable for most NLS1s. Therefore, for the NLS1s we subtracted 10% and 30% of the  $[\text{OIII}]\lambda 5007\text{\AA}$  line flux from the total  $\text{H}\beta$  and  $\text{H}\alpha$  flux, respectively (c.f. Cohen 1983). As expected, most NLS1s do not show significant reddening, while the Balmer decrements of some BLS1s do suggest significant reddening in the optical/UV. The Balmer decrements were converted into  $E_{B-V}$  by assuming a zero point  $\text{H}\alpha/\text{H}\beta=3.06$  as derived by Dong et al. (2008) for a sample of 446 blue AGN<sup>4</sup>. All AGN in our sample for which the Balmer decrement is found to be below this value were considered to have no intrinsic reddening. For 16 AGN, we do not have a measurement of the  $\text{H}\alpha$  line flux, and therefore we could not determine the Balmer decrement and correct for intrinsic reddening. Out of the remaining 76 AGN, 38 have Balmer decrements  $\text{H}\alpha/\text{H}\beta > 3.06$ . In 21 AGN significant reddening is expected from their  $\text{H}\alpha/\text{H}\beta > 3.40$ . The applied reddening correction influenced the estimates of several parameters such as  $\alpha_{\text{ox}}$ ,  $\alpha_{\text{UV}}$ , and  $L/L_{\text{Edd}}$ . In almost all fig-

<sup>2</sup>We are aware of the uncertainties inherent in determining  $M_{\text{BH}}$  from extrapolation of reverberation data (e.g. Bentz et al. 2006, 2009), especially in NLS1s. However, this method is still the most reliable way to estimate  $M_{\text{BH}}$ .

<sup>3</sup>MIDAS is the European Southern Observatory’s Munich Image Data Analysis System

<sup>4</sup>We note that we assume Galactic dust properties when converting  $A_V$  to  $N_{\text{H}}$  and vice versa. We also assume that deviations from the assumed zero-point broad Balmer decrement are a consequence of reddening rather than evidence for a range of physical conditions (such as optical depth) in the broad-line region.

<sup>1</sup>The *ROSAT* PSPC hardness ratio was defined as  $\text{HR} = (\text{H-S})/(\text{H+S})$  with S and H are the counts in the 0.1-0.4 keV and 0.5-2.4 keV energy ranges, respectively

ures, we show results with and without reddening correction.

The majority of the *Swift* observations were performed as a *Swift* fillin target program. Additional AGN were observed as calibration targets and ToOs. In total, *Swift* has observed 92 bright soft X-ray selected AGN so far. A summary of all XRT and UVOT observations is given in Table 2 listing the target ID, segment number<sup>5</sup>, the start and end times of each observing segment and the exposure times in the XRT and each of the UVOT filters. Note that most AGN have been observed multiple times allowing us also to search for UV and X-ray variability.

For all observations<sup>6</sup> the XRT was operating in photon counting mode (Hill et al. 2004) and the data were reduced by the task *xrtpipeline* version 0.11.6., which is included in the HEASOFT package 6.4. Source photons were selected in a circular region with a typical radius of 47'' and background region of a close-by source-free region with  $r=188''$ . In cases when the AGN was brighter than 0.4 counts  $s^{-1}$ , in order to avoid the effects of pileup, source photons from an inner radius of 10'' were excluded from the spectral analysis. Photons with grades 0-12 were selected. The photons were extracted with *XSELECT* version 2.4. The spectral data were re-binned by using *grppha* version 3.0.1 to 20 photons per bin. The spectra were analyzed using *XSPEC* version 12.4.0 (Arnaud 1996). In 2007 August the substrate voltage of the XRT CCD was raised from 0 to 6V in order to lower the dark current and as a result the detector can operate at slightly higher temperatures (Godet et al., 2009). Therefore, for XRT data taken before 2007 September, we used the standard response matrix *swxpc0to12s0\_20010101v010.rmf*, and used the *swxpc0to12s6\_20010101v010.rmf* response matrix for observations taken after that date. All spectral fits were performed in the observed 0.3–10.0 keV energy band. For each X-ray spectrum we created an Ancillary Response Function (ARF) file using the *Swift* XRT task *xrtmkarf* to correct for vignetting and bad CCD columns and pixels.

In total, 88 out of 92 AGN were observed at

least once in all 6 UVOT filters or in the three UV filters only. The rest had only sporadic observations in one or two of the UVOT filters, because these AGN were observed as calibration targets. In the case of RX J2248.6–5109, UVOT was unable to observe the AGN due to a bright star in the UVOT field-of-view. Before analyzing the data, the data from each segment were co-added by the UVOT task *uvotimsum*. Source counts were selected within the standard 5'' radius for all UVOT filters according to the most recent UVOT photometry calibration as described by Poole et al. (2008). As we will discuss in § 3.3, with this source extraction radius some contamination from host galaxy star light can be expected for some of the nearby AGN. Background photons were selected in a source-free region close-by with a radius of 20''. The data were analyzed with the UVOT software tool *uvotsource*. This tool uses the count rate to flux/magnitude conversion as described in Poole et al. (2008) assuming a GRB-like power-law spectrum, which is also appropriate for AGN. The magnitudes as listed in Table 3 and fluxes used for the spectral energy distributions were all corrected for Galactic reddening using the  $E_{B-V}$  values by Schlegel et al. (1998) as listed in Table 1. The correction factor in each filter was calculated with equation (2) in Roming et al. (2009) who used the standard reddening correction curves by Cardelli et al. (1989).

### 3. Results

#### 3.1. A note on the Computation of the Eddington ratio

The Eddington ratio is an important parameter in AGN studies. It determines the time scale of black hole growth across cosmic times, and it is suspected to drive a number of the observed AGN spectral properties. Its reliable determination is therefore of great interest. However, both of the parameters that determine this ratio (the black hole masses and bolometric luminosities) are not very easily accessible observationally. Direct determinations of black hole masses through reverberation mapping still only exist for a small fraction of all AGN (e.g., Peterson et al. 2004; Bentz et al. 2009), bolometric luminosities are rarely based on SEDs which are measured in all wave-bands simultaneously, and, in any case,

<sup>5</sup>Segments are used for *Swift* planning purposes. Typically one segment covers a time span of one or two days.

<sup>6</sup>Except 3C 273 for which we used observations made in Windowed Timing mode.

the EUV part of the SED is not directly observable in all low-redshift sources.

Our study significantly improves on the determination of bolometric luminosities and their uncertainties. However, when reporting Eddington ratios, we still make the common assumption that the BH mass scaling relation derived for the reverberation-mapped AGN sample (e.g., Kaspi et al. 2000; Peterson et al. 2004; Kaspi et al. 2005) is applicable to all of our sources. This does not need to be the case; especially, since few NLS1 galaxies have been reverberation-mapped, since radiation-pressure corrections may be relevant in some cases (Marconi et al. 2008), and since other processes might affect the Broad Line Region kinematics in individual galaxies (e.g., jet-cloud interactions). While the focus of this work is on SEDs, we do show results involving the Eddington ratio, and would like to emphasize, that the above-mentioned limitations have to be kept in mind when interpreting those results.

### 3.2. X-ray Spectral Analysis

Figure 1 shows three examples of *Swift* XRT spectra with low, medium and high signal-to-noise ratios (RX J0117.5–3826 (segment 002, 188 counts), Fairall 1119 (segment 001, 600 counts), and RX J0128.1–1848 (segment 004, 4350 counts), respectively). Table 4 summarizes the results of the spectral analysis of the X-ray data. All spectra were fitted with an absorbed single power-law model in the 0.3–10 keV energy range with the absorption column density fixed to the Galactic value from Dickey & Lockman (1990) as listed in Table 1. This model fits the majority of the spectra quite well. A few AGN require additional components, and we fitted those spectra with an absorbed broken power-law model. All model fit parameters, the X-ray fluxes, the count rates in the 0.3–10 keV band, and hardness ratios<sup>7</sup> are listed in Table 4. The X-ray fluxes are the rest-frame absorption-corrected 0.2–2.0 keV fluxes. We have selected this energy band to allow for a direct comparison with the RASS data given in Grupe et al. (2001a). As a consequence of the soft X-ray selec-

tion criterion using the *ROSAT* PSPC hardness ratio (Grupe et al. 1998a; Thomas et al. 1998; Grupe et al. 2001a), the AGN in our sample do not show any evidence for excess absorption above the Galactic value, with the exception of a few cases. The new spectral fits confirm our previous findings from the RASS data that these soft X-ray selected AGN are intrinsically unabsorbed in X-rays (Grupe et al. 2001a), as the majority of AGN can be fit sufficiently well by an absorbed single power-law model with the absorption column density fixed to the Galactic value.

### 3.3. UVOT Photometry

Table 3 lists the magnitudes in each of the 6 UVOT filters (if available). All magnitudes are corrected for Galactic reddening using the  $E_{B-V}$  values given by (Schlegel et al. 1998) as listed in Table 1. A correction for intrinsic reddening was not applied at this point. Concerning source variability, previous studies have shown (e.g. Grupe et al. 2007a, 2008a) that the UVOT is relatively stable between observations suggesting that any variability  $\Delta\text{mag} > 0.05$  mag seen between epochs is real.

Does the UVOT photometry measure the intrinsic continuum from the AGN? There are three possible reasons why it may not: a contribution from the host galaxy star light, intrinsic reddening, and the presence of emission lines in the filter band-passes. For our relatively low redshift objects, the most likely contaminant is Mg II  $\lambda 2800$  which will contribute to the flux measured in the U filter if the redshift of the AGN is around  $z = 0.2$ . To a smaller extent, we can also expect some contributions by C IV and C III] in the W2 and M2 filters for objects with higher redshifts. However, the photometry of the majority of the AGN in our sample will not be affected by emission lines. Therefore, none of the UVOT values listed in our paper takes contributions by emission lines into account.

Host galaxy star light potentially presents a more serious problem. Most of the AGN in our sample are rather low-luminosity AGN and the contribution in the V, B and even U bands can be significant. As pointed out by Bentz et al. (2006), even for images with a spatial resolution of about  $1''$  it is almost impossible to disentangle the nuclear from the host galaxy bulge emission.

<sup>7</sup>We define the hardness ratio as  $\text{HR} = (\text{H}-\text{S})/(\text{H}+\text{S})$  where S and H are the background-corrected number of counts in the 0.3–1.0 and 1.0–10.0 keV energy bands, respectively

The Point Spread Function of the UVOT images, however, is about  $2''$  (Poole et al. 2008). As another example, Leighly et al. (2009) showed that in the *XMM-Newton* OM, the *Swift* UVOT sister instrument, the host galaxy contribution in V can be 70% in the case of the low-luminosity NLS1 Mkn 493. The problem may not be as severe in the UVOT, however. The difference between the UVOT and the OM is that the UVOT has less stray light than the OM and the source extraction radius in the UVOT is  $5''$  instead of  $12''$  which is used for the OM. We checked several nearby AGN including Mkn 493 and found that in the optical filters (V, B, and U) the contribution by the host galaxy can be significant. We estimated the host galaxy contribution by decreasing the source extraction radius in *wvotsource* to  $3''$  and applying an aperture correction by setting the *wvotsource* parameter *apercorr=curveofgrowth*. In cases like Mkn 493 we measured a difference in the V filter magnitudes of 0.25 mag between the  $5''$  and  $3''$  extraction radii. In the UV filters, however, we found only a difference of 0.05 mag. As for changes in the optical/UV slopes, we noticed that in our most extreme case, Mkn 493, the difference is 0.15 in  $\alpha_{UV}$ . This is similar to the measurement uncertainty in  $\alpha_{UV}$  for most of our objects. For distant sources, we cannot spatially resolve the host from the AGN, but expect that the errors are no larger than the ones we determined for the nearby sources. Therefore, we can conclude that the star light from the host galaxy can affect our measurements of the nuclear emission using the UVOT data. However, for the majority of our objects this contribution should not affect our results. Therefore, all measurements have been performed using the standard  $5''$  source extraction radius. Note that in order to determine the optical/UV slope  $\alpha_{UV}$ , we fitted a single power law model to the data of all 6 UVOT filters. However, in cases where we noticed a flattening or an increase in the fluxes at longer wavelengths which indicates galaxy contamination, we only fitted the data of the u, w1, m2, and w2 filters.

The final effect that can influence the optical/UV slope is intrinsic reddening. The measured Balmer decrements indicate that a fair number of objects have intrinsic reddening of their broad lines. One might expect that the reddening indicated by the Balmer decrements would be mir-

rored in a flattening of the optical/UV slope.<sup>8</sup> We have therefore searched for evidence of continuum reddening associated with the Balmer decrement by plotting the observed (but corrected for Galactic reddening) optical/UV spectral slope  $\alpha_{UV}$  as a function of the Balmer decrement as listed in Table 1 (Figure 2). NLS1s are displayed as blue triangles and BLS1s as red circles. This  $\alpha_{UV}$ -  $H\alpha/H\beta$  relation is clearly dominated by three outliers with  $H\alpha/H\beta > 5.0$ : Mkn 766, IRAS 1334+24, and NGC 4593. Excluding those three objects from the correlation analysis we do not find any statistically significant correlation between  $\alpha_{UV}$  and  $H\alpha/H\beta$  ( $r_1=0.133$ ,  $P=0.272$ ;  $r_s=0.123$ ,  $T_s=1.00$ ,  $P=0.309$ ). This result suggests that the intrinsic reddening inferred from the Balmer decrement does not significantly flatten  $\alpha_{UV}$ . Nevertheless, we applied a reddening correction to the optical/UV spectra and list both the non-corrected values and those corrected for intrinsic reddening. Although the mean, standard deviation and median of  $H\alpha/H\beta$  of NLS1s are 3.10, 0.61, and 3.00, respectively compared with 3.43, 0.82, and 3.18 which seem to suggest that BLS1 are generally more reddened than NLS1s, a KS test of the  $H\alpha/H\beta$  distributions results in  $D=0.280$  with a probability  $P=0.087$  of a random result. This result shows that the distributions are not significantly different.

### 3.4. Spectral Energy Distributions

Table 5 summarizes the results from the analysis of the SEDs. For each object we typically selected the segment/observation with the longest observing time to get the best signal-to-noise ratio. The X-ray spectral slope  $\alpha_X$  was taken from the power law fits to the XRT data as listed in Table 4. The UV/optical spectral slopes  $\alpha_{UV}$  were determined from a single power-law model fit to the UVOT fluxes. We determined the optical-to-X-ray spectral slope  $\alpha_{ox}$ <sup>9</sup> by measuring the flux den-

<sup>8</sup>We note in passing that the majority of the objects of our sample show no strong excess X-ray absorption. Objects with a dusty warm absorber may be reddened in the optical and UV but have little evidence for X-ray absorption (e.g., Brandt et al. 1996; Komossa & Bade 1998). However, additional evidence that this is not generally true for our objects is the lack of optical polarization (Grupe et al. 1998b) characteristic of dust (Leighly et al. 1997).

<sup>9</sup>The X-ray loudness is defined by (Tananbaum et al. 1979) as  $\alpha_{ox} = -0.384 \log(f_{2keV}/f_{2500\text{\AA}})$ .

sities at rest-frame 2500Å and 2 keV. The X-ray luminosities  $L_X$  were derived from the absorption-corrected rest-frame 0.2-2.0 keV fluxes as given in Table 4.

In the UV-to-X-ray part of the SED we fitted two different models to the UVOT and XRT data. The first (henceforth Model A) consists of a power-law with an exponential cut-off describing the optical-EUV part of the SED, added to an “absorbed” power law model to describe the X-ray part of the SED. Note that this “absorption” merely serves as a mathematical description to ensure the appropriate decrease of the X-ray power law at low energies in order to prevent it from over-predicting the UV part of the SED (see also Grupe et al. 2004a). The second (henceforth Model B) is a double broken power-law model; that is, a power law was fitted to the UV part of the SED and a second one separately to the X-ray part, and a third power law was then used to connect these two models across the EUV. The break points in Model B are at 2000Å and 0.3 keV, where the UVOT observing window ends and the XRT window starts. At 0.3 keV, the break point flux density was set to that of the unabsorbed power law model in X-rays. Model A was applied to both observed and the intrinsic-reddening-corrected UVOT data. In some cases where a very large Balmer decrement was found, e.g., IRAS 1334+2438, this procedure may overestimate the luminosity in the BBB,  $L_{\text{BBB}}^{\text{10}}$ . Model B was applied only to the data not corrected for intrinsic reddening.

Since we do not know the shape of the BBB in the EUV band, we apply both models (A and B) to estimate the SED. This approach allows us to get an impression on the uncertainties in the bolometric luminosities, given the uncertainties in the EUV shape of the SED. The reddening-corrected model A serves as a kind of upper limit on the EUV luminosity, since the extrapolation of the reddening-corrected UV spectrum produces a strong EUV bump. On the other hand, the piece-

wise power law approach of model B introduces a break from the last observed UV point to the first observed X-ray data point, and serves as a reasonable lower limit to the EUV luminosity.

The BBB luminosity  $L_{\text{BBB}}$  was estimated by integrating over these continuum spectra in the rest frame energy range between 1  $\mu\text{m}$  and 2 keV. As mentioned before, the fits with Model A give an upper limit on  $L_{\text{BBB}}$  while the fits with Model B may be regarded as lower limits. Both values of  $L_{\text{BBB}}$  are listed in Table 5. We found that typically  $L_{\text{BBB}}$  calculated from Model A is a factor of 2 higher than that of Model B. In other words, although we do not know the real shape of the BBB in the EUV, we may overestimate  $L_{\text{BBB}}$  by a factor of only a few at the most and not by orders of magnitude. The Eddington ratios were calculated from  $L_{\text{BBB}}$  and the Eddington luminosity. To derive the latter, we used the black hole masses of Grupe (2004) as listed in Table 1. Note that  $\alpha_{\text{UV}}$ ,  $\alpha_{\text{ox}}$ ,  $L_{\text{BBB}}$ ,  $L/L_{\text{Edd}}$ , and  $L_{5100}$  are listed with and without the correction for intrinsic reddening.

The mean SEDs, corrected and uncorrected for intrinsic reddening for NLS1s (blue lines) and BLS1s (red lines) are displayed in Figure 3. In general, NLS1s appear to be fainter in the UV and at hard X-ray energies than BLS1s. Nevertheless, their mean and median  $\alpha_{\text{UV}}$  and  $\alpha_{\text{ox}}$  are very similar as also shown in Table 6. This table summarizes the mean, standard deviation and median of the whole sample, NLS1s and BLS1s for the spectral slopes, luminosities, flux ratios and redshifts. Due to the sample selection criteria, the distributions are generally skewed and non-Gaussian and therefore the medians are better estimators than the means. BLS1s and NLS1s show clear differences in their  $\alpha_X$ ,  $L/L_{\text{Edd}}$ , and X-ray variability. NLS1s show, as expected from previous studies, significantly steeper X-ray spectra than BLS1s. From previous studies (Walter & Fink 1993; Grupe et al. 1998a) we had expected that NLS1s would have bluer optical-UV spectra. As we will show later in Section 3.5, we do confirm that AGN with steeper X-ray spectra have bluer optical-UV spectra, but this relation holds only among those AGN that have relatively flat X-ray spectral slopes in the first place.

Figure 4 displays the distributions of the 0.3-10 keV X-ray spectral slope  $\alpha_X$  of NLS1s and BLS1s (solid blue line and dotted red line, respectively).

<sup>10</sup>Note that throughout this paper we use the Big-Blue-Bump luminosity  $L_{\text{BBB}}$  rather than the bolometric luminosity  $L_{\text{bol}}$ . Although most of the SED continuum energy in a Seyfert galaxy is deposited in the optical-to-X-ray band, we miss emission in the radio band. However, we do not consider the radio contribution significant in most of our AGN. Therefore  $L_{\text{BBB}}$  basically represents  $L_{\text{bol}}$ . This luminosity is used to determine  $L/L_{\text{Edd}}$ .



NLS1s and BLS1s clearly show different distributions in the X-ray spectral slopes  $\alpha_X$  (a KS test results in  $D=0.557$  with a corresponding probability  $P < 0.0001$  of being the same distribution).

Figure 5 shows the distributions of the optical/UV slope  $\alpha_{UV}$  uncorrected and corrected for intrinsic reddening. We found no significant difference in the observed  $\alpha_{UV}$  distributions between NLS1s and BLS1s ( $D=0.140$ ,  $P=0.757$ ) but there is a slight difference in the distribution in the reddening-corrected UV slope  $\alpha_{UV-corr}$  ( $D=0.385$ ,  $P=0.007$ ), with the BLS1s having bluer continua, resulting in steeper  $\alpha_{UV}$ .

Figure 6 shows the distributions of the optical-to-X-ray spectral slope  $\alpha_{ox}$  uncorrected and corrected for intrinsic reddening. For the observed  $\alpha_{ox}$ , the distributions between NLS1s and BLS1s are slightly different with  $D=0.292$  and  $P=0.039$ . NLS1s appear to be X-ray weaker at 2 keV than BLS1s which results in larger values of  $\alpha_{ox}$  in NLS1s. However, this difference disappears when the distributions for the  $\alpha_{ox}$  with the correction for intrinsic reddening are used. Here a KS test gives  $D=0.104$  and  $P=0.986$ .

Figure 7 shows the distributions of the Eddington ratio  $L/L_{Edd}$  uncorrected and corrected for intrinsic reddening. The distributions for NLS1s and BLS1s are different. A KS test for the observed  $L/L_{Edd}$  (uncorrected for intrinsic reddening) gives  $D=0.443$  with a corresponding probability  $P < 0.001$ . However, for  $L/L_{Edd}$  corrected for intrinsic reddening the samples are almost identical with  $D=0.273$  and a probability  $P=0.118$ .

Figure 8 displays the distributions of the 0.2-2.0 keV luminosity  $\log L_X$  of NLS1s and BLS1s. These distributions are essentially identical ( $D=0.125$ ,  $P=0.851$ ). Figure 9 displays the distributions of the luminosities in the BBB emission uncorrected and corrected for intrinsic reddening (left and right panels, respectively). As for the reddening-uncorrected luminosities the distributions of NLS1s and BLS1s are almost identical ( $D=0.151$  and  $P=0.669$ ). However, for the data corrected for intrinsic reddening, BLS1s seem to have slightly more luminous Big Blue Bumps than NLS1s ( $D=0.299$  and  $P=0.070$ ).

### 3.5. Correlation analysis

We have searched for correlations among the measured parameters. For all correlations we determined the linear correlation coefficient  $r_l$  and the Spearman rank order correlation coefficient  $r_s$  plus the Student's T-test value  $T_s$ . The probability  $P$  of a null correlation was determined also for both correlation coefficients. The results of the correlation analysis are listed in Table 7. The part above the diagonal in Table 7 gives the linear correlation coefficient  $r_l$ , the corresponding probability  $P$  and number of sources involved. The lower part of the table lists  $r_s$ ,  $T_s$ , number of sources, and the probability. Note that we did not do a correlation analysis between reddening-corrected and uncorrected properties, such as  $\alpha_{ox}$  and  $\alpha_{ox-corr}$  or  $\alpha_{UV}$  and  $\alpha_{UV-corr}$ .

One of the principal motivations of this study is to see whether there is a relation between the X-ray spectral slope  $\alpha_X$  and the optical/UV slope  $\alpha_{UV}$ . This is motivated by earlier studies by e.g. Walter & Fink (1993) and Grupe et al. (1998a) who found that AGN with bluer optical/UV spectra have steeper X-ray spectra. Figure 10 displays the 0.3-10 keV X-ray energy spectral slope  $\alpha_X$  versus the optical-UV slope  $\alpha_{UV}$ . The left side of Figure 10 displays the relation with  $\alpha_{UV}$  corrected for only Galactic reddening. The right panel shows  $\alpha_{UV}$  corrected for both intrinsic and Galactic reddening. For the UVOT data uncorrected for intrinsic reddening we found linear and Spearman rank order correlation coefficients  $r_l = -0.15$ ,  $r_s = -0.19$  with a Student's T-test  $T_s = -1.8$ , and probabilities  $P=0.1606$  and  $0.077$  of null correlations, respectively. The trend does not improve when we consider the reddening-corrected optical/UV slope  $\alpha_{UV-corr}$  ( $r_l = -0.24$ ,  $r_s = -0.14$ ,  $T_s = -1.2$ ). However, there seems to be a saturation in the optical/UV slope when the X-ray spectral slope becomes steeper than  $\alpha_X \approx 1.6$ . As we will see below, this saturation is due to the fact that at this X-ray spectral slope  $L/L_{Edd}$  reaches unity. When we limited the sample to the 63 AGN with  $\alpha_X < 1.6$  (63 AGN) we found that there is a relatively strong correlation between  $\alpha_X$  and  $\alpha_{UV}$  with  $r_l = -0.36$  and  $r_s = -0.30$ ,  $T_s = 2.5$  and probabilities  $P=0.0038$  and  $0.0151$ , respectively. Because NLS1s typically have steeper X-ray spectra than BLS1s, this effect is basically dominated by BLS1s. Excluding IRAS 1334+2438

which has a highly reddened spectrum ( $\alpha_{UV}=2.8$ ,  $H\alpha/H\beta=6.2$ ), we found a linear correlation coefficient for the BLS1s of  $r_1 = -0.46$  with a probability  $P = 0.0011$ . For the Spearman rank order correlation we found  $r_s = -0.48$  and  $T_s = -3.56$  with  $P=0.009$ . For the NLS1s, however, there is only a marginal trend ( $r_1 = -0.21$ ). In summary, we can confirm the earlier results from ROSAT (Walter & Fink 1993; Grupe et al. 1998a) that  $\alpha_X$  and  $\alpha_{UV}$  are correlated, but the correlation appears to be dominated by AGN with  $\alpha_X < 1.6$ , i.e., mainly BLS1s.

There are clear correlations between the optical-to-X-ray spectral slope  $\alpha_{ox}$  with the X-ray spectral slope  $\alpha_X$  and the optical/UV slope  $\alpha_{UV}$ , such that AGN with steeper X-ray spectra appear to be X-ray weaker (*at 2 keV*; note that their X-ray luminosities are similar) than those with flatter  $\alpha_X$ . Figure 11 displays this relationship. The linear and Spearman rank order correlation coefficients are  $r_1=+0.47$  and  $r_s=+0.47$  ( $T_s=5.0$ ), respectively; in both cases the probability of a null correlation is  $P < 0.0001$ . These correlations also hold for the UVOT data corrected for intrinsic reddening. The trend that AGN with steep X-ray spectra tend to be X-ray weak *at hard X-rays*<sup>11</sup> has also been found by Atlee & Mathur (2009). For comparison, Young et al (2009) found among their sample of SDSS quasars with simultaneous X-ray observations that X-ray faint quasars have flatter X-ray spectra. Correlations are also found between  $\alpha_{ox}$  and the optical/UV spectral slope  $\alpha_{UV}$  (Figure 12); there is a clear anti-correlation with  $r_1=-0.63$  and  $r_s=-0.57$  and  $T_s=-6.4$ . For both correlation coefficients the probability of a null-result is  $P < 0.0001$ .

Figure 13 displays the relationships between the Eddington ratio  $L/L_{Edd}$  and  $\alpha_X$ ,  $\alpha_{UV}$ , and  $\alpha_{ox}$ . The X-ray spectral slope  $\alpha_X$  and the Eddington ratio  $L/L_{Edd}$  are correlated with a Spearman rank order correlation coefficient  $r_s=0.55$  and a Student's T-test  $T_s=+6.1$  and the linear correlation coefficient is  $r_1=0.51$ . This correlation is similar to those found previously by Grupe (2004) and Shemmer et al. (2008) who reported strong correlations between the Eddington ratio  $L/L_{Edd}$  and

the soft and hard X-ray spectral slopes, respectively. The upper panel of Figure 13 suggests that, however, at an Eddington ratio  $L/L_{Edd} \approx 1$  the relationship saturates. This implies that  $\alpha_X$  cannot be used to estimate  $L/L_{Edd}$  universally; the relationship only works for X-ray spectral indices with  $\alpha_X$  up to  $\approx 1.6$ , similar to the  $\alpha_X$ - $\alpha_{UV}$  relation. Again considering only the AGN with  $\alpha_X < 1.6$ , we found correlation coefficients  $r_1 = +0.64$ ,  $r_s = +0.60$  and  $T_s = +5.7$  with probabilities of a random result  $P < 0.001$  in both cases. For this subsample of objects with  $\alpha_X < 1.6$ , we found the following relation between  $\alpha_X$  and  $\log L/L_{Edd}$ :

$$\log L/L_{Edd} = (1.65 \pm 0.26) \times \alpha_X - (2.41 \pm 0.30) \quad (1)$$

This relationship is shown as a dotted line in the upper left panel of Figure 13. It is dominated by BLS1s, because the majority of the NLS1s in our soft X-ray selected sample accrete at the Eddington limit or even at super-Eddington rates. For the super-Eddington accretors, the relationship breaks down; this is similar to the behavior of the  $\alpha_X$ - $\alpha_{UV}$  relationship as shown below. It is interesting to mention that Winter et al (2009) did not find a correlation between the hard X-ray 2-10 keV spectral slope and  $L/L_{Edd}$ , although their sources are all low  $L/L_{Edd}$  AGN. From our results and those of Shemmer et al. (2008), we would have expected to see a correlation between  $\alpha_X$  and  $L/L_{Edd}$ .

The middle panels in Figure 13 display the anti-correlation between the optical/UV spectral slope  $\alpha_{UV}$  and the Eddington ratio  $L/L_{Edd}$ . AGN with bluer UV continua ( $\alpha_{UV} < 1$ ) tend to have higher Eddington ratios. The correlation coefficients for a Spearman and linear correlation analysis are  $r_s=-0.57$  with a T-test  $T_s=-6.4$  and  $r_1=-0.63$  with a probabilities  $P < 0.001$ . Note that there is an offset by 0.6 dex between NLS1s and BLS1s in these plots: For a given  $\alpha_{UV}$ , NLS1s have a  $\sim 4$  times higher Eddington ratio than BLS1s. This division becomes even stronger when considering the data corrected for intrinsic reddening (right panel). Considering only the NLS1s, we found linear and Spearman rank order correlation coefficients of  $r_1=-0.73$  and  $r_s=-0.70$ ,  $T_s$ , respectively. For the BLS1s, the linear correlation coefficient is  $r_1=0.75$  and the Spearman rank order

<sup>11</sup>Note that this result may be an artifact of assuming a single power law to fit the whole X-ray spectrum. More complicated spectral models involving soft excesses on flatter power laws could reduce this trend.

correlation coefficient  $r_s = -0.67$ ,  $T_s = -5.9$ . In all these cases, the probability of a random correlation is  $P < 0.0001$ . Clearly,  $\alpha_{UV}$  is strongly correlated with  $L/L_{Edd}$ . Note, however, that in the model for the UV-EUV SED employing a power law with exponential cut off (Model A),  $\alpha_{UV}$  and  $L/L_{Edd}$  are not necessarily independent parameters. Thus, a steeper  $\alpha_{UV}$  when extrapolated, will lead to a stronger bump and therefore higher  $L_{BBB}$  and  $L/L_{Edd}$ . If the  $\alpha_{UV} - L/L_{Edd}$  relation is real it must hold also when the double broken power law model is used (Model B). This is indeed the case. For the whole sample we found a linear correlation coefficient  $r_1 = -0.46$  and a Spearman rank order correlation coefficient  $r_s = -0.34$  with  $T_s = -3.4$  with probabilities  $P < 0.0001$  and  $0.0010$ , respectively. Looking at the NLS1 and BLS1 samples separately, the correlations are very strong with  $r_1 = -0.65$  and  $-0.62$ , respectively. In both cases the probabilities of a null correlation are  $P < 0.0001$ . Therefore we consider the anti-correlation between  $\alpha_{UV}$  and  $L/L_{Edd}$  to be real.

For the whole sample we derived the following relationship between  $\alpha_{UV}$  and  $L/L_{Edd}$ :

$$\log L/L_{Edd} = (-0.65 \pm 0.09) \times \alpha_{UV} + (0.08 \pm 0.09). \quad (2)$$

For the NLS1s alone, we find:

$$\log L/L_{Edd} = (-0.62 \pm 0.09) \times \alpha_{UV} + (0.41 \pm 0.10). \quad (3)$$

However, BLS1s show an offset by 0.58 dex:

$$\log L/L_{Edd} = (-0.74 \pm 0.10) \times \alpha_{UV} - (0.17 \pm 0.10). \quad (4)$$

The dotted lines in the left middle panel in Figure 13 show equations (3) and (4).

For the reddening-corrected data  $\alpha_{UV,corr}$  and  $L/L_{Edd-corr}$  we found the following relationships for the whole sample, the NLS1s, and BLS1s, respectively:

$$\log L/L_{Edd-corr} = (-0.77 \pm 0.09) \times \alpha_{UV-corr} + (0.17 \pm 0.07)_{\alpha_{UV-corr}} \quad (5)$$

$$\log L/L_{Edd-corr} = (-0.99 \pm 0.14) \times \alpha_{UV-corr} + (0.57 \pm 0.10), \quad (6)$$

$$\log L/L_{Edd-corr} = (-0.96 \pm 0.10) \times \alpha_{UV-corr} - (0.08 \pm 0.08). \quad (7)$$

The relationships for the NLS1s and the BLS1s are shown as dotted lines in the right middle panel of Figure 13.

Thus,  $\alpha_{UV}$  and  $\alpha_{UV-corr}$  can be used in order to determine the Eddington ratio  $L/L_{Edd}$  and  $L/L_{Edd-corr}$ , respectively. However, one has to keep in mind that there is an offset between BLS1s and NLS1s.

Similar relationships also hold for the Eddington ratios derived from the double broken power law fits to the SEDs as shown in Figure 14. The relationships for the whole sample, the NLS1s, and the BLS1s are as follows:

$$\log L/L_{Edd-bknp0} = (-0.47 \pm 0.10) \times \alpha_{UV} - (0.30 \pm 0.10), \quad (8)$$

$$\log L/L_{Edd-bknp0} = (-0.41 \pm 0.09) \times \alpha_{UV} + (0.12 \pm 0.09), \quad (9)$$

$$\log L/L_{Edd-bknp0} = (-0.58 \pm 0.10) \times \alpha_{UV} - (0.69 \pm 0.10). \quad (10)$$

Again, the slopes in the relations are similar, however, there is an offset between NLS1s and BLS1s by 0.8 dex.

The lower panels in Figure 13 show the relationship between  $\alpha_{ox}$  and  $L/L_{Edd}$ . We found a rather strong correlation between  $\alpha_{ox}$  and  $L/L_{Edd}$ . For the observed  $\alpha_{ox}$  we found a linear correlation coefficient  $r_1 = +0.51$  and a Spearman rank order correlation coefficient  $r_s = +0.55$ . This result, however, is different from that reported by Shemmer et al. (2008) who did not find such a correlation. Our result becomes even stronger when we consider the reddening corrected values  $\alpha_{ox}$  and  $L/L_{Edd}$  is given by

$$\alpha_{ox} = (0.11 \pm 0.02) \log L/L_{Edd} + (1.39 \pm 0.02) \quad (11)$$

The slope in this relation is flatter than what has been reported recently by Lusso et al. (2010). Note that the scatter in our relation is significantly smaller than in the Lusso et al. (2010) sample.

Figure 15 displays the relationship between the optical-to-X-ray spectral slope  $\alpha_{\text{ox}}$  as a function of the luminosity density at 2500Å,  $l_{2500}$ . Also our sample shows the well-known relation found by e.g. Yuan et al. (1998); Strateva et al. (2005); Just et al. (2007); Gibson et al. (2008) that AGN with higher luminosity density at 2500Å appear to be X-ray weaker at 2 keV. We found a relation between  $\alpha_{\text{ox}}$  and the luminosity density at 2500Å:

$$\alpha_{\text{ox}} = (0.114 \pm 0.014) \times \log l_{2500} - (1.177 \pm 0.305) \quad (12)$$

with the luminosity density at 2500Å given in units of  $\text{W Hz}^{-1}$ . This relationship is in excellent agreement with those given by Strateva et al. (2005) and Just et al. (2007). Dashed and solid lines in the upper left panel of Figure 15 show our  $\alpha_{\text{ox}} - \log l_{2500}$  relation and that of Strateva et al. (2005), respectively. Our relationship, however, deviates significantly from those given by Gibson et al. (2008) and Vasudevan et al. (2009b) who found much steeper slopes between  $\alpha_{\text{ox}}$  and  $\log l_{2500}$ . The most likely reason for this deviation is that the Gibson et al. (2008) sample contains more luminous AGN and stretches only over one order of magnitude in  $\log l_{2500}$  while ours and that of Strateva et al. (2005) stretch 4 and 5 orders, respectively. As shown in Figure 15, there are also relationships between  $\alpha_{\text{ox}}$  and  $L_{\text{BBB}}$ ,  $L_{\text{X}}$ , and  $L_{5100\text{Å}}$ . Also here we find correlations with  $\alpha_{\text{ox}}$  as listed in Table 7.

Figure 16 displays the relations between the X-ray spectral slope  $\alpha_{\text{X}}$  with  $L_{\text{X}}$  and  $L_{\text{BBB}}$  in the left and right panels, respectively. In both cases we found marginal evidence that more luminous AGN have steeper X-ray spectra. Note that there is an offset between NLS1s and BLS1s. Thus, for a given  $L_{\text{X}}$  or  $L_{\text{BBB}}$  NLS1s have steeper X-ray spectra; this may be a consequence of their typically smaller black hole masses.

Figure 17 displays the relationships between the luminosity at 5100Å and the 0.2-2.0 keV X-ray luminosity  $L_{\text{X}}$  with the luminosity in the Big-Blue-Bump  $L_{\text{BBB}}$ . These relationships give the bolometric

metric corrections for optical and X-ray luminosities. The bolometric correction for the 5100Å luminosity  $L_{5100\text{Å}}$  (shown in the left panel of figure 17) is given by;

$$\log L_{\text{BBB}} = (1.32 \pm 0.06) \times \log L_{5100} - (10.84 \pm 2.21). \quad (13)$$

The right panel of Figure 17 shows the correlation between the rest frame 0.2-2.0 keV luminosity and  $\log L_{\text{BBB}}$ . Here we found the following relationship:

$$\log L_{\text{BBB}} = (1.23 \pm 0.06) \times \log L_{\text{X}} - (7.36 \pm 2.01). \quad (14)$$

The left panel of Figure 18 displays the well-known relationship between  $\text{FWHM}(\text{H}\beta)$  and the X-ray spectral slope  $\alpha_{\text{X}}$ . The right panel shows  $\text{FWHM}(\text{H}\beta)$  vs.  $L/L_{\text{Edd}}$ . The  $\text{FWHM}(\text{H}\beta)$  were taken from (Grupe et al. 2004a). As expected from previous work (e.g. Boller et al. 1996; Brandt et al. 1997; Grupe et al. 1999; Leighly 1999b; Grupe 2004; Zhou et al. 2006) a clear anti-correlation between the width of  $\text{H}\beta$  and  $\alpha_{\text{X}}$  is found. The Spearman rank order correlation coefficient for the  $\text{FWHM}(\text{H}\beta) - \alpha_{\text{X}}$  relation is  $r_s = -0.65$  with a Student's T-test  $T_s = -7.9$  and a probability  $P < 0.0001$ . The linear correlation coefficient is  $r_l = -0.58$  with a probability  $P < 0.0001$ . We also find a strong anti-correlation between  $\text{FWHM}(\text{H}\beta)$  and  $L/L_{\text{Edd}}$ , as seen in the right panel of Figure 18. The correlation coefficients are  $r_l = -0.56$  and  $r_s = -0.50$  with  $T_s = -5.3$ , and in both cases the probability of a null result is  $P < 0.0001$ . Note that  $\text{FWHM}(\text{H}\beta)$  and  $L/L_{\text{Edd}}$  are not independent properties.  $L/L_{\text{Edd}}$  depends on  $\text{FWHM}(\text{H}\beta)$  because we used the Kaspi et al. (2000) relation to determine  $M_{\text{BH}}$  which is then used to determine  $L_{\text{Edd}}$ . In any case, the correlation between  $\text{FWHM}(\text{H}\beta)$  and  $\alpha_{\text{X}}$  is a robust result, because both are independent.

Figure 19 shows the relationship of  $\text{FWHM}(\text{H}\beta)$  with the optical UV slope  $\alpha_{\text{UV}}$  and  $\alpha_{\text{ox}}$ . We do not find a correlation between  $\text{FWHM}(\text{H}\beta)$  and  $\alpha_{\text{UV}}$ , even among those AGN with  $\alpha_{\text{X}} < 1.6$ .

### 3.6. Variability

All of our objects are members of the *ROSAT* bright soft X-ray selected sample of AGN (Grupe et al.

2001a), and thus have at least one *ROSAT* PSPC and one *Swift* observation. This enables us to search for long-term variability on a time scale of more than 15 years. Also, the majority of the AGN (86 out of 92) have been observed at least twice by *Swift*, with the majority having more than two observations. Note that due to the nature of the fill-in target program this sampling is not homogeneous. Some AGN have been observed twice within a few days while for others the interval was more than a year. Nevertheless, our study shows again that most AGN vary in X-rays by a factor of 3 at the most on all timescales. We note, however, X-ray variability by factors of more than 10 have been observed in some AGN including Mkn 335, PG 1211+143, and RX J2217.9–5941 (Grupe et al. 2007b; Bachev et al. 2009; Grupe et al. 2004b, respectively).

The AGN in our sample are also variable in the UV. Except for the study of variability using *IUE* and *HST* data by Dunn et al. (2006), ours is the largest sample of data suitable to study UV variability. We found that the majority of AGN vary by up to 0.4 mag over the time scale of a few months, though as discussed below, some AGN can vary by up to 1.5 mags within just a few months.

Figure 20 displays the short and long term X-ray flux variability in the AGN sample. The left panel shows a comparison of the count rate from the brightest and faintest AGN with multiple *Swift* observations. The right panel shows the long-term flux variability between the RASS and the *Swift* observations where we again plot the data from the *Swift* observation with the largest difference from the RASS observation. The dashed lines in Figure 20 mark a variability by a factor of 3. While the *Swift* observations in the left panel show that most AGN vary over a time scale of about a year by a factor of 3 or less, the comparison of the *Swift* data with the RASS data displays a slightly different picture: in general we see a trend that the AGN were slightly more luminous during the RASS observations. While during the RASS the mean and median 0.2-2.0 keV luminosities were  $\log L_X=37.02$  and  $37.13$  [W], respectively, during our *Swift* observations we found  $\log L_X=36.94$  and  $37.00$  [W]. We note that this small differences is likely to be a consequence of the sample selection by soft X-ray count rate.

Figure 21 shows the spectral variability among the AGN in the sample. The left panel shows the changes in the hardness ratio between the two *Swift* observations with the largest differences. The right panel displays the long-term change of the 0.2-2.0 keV X-ray spectral slope  $\alpha_X$  between the RASS and the *Swift* observations. The left panel of Figure 21 suggests that the majority of AGN do not show strong spectral variability on time scales of a year or two. The long-term  $\alpha_X$  between the RASS and the XRT observations, at first glance, appears to indicate a systematic flattening of the X-ray spectra over the last 15-18 years.

A very obvious explanation of this apparent flattening is the fact, that *ROSAT* spectra were only fit in the 0.1-2 keV regime, where spectral complexity is known to be common, while *Swift* spectra were fit over a much larger energy band, but still assuming one single power law. Any spectral hardening beyond a few keV would naturally produce most or all of the observed trend. We argue that it is unlikely that cross-calibration uncertainties contribute significantly to the observed trend, even though that has apparently been identified as a potential problem in comparison of *ROSAT* and *ASCA* data (Iwasawa et al. 1999). As shown by Beuermann et al. (2006) and Beuermann (2008) for the *ROSAT* PSPC and Godet et al., (2009) for the *Swift* XRT, both instruments are well-calibrated and reliable. However, an additional selection effect could contribute to the observed apparent flattening. The objects were required to have *ROSAT* PSPC count rates higher than  $0.5 \text{ counts s}^{-1}$  as well as *ROSAT* PSPC hardness ratios  $\text{HR} < 0.0$  to be a member of our sample (Thomas et al. 1998; Grupe et al. 1998a). Objects that were only temporarily soft may have been included in our sample. In fact, we have observed dramatic spectral hardening in follow-up observations of several objects in our sample including RX J0134.2–4258 and RX J0148.3–2758 (Grupe et al. 2000; Komossa & Meerschweinchen 2000; Grupe et al. 2006a, respectively). The apparent hardening of the X-ray spectra may thus be partly a consequence of the selection due to hardness ratio. Just as selection by the flux limit shows that a majority of our AGN appear slightly X-ray fainter than during the RASS observations. Specifically, 52

AGN have lower *Swift* flux than RASS flux, while the opposite is true for only 40 AGN.

The left panel of Figure 22 shows the *Swift* XRT difference in hardness ratio as a function of corresponding count ratio, while the right panel displays the flux ratio between the RASS and *Swift* observations as a function of the difference in the *Swift* and RASS X-ray spectral slopes  $\alpha_X$ . The purpose of these plots is to test whether there is a general trend of a source spectrum to become harder (or softer) when the source becomes fainter or brighter. In neither case do we see any correlation between a change in the flux and any type of spectral variations. Note that this is a general trend based on only two epochs. For an individual source this picture might indeed be different when it is monitored as we have shown in cases like RX J0148.3–2758 or Mkn 335 (Grupe et al. 2006a; Grupe et al. 2008a).

Figure 23 displays the variability in the UVOT W2 filter. We selected this filter because it is the bluest filter which therefore shows a much stronger response to changes in the BBB emission than any other filter. The left panel of Figure 23 displays the difference between the two observations with the brightest and faintest magnitudes in UVW2. The right panel shows the difference between these magnitudes as a function of the ratio of the count rates in the 0.3–10.0 keV XRT X-ray band. Clearly, the majority of the AGN in our sample show some UV variability. Typically, however, this variability is less than 0.4 mag, corresponding to a flux ratio of 1.5. Four AGN do show a variability in the UVW2 filter by more than 0.5 mag: RX J0148.3–2758, ESO 242-G8, RX J0319.8–2627, and RX J2349.4–3126. The last object has also been seen to show strong spectral variability in X-rays from *ROSAT* observations (Grupe et al. 2001a). It is interesting to note that except for RX J0148.3–2758 all these very variable AGN are BLS1s. RX J0319.8–2627 and RX J2349.4–3126 varied in W2 by more than 1.2 mag.

The right panel of Figure 23 shows the XRT count rate ratio between two epochs and the change in the UVOT W2 filter. Note that here we took the UVW2 magnitudes from the same epochs as the maximum and minimum count rates in the XRT. We found a clear correlation between the amplitude of the UVW2 variability and the ra-

tio of the XRT count rate ( $r_1=-0.41$ ,  $r_s=-0.47$ ,  $T_s=-4.55$ , and the probabilities of random results  $P < 0.0001$  for both correlation coefficients). Thus, AGN that have become brighter in X-rays in the second epoch also appear to be brighter in the UV, generally speaking. There is one interesting trend to note: The AGN with the strongest UV variability tend to be BLS1.

It has long been known that the variability time scales are strongly correlated with the luminosity and the black hole mass (e.g. Barr & Mushotzky 1986; Lawrence & Papadakis 1993; Green et al. 1993; Nandra et al. 1997; Leighly 1999; O’Neill et al. 2005; Kelly et al. 2008). We correlated the ratio in the XRT count rates between two epochs with the 0.2–2.0 keV X-ray luminosity  $\log L_X$  and the black hole mass as shown in Figure 24 (left and right panels, respectively). While we found a clear trend that AGN with smaller black hole masses show higher X-ray variability (85 AGN,  $r_1 = -0.22$ ,  $P=0.0406$ ;  $r_s = -0.29$ ,  $T_s = -2.7$ ,  $P=0.0084$ ), we do not see this trend with the X-ray luminosity. Here there seems to be a relatively large group of AGN, predominantly NLS1s with luminosities around  $L_X=37$  [W] that show very strong variability. Again, because of our inhomogeneous sampling due to the nature of the fill-in program, as well as the soft X-ray selection, one has to take the latter statement with caution. We cannot exclude at all that there is not an anti-correlation in our sample as well between the X-ray variability and the X-ray luminosity.

### 3.7. Individual target notes

#### 3.7.1. Mkn 335

Mkn 335 was discovered in May 2007 by *Swift* in an historical X-ray low state (Grupe et al. 2007b). Consequently we started a monitoring campaign with *Swift* and initiated a 20 ks ToO observation with *XMM-Newton*. The *XMM-Newton* observation confirmed the X-ray low-state and revealed the presence of strong soft X-ray emission lines in the RGS spectra (Grupe et al. 2008a; Longinotti et al. 2008). We are currently monitoring Mkn 335 with *Swift*. Since 2007 September it has returned to a high state (Grupe et al. in prep). As discussed in Grupe et al. (2008a) the cause of the low-state was either a strong variable partial covering absorber or reflection of X-rays on the

accretion disk. For the study presented here we used the data from one of the high state observations in September 2008 which seem to represent the 'normal' state of Mkn 335. Nevertheless, recent monitoring of Mkn 335 with *Swift* starting in May 2009 showed it again in a very low flux state (Grupe et al. in prep).

### 3.7.2. *RX J0134.2–4258 and RX J0136.9–3510*

Although the NLS1s RX J0134.2–4258 and RX J0136.9–3510 are not members of the sample of 110 bright soft X-ray selected AGN by Grupe et al. (2001a) and Grupe (2004), they were added to our observing program. Both AGN are very interesting NLS1s. RX J0134.2–4258 is one of a few radio-loud NLS1s (Grupe et al. 2000; Komossa et al. 2006) and had shown one of the softest X-ray spectra of any AGN during the RASS. However, when it was observed by the ROSAT PSPC about two years after the RASS, its X-ray spectrum had dramatically hardened. An ASCA observation in December 1997 confirmed this hard X-ray spectrum Grupe et al. (2000). While Komossa & Fink (1997) and Komossa & Meerschweinchen (2000) suggested that this variability is due to a variable 'warm' ionized absorber, Grupe et al. (2000) discussed that the spectral variability maybe due to the absence and recovery of the accretion disk corona. RX J0136.9–3510 also had one of the steepest X-ray spectra seen of any AGN during the RASS. Ghosh et al. (2004) also discussed the presence of a highly blueshifted Fe  $K\alpha$  line seen by ASCA in this NLS1 and Jin et al. (2009) reported on super-Eddington accretion flows. Our results presented here also suggest super-Eddington accretion.

### 3.7.3. *RX J0148.3–2753*

The NLS1 RX J0148.3–2753 has been the target of several *Swift* fill in and ToO observations. The results of the *Swift* observations performed in 2005 May and December have been published by Grupe et al. (2006a). This NLS1 is highly variable in X-rays by factors of more than 5. We found that the flux variability is associated with strong X-ray spectral variability. In this paper we only present the data previously not published in Grupe et al. (2006a).

### 3.7.4. *Mkn 110*

Mkn 110 has been a highly variable AGN in X-rays as well as at optical/UV wavelengths (e.g. Grupe et al. 2001a; Kollatschny et al. 2001, 2006). Some caution has to be taken into account regarding the Balmer decrement. Because the fluxes in the optical emission lines are highly variable as show by Kollatschny et al. (2001, 2006), we do not know what the exact Balmer decrement was during the time of the *Swift* observation. For the correction for intrinsic reddening we used the optical spectrum published in Grupe et al. (2004a).

Véron-Cetty et al. (2007) discussed the nature of Mkn 110 and concluded that most-likely it is a BLS1s although its FWHM( $H\beta$ ) is less than 2000 km s<sup>-1</sup>. Our continuum measurements presented here seem to support this assumption. In most plots Mkn 110 appears to be among BLS1s and not NLS1s.

### 3.7.5. *PG 1211+143*

The NLS1 PG 1211+143 was monitored by *Swift* simultaneously with ground-based optical photometry between March and May 2007 (Bachev et al. 2009). It was caught by *Swift* in a low state, about 10 times fainter than expected from previous ROSAT and *XMM-Newton* observations. At the end of our two-month monitoring campaign PG1211+143 returned into its normal high state. For this paper we used the observation from 2007 April 02 which was one of the high state observations.

### 3.7.6. *Mkn 766*

The NLS1 Mkn 766 was monitored by *Swift* for half a year between 2006 December and 2007 May (Grupe et al. in prep.) quasi-simultaneously with RXTE and ground-based optical photometry. For this paper we used the first of these observations from 2006 December 21.

### 3.7.7. *3C 273*

The first quasar ever discovered, 3C 273 (Schmidt 1963), has been the target of many *Swift* observations since the start of the mission. 3C 273 is a standard calibration source and also has been the target of several monitoring campaigns. However, not all observations are suitable

for our study. 3C 273 is the brightest AGN in our sample and if observed in our standard observing modes (XRT in PC mode, UVOT in full frame) the observations are strongly compromised by pileup/coincident losses. In order to obtain usable data, 3C 273 has to be observed in Windowed Timing mode in XRT and in the  $5' \times 5'$  hardware window mode in the UVOT. Because it is beyond the scope of his paper to list all observations performed so far, we picked some more recent observation from the beginning of 2009 where 3C 273 was observed in WT in XRT and the UVOT  $5' \times 5'$  hardware window. Other *Swift* observations of 3C 273 are listed in e.g. Pacciani et al. (2009).

### 3.7.8. NGC 5548

The Seyfert 1.5 galaxy NGC 5548 has been the target of two *Swift* monitoring campaigns, one in 2005 April/May (Goad & Page 2006) and in 2007 June to August (Grupe et al. 2010, in prep). The latter one was simultaneous with Suzaku (Krongold et al. 2010; Liu et al. 2010) in order to study the variable 'warm' absorber in this AGN. In the study presented here we used the XRT and UVOT observation from segment 059 from the beginning of the 2007 monitoring campaign on 2007 June 19. Note that NGC 5548 is the AGN with the lowest Eddington ratio  $L/L_{\text{Edd}}$  in our sample.

### 3.7.9. RX J2217.9–5941

The NLS1 RX J2217.9–5941 was discovered during the RASS as a bright X-ray AGN with a very soft X-ray spectrum (Grupe et al. 1998a). However, when it was observed in May 1997 and April 1998 by the *ROSAT* High-Resolution Imager and in May 1998 by *ASCA* it appeared to have become significantly fainter (Grupe et al. 2001b). Two follow-up observations with *Chandra* confirmed this low state (Grupe et al. 2004b). The spectra derived from the *Chandra* data suggest the presence of a partial covering absorber. Our *Swift* observations also found this AGN in a low state. Between the RASS observation and the last *Swift* observation RX J2217.9–5941 has shown a decay in its 0.2–2.0 keV flux by a factor of about 30.

## 4. Discussion

In this paper we presented a sample of 92 bright soft X-ray selected AGN with simultaneous op-

tical/UV and X-ray observations using *Swift* in order to study the optical to X-ray spectral energy distribution in AGN. Many of these AGN exhibit strong variability in X-rays as well as at UV wavelengths. Therefore, studying the SEDs of AGN, performing the observations in the UV and in X-ray simultaneously is critical. The NASA GRB Explorer mission *Swift* has the unique ability to perform this type of multi-wavelength observations with relatively short snap-shot observations. As a result, more than 95% of the AGN in our sample have been observed by *Swift* multiple times.

The mean and median values of  $\alpha_{\text{ox}}$  and  $\alpha_{\text{UV}}$  of NLS1s and BLS1s suggest that the SEDs are relatively similar. However, NLS1s appear to be intrinsically fainter in the UV compared with BLS1s. This result is most likely due to the accretion disk temperatures in NLS1s and BLS1s. NLS1s have, generally speaking, smaller black hole masses. Because of the  $T \propto M^{-1/4}$  relation between the temperature of the accretion disk and the mass of the central black hole, NLS1s have hotter accretion disks than BLS1s. Therefore their BBB thermal spectra are shifted towards higher energies making the UV spectra appear fainter. Our result reflects very well the SED models used by Kelly et al. (2008) shown in their Figure 13. This interpretation also explains the findings by Atlee & Mathur (2009) and Rodríguez-Pascual et al. (1997) that NLS1s appear to be fainter in the UV when compared with other samples.

One of our main interests in our study was to investigate whether AGN with steep X-ray spectra also show blue optical/UV spectra as previously reported by e.g. Walter & Fink (1993) and Grupe et al. (1998a) using non-simultaneous data. On a first glance there seems to be only a slight correlation between  $\alpha_{\text{X}}$  and  $\alpha_{\text{UV}}$ . Certainly reddening in the UV may produce scatter in this relationship, but that is not a plausible explanation for the lack for correlation in the whole sample. The answer regarding the relationship between  $\alpha_{\text{X}}$  and  $\alpha_{\text{UV}}$  seems to be a bit more complicated. Examining the BLS1s (filled red circles in Figure 10) first, and excluding IRAS 1334+24, the AGN in the upper right corner which is known to have very strong reddening in the optical/UV (Wills et al. 1992; Grupe et al. 1998b), we find a fairly strong correlation between  $\alpha_{\text{X}}$  and  $\alpha_{\text{UV}}$ . Now the correlation coefficient is  $r_1 = -0.49$



with a probability  $P=0.0011$  of a random result. For a Spearman rank order correlation we found  $r_s = -0.53$  and  $T_s = -3.9$  with  $P=0.0004$ . For the NLS1s, however, there appears to be nearly no relationship between  $\alpha_X$  and  $\alpha_{UV}$  ( $r_1 = -0.21$ ). The reason for this appears to be related to the fact that NLS1s operate close to or above the Eddington limit. This is not the case, however, for BLS1s which operate at lower  $L/L_{Edd}$ . Looking back at the entire sample, we see that the relationship saturates at about  $\alpha_X=1.6$ . For objects with an X-ray spectrum steeper than  $\alpha_X=1.6$  the optical/UV slope remains nearly constant, and these AGN are dominated by NLS1s. When excluding all AGN with  $\alpha_X>1.6$ , we find a clear correlation that AGN with steeper X-ray spectra also show bluer optical/UV continua ( $r_1 = -0.43$ ,  $P=0.0009$ ;  $r_s = -0.36$ ,  $T_s = -2.8$ ,  $P=0.0071$ ). Our results, therefore, confirm the findings by Walter & Fink (1993) and Grupe et al. (1998a).

Another aspect of our study was to determine if there are observable properties that can be used to describe the SEDs and estimate  $L/L_{Edd}$ . As shown previously by Grupe (2004) and Shemmer et al. (2008),  $L/L_{Edd}$  can be estimated from the X-ray spectral slope  $\alpha_X$ . However, we find that this relationship is only valid for AGN with X-ray spectral slope  $\alpha_X<1.6$ . At about this point,  $L/L_{Edd}$  reaches unity. For AGN with steep X-ray spectra, thus predominantly NLS1s, this  $\alpha_X$ -  $\alpha_{UV}$  relation breaks down. As shown in the middle panels of Figure 13,  $\alpha_{UV}$  can be used as an estimator of  $L/L_{Edd}$ . This slope can actually predict  $L/L_{Edd}$  even better than the X-ray spectral slope  $\alpha_X$  because it does not show the saturation that we see in the  $\alpha_X$ - $L/L_{Edd}$  relation. One interesting result of the  $\alpha_{UV}$ -  $L/L_{Edd}$  relation is that there is an offset between NLS1s and BLS1s by about 0.6 dex. So, for a given optical/UV slope  $\alpha_{UV}$ , BLS1s show a lower Eddington ratio by a factor of  $\approx 4$  compared with NLS1s (see Eqs. 2 to 10). The main effect here is from the larger black hole masses found in BLS1s; on average, BLS1s have a 10 times larger black hole mass than NLS1s. As an alternative this result may also suggest that there is a physical difference in the accretion disk properties of NLS1s and BLS1s. As shown by Wandel & Petrosian (e.g. 1988), accretion discs with a blackbody spectrum modified by Comptonization have redder optical/UV spectra for a

given central black hole mass than those without Comptonization. It could be that because NLS1s do accrete at high  $L/L_{Edd}$  a wind from the accretion disk causes the Comptonization layer above the disk to be smaller than in BLS1s. Our conclusion differs from that by Atlee & Mathur (2009) who suggested that the accretion disk properties are independent of the mass of the central black hole and  $L/L_{Edd}$ .

The immediate application of these relations is for high-redshift quasars. In that case it is difficult to estimate  $L/L_{Edd}$  based on their X-ray data because their rest-frame soft X-ray 0.2-2.0 keV spectra are mostly shifted out of the observed energy window and the majority of them are too X-ray faint to derive useful X-ray spectra (e.g. Grupe et al. 2006a). Because rest-frame optical/UV spectra exist for most of these AGN, one can use the spectral slope  $\alpha_{UV}$  in order to determine  $L/L_{Edd}$ . When applying this method to an AGN one has to make sure that one has the correct classification of the AGN because of the offset between NLS1s and BLS1s. As a test, we applied our relation to the sample of 10 intermediate redshift QSOs presented by Dietrich et al. (2009) for which rest-frame spectra of the  $H\beta$  line region were taken. From the rest-frame UV spectra we derived the Eddington ratios using the relation for BLS1s (equation #4) and found that our estimates are in good agreement with those  $L/L_{Edd}$  values reported in Dietrich et al. (2009). This suggests that our method is quite reliable. However, it still requires a much larger sample of intermediate and high redshift QSOs to verify this result.

Regarding the bolometric corrections, in Figure 17 we show the relationships between the luminosity at  $5100\text{\AA}$  and in the rest-frame 0.2-2.0 keV band vs. the luminosity in the BBB  $L_{BBB}$ . In both panels the solid lines are the relations found in our sample as given in equations (12) and (13). The dashed line in the left panel shows the relation found by Elvis et al. (1994). Our sample shows only a slight luminosity dependence of the bolometric correction (i.e.,  $L_{bbb}$ ) on  $5100\text{\AA}$  or 0.2-10 keV luminosity.

One interesting result we found is the trend that BLS1s appear to be more variable in the UV compared with NLS1s. At first glance, because they vary strongly in X-rays, one might expect that NLS1s would also be highly variable in the

UV. However, they are not. This may be because the UV in lower accretion rate objects comes from relatively close to the black hole, where time scales are shorter, while the UV in NLS1s comes from a more extended part of the accretion disk, where less variability is expected. Another reason may be the effect of partial covering absorption on the X-ray emission. As we have seen in, e.g., Mkn 335 and WPVS 007 (Grupe et al. 2007a; Grupe et al. 2007b; Grupe et al. 2008a; Grupe et al. 2008b; Leighly et al. 2009), some NLS1s can vary strongly in X-rays, but only show minor variability in the UV. In both cases, a possible explanation is the presence of a partial covering absorber that affects the spectrum at X-ray energies, but does not affect the UV range that much, assuming it is dust-free and compact.

One of our main concerns regarding our study was that the optical/UV and X-ray data were taken simultaneously. Nevertheless we found similar results for the whole sample as have been reported earlier from samples with non-simultaneous observations, such as Walter & Fink (1993) or Grupe et al. (1998a). Is there still an advantage in simultaneous data? The answer is 'yes'. There are several arguments that make simultaneous observations crucial for this type of study: 1) Non-simultaneity smears out trends. While this may not be a problem for very large samples (e.g., those considered by Grupe et al. 1998a; Atlee & Mathur 2009), in which the trends dominate the effect of smearing, this would not apply for individual sources. One of our aims was to find relations between observed parameters to get an estimate of  $L/L_{\text{Edd}}$ . As we have shown in some examples, this will not work if the AGN is highly variable in the UV as well as in the X-rays (such as ESO242-G008, or RX J2349.4-3126) as shown in the SEDs displayed in the appendix. 2) Observing the data simultaneously in the optical/UV and in X-rays reduces the scatter in the relationships. As shown above this is especially important if the sample contains BLS1s, which tend to show stronger UV variability than NLS1s. One example here is the  $\alpha_{\text{ox}}\text{-log } l_{2500\text{\AA}}$  relation. While the scatter in our relation is relatively small it appears to be significantly larger in the sample of Gibson et al. (e.g., 2008) and Yuan et al. (1998). In other words, in a sample with simultaneous data, relations can be constrained better

than with non-simultaneous data sets.

Future work on our SED project includes obtaining *Swift* observations for the entire sample of 110 bright soft X-ray selected AGN Grupe et al. (2001a); Grupe (2004) and extending the sample to hard X-ray selected AGN by making use of existing data either from *Swift* or *XMM-Newton* observations. The goal here is to increase the statistics on the results and to avoid the selection effects that are currently in our soft X-ray flux-selected AGN sample. In a second paper we will also perform a more detailed statistical analysis including a Principal Component and cluster analysis to examine the connections between continuum and optical emission line properties, and will then carry out a rigorous interpretation of these results with respect to implications for NLS1 models.

## 5. Conclusions

We have derived SEDs for a sample of 92 AGN with *simultaneous* optical-UV and X-ray observations with *Swift*. 88 of these AGN are observed in at least 3 of the 6 UVOT filters. This is the largest sample of AGN with simultaneous multi-wavelength coverage, and one of the largest with repeated UV observations. Our results can be summarized as follows:

- We provide bolometric corrections (Equations (12) and (13)) starting from the optical or X-ray luminosity, covering several decades in luminosity.
- NLS1s appear to be fainter in the UV and at hard X-ray energies and show steeper X-ray spectra than BLS1s.
- NLS1s and BLS1s have very similar  $\alpha_{\text{UV}}$  and  $\alpha_{\text{ox}}$ .
- We found a strong correlation between  $\alpha_{\text{X}}$  and  $\alpha_{\text{UV}}$ . However, this relation saturates for AGN with  $\alpha_{\text{X}} > 1.6$  (i.e., predominantly for NLS1 galaxies).
- We confirm earlier findings by e.g. Grupe (2004) and Shemmer et al. (2008) that AGN with steeper X-ray spectral indices have higher  $L/L_{\text{Edd}}$ . Again, the relation saturates for AGN with  $\alpha_{\text{X}} > 1.6$ .

- There is a clear anti-correlation between the optical/UV spectral slope  $\alpha_{UV}$  and  $L/L_{Edd}$ . AGN with bluer  $\alpha_{UV}$  have higher  $L/L_{Edd}$ . However, there is an offset between NLS1s and BLS1s and for a given  $\alpha_{UV}$  NLS1s have about 4 times higher  $L/L_{Edd}$  than BLS1s.
- The relationships we found between  $\alpha_{UV}$  and  $L/L_{Edd}$  for NLS1s and BLS1s can be used to estimate  $L/L_{Edd}$  in, e.g., high-redshift QSOs.
- Although NLS1s show strong X-ray variability, they vary only marginally in the UV.

We would like to thank the *Swift* team for performing the observations of our AGN sample, in particular the *Swift* PI Neil Gehrels for approving our various ToO requests for observing the AGN when they were found in an interesting flux state. Special thanks to the *Swift* science planners Judy Racusin, Sally Hunsberger, Claudio Pagani, David Morris, Mike Stroh and Peter Brown, and our referee Lisa Winter for excellent comments and suggestions that significantly improved the paper. This research has made use of the NASA/IPAC Extragalactic Database (NED) which is operated by the Jet Propulsion Laboratory, Caltech, under contract with the National Aeronautics and Space Administration. *Swift* at PSU is supported by NASA contract NAS5-00136. This research was supported by NASA contract NNX07AH67G (D.G.).

## REFERENCES

- Arnaud, K.A., et al., 1985, MNRAS, 217, 105
- Arnaud, K. A., 1996, ASP Conf. Ser. 101: Astronomical Data Analysis Software and Systems V, 101, 17
- Atlee, D.W., & Mathur, S., 2009, ApJ, 703, 1597
- Bachev, R., Grupe, D., Boeva, S., Ovcharov, E., Valcheva, A., Semkov, E., Georgie, & Gallo, L.C., 2009, MNRAS, 399, 750
- Barr, P., & Mushotzky, R.F., 1986, Nature, 330, 421
- Barthelmy, S.D., 2005, Space Science Reviews, 120, 143
- Bentz, M.C., Peterson, B.M., Pogge, R.W., Vestergaard, M., & Onken, C.A., 2006, ApJ, 644, 133
- Bentz, M.C., Peterson, B.M., Netzer, H., Pogge, R.W., & Vestergaard, M., 2009, ApJ, 697, 160
- Beuermann, K., 2008, A&A, 481, 919
- Beuermann, K., Thomas, H.-C., Reinsch, K., et al., 1999, A&A, 347, 47
- Beuermann, K., Burwitz, V., & Rauch, T., 2006, A&A, 458, 541
- Boller, T., Brandt, W.N., & Fink, H.H., 1996, A&A, 305, 53
- Boroson, T.A., & Green, R.F., 1992, ApJS, 80, 109
- Boroson, T.A., 2002, ApJ, 565, 78
- Brandt, W. N., Fabian, A. C., & Pounds, K. A. 1996, MNRAS, 278, 326
- Brandt, W.N., Mathur, S., & Elvis, M., 1997, MNRAS, 285, L25
- Brocksopp, C., Starling, R.L.C., Schady, P., Mason, K.O., Romero-Comenere, E., & Puchnarewicz, E.M., 2006, MNRAS, 366, 953
- Burrows, D., et al., 2005, Space Science Reviews, 120, 165
- Cardelli, J.A., Clayton, G.C., Mathis, J.S., 1989, ApJ, 345, 245
- Cohen, R.D., 1983, ApJ, 273, 489
- Crummy, J., Fabian, A.C., Gallo, L.C., & Ross, R.R., 2006, MNRAS, 365, 1067
- Czerny, B., & Elvis, M., 1987, ApJ, 321, 305
- Dickey, J.M., & Lockman, F.J., 1990, ARA&A, 28, 215
- Dietrich, M., Mathur, S., Grupe, D., & Komossa, S., 2009, ApJ, 696, 1998
- Done, C., Sobolewska, M.A., Gierlinski, M., & Schurch, MNRAS374, L15
- Dong, X., Wang, T., Wang, J., Yuan, W., Zhou, H., Dai, H., & Zhang, K., 2008, MNRAS, 383, 581

- Dunn, J.P., Jackson, B., Deo, R.P., Farrington, C., Das, V., & Crenshaw, D.M., 2006, *PASP*, 118, 572
- Elvis, M., et al., 1994, *ApJS*, 95, 1
- Fabian, A.C., Miniutti, G., Gallo, L.C., Boller, T., Tanaka, Y., Vaughan, S., & Ross, R.R., 2004, *MNRAS*, 353, 1071
- Fabian A.C., Vasudevan, R.V., Mushotzky, R.F., Reynolds, L.M., & Winter, C.S., 2009, *MNRAS*, in press, arXiv:0901.0250
- Gallo, L.C., 2006, *MNRAS*, 368, 479
- Gallo, L.C., Tanaka, Y., Boller, T., Fabian, A.C., Vaughan, S., & Brandt, W.N., 2004, *MNRAS*, 353, 1064
- Gehrels, N., et al., 2004, *ApJ*, 611, 1005
- Ghosh, K.K., Swartz, D.A., Tennant, A.F., Wu, K., & Ramsey, B.D., 2004, *ApJ*, 607, L111
- Gibson, R.R., Brandt, W.N., & Schneider, D.P., 2008, *ApJ*, 685, 773
- Gierlinski, M., & Done, C., 2004, *MNRAS*, 349, L7
- Goad, M.R., & Page, K.L., 2006, *Proceedings of the The X-ray Universe 2005 (ESA SP-604)*. 26-30 September 2005, El Escorial, Madrid, Spain. Editor: A. Wilson, p.621
- Godet, O., et al., 2009, *A&A*, 494, 775
- Goodrich, R.W., 1989, 342, 224
- Green, A.R., McHardy, I.M., & Lehto, H.J., *MNRAS*, 265, 664
- Grupe, D., 2004, *AJ*, 127, 1799
- Grupe, D., Beuermann, K., Thomas, H.-C., Mannheim, K., & Fink, H.H., 1998a, *A&A* 330, 25
- Grupe, D., Wills, B.J., Wills, D., Beuermann, K., 1998b, *A&A*, 333, 827
- Grupe, D., Beuermann, K., Mannheim, K., & Thomas, H.-C., 1999, *A&A*, 350, 805
- Grupe, D., Leighly, K.M., Thomas, H.-C., & Laurent-Muehleisen, S.A., 2000, *A&A*, 356, 11
- Grupe, D., Thomas, H.-C., & Beuermann, K., 2001a, *A&A*, 367, 470
- Grupe, D., Thomas, H.-C., & Leighly, K.M., 2001b *A&A*, 369, 450
- Grupe, D., Wills, B.J., Leighly, K.M., & Meusinger, H., 2004a, *AJ*, 127, 156
- Grupe, D., Leighly, K.M., Burwitz, V., Predehl, P., & Mathur, S., 2004b, *AJ*, 128, 1524
- Grupe, D., Mathur, S., & Komossa, S., 2004c, *AJ*, 127, 3161
- Grupe, D., Leighly, K.M., Komossa, S., Schady, P., O'Brien, P.T., Burrows, D.N., & Nousek, J.A., 2006a, *AJ*, 132, 1189
- Grupe, D., Mathur, S., Wilkes, B., & Osmer, P., 2006b, *AJ*, 131, 55
- Grupe, D., Schady, P., Leighly, K.M., Komossa, S., O'Brien, P.T., & Nousek, J.A., 2007a, *AJ*, 133, 1988
- Grupe, D., Komossa, S., & Gallo, L.C., 2007b, *ApJ*, 668, L111
- Grupe, D., Komossa, S., Gallo, L.C., Fabian, A.C., Larsson, J., Pradhan, A.K., Xu, D., & Miniutti, G., 2008a, *ApJ*, 681, 982
- Grupe, D., Leighly, K.M., & Komossa, S., 2008, *AJ*, 136, 2343
- Hill, J.E., et al., 2004, *SPIE*, 5165, 217
- Hopkins, P.F., Gordon, R.T. & Hernquist, L. 2007, *ApJ*, 654, 731
- Iwasawa, K., Fabian, A. C., & Nandra, K. 1999, *MNRAS*, 307, 611
- Jin, C., Done, C., Ward, M., Gierlinski, M., & Mullaney, J., 2009, *MNRAS*, in press, arXiv:0903.4698v1
- Just, D., Brandt, W.N., Shemmer, O., Steffen, A.T., Schneider, D.P., Chartas, G., & Garmire, G.P., 2007, *ApJ*, 665, 1004
- Kaspi, S., Smith, P. S., Netzer, H., Maoz, D., Januzzi, B. T., & Giveon, U., 2000, *ApJ*, 533, 631
- Kaspi, S., et al. 2005, *ApJ*, 629, 61

- Kelly, B.C., Bechtold, J., Trump, J.R., Vestergaard, M., & Siemiginowska, A., 2008, *ApJS*, 176, 355
- Kollatschny, W., Bischoff, K., Robinson, E.L., Welsh, W.F., & Hill, G.J., 2001, *A&A*, 379, 125
- Kollatschny, W., Zetzl, M., & Dietrich, M., 2006, *A&A*, 454, 459
- Komossa, S., & Fink, H.H., 1997, *Accretion Disks - New Aspects. Lecture Notes in Physics*, 487, 250
- Komossa, S., & Bade, N. 1998, *A&A*, 331, L49
- Komossa, S., & Meerschweinchen, J. 2000, *A&A*, 354, 411
- Komossa, S., Voges, W., Xu, D., Mathur, S., Adorf, H.-M., Lemson, G., Duschl, W.J., & Grupe, D., 2006, *AJ*, 132, 531
- Krongold, Y, Elvis, M., et al., 2010, *ApJ*, in press, arXiv:1001.1339
- Lawrence, A., & Papadakis, I., 1993, *ApJ*, 414, L85
- Leighly, K.M., 1999, *ApJS*, 125, 297
- Leighly, K.M., 1999b, *ApJS*, 125, 317
- Leighly, K.M., Kay, L. E., Wills, B. J., Wills, D. & Grupe, D. 1997, *ApJ*, 489L, 137
- Leighly, K.M., Halpern, J.P., Jenkins, E.B., Grupe, D., Choi, J., & Prescott, K.B., 2007, *ApJ*, 663, 103
- Leighly, K.M., Hamann, F., Casebeer, D.A., & Grupe, D., 2009, *ApJ*, 701, 176
- Lira, P., Lawrence, A., O'Brien, P., Johnson, R.A., Terlevich, R., & Bannister, N., 1999, *MNRAS*, 305, 109
- Liu, Y., et al., 2010, *ApJ*, accepted, arXiv:1001.0356
- Longinotti, A.L., Nucita, A., Guainazzi, M., et al., 2008, *A&A*, 484, 311
- Lusso, E., et al., 2010, *A&A*, accepted, arXiv:0912.4166v1
- Mannheim, K., Schulte, M., Rachen, J., 1995, *A&A*, 303, L41
- Marconi, A., Risaliti, G., Gilli, R., Hunt, L.K., Maiolino, R., & Salvati, M., 2004, *MNRAS*, 351, 169
- Marconi, A., et al. 2008, *ApJ*, 678, 693
- Markwardt, C.B., Tueller, J., Skinner, G.K., Gehrels, N., Barthelmy, S.D., & Mushotzky, R.F., 2005, *ApJ*, 633, L77
- Mason, K.O., et al., 2001, *A&A*, 365, L36
- Mathur, S., 2000, *MNRAS*, 314, L17
- Nandra, K., George, I.M., Mushotzky, R.F., Turner, T.J., & Yaqoob, T., 1997, *ApJ*, 476, 70
- O'Neill, P.M., Nandra, K., Papadakis, I.E., & Turner, T.J., 2005, *MNRAS*, 358, 1405
- Osterbrock, D.E. & Pogge, R.W., 1985, *ApJ*, 297, 166
- Pacciani, L., et al. 2009, *A&A*, 494, 49
- Peterson, B., et al. 2004, *ApJ*, 613, 682
- Pfeffermann, E., Briel, U.G., Hippmann, H., et al., 1986, *SPIE*, 733, 519
- Poole, T.S., et al., 2008, *MNRAS*, 383, 627
- Pounds, K.A., Done, C., & Osborne, J.P., 1995, *MNRAS*, 277, L5
- Rodríguez-Pascual, P. M.; Mas-Hesse, J. M.; Santos-Lleo, M., 1997, *A&A*, 327, 72
- Roming, P.W.A., et al., 2005, *Space Science Reviews*, 120, 95
- Roming, P.W.A., et al., 2009, *ApJ*, 690, 163
- Ross, R.R., Fabian, A.C., & Mineshige, S., 1992, *MNRAS*, 58, 189
- Schlegel, D. J., Finkbeiner, D. P., & Davis, M. 1998, *ApJ*, 500, 525
- Schmidt, M., 1963, *Nature*, 197, 1040
- Shemmer, O., Brandt, W.N., Netzer, H., Maiolino, R., & Kaspi, S., 2008, *ApJ*, 682, 81

- Shields, G.A., 1978, *Nature*, 272, 706
- Strateva, I.V., Brandt, W.N., Schneider, D.P., Vanden Berk, D.G., & Vignali, C., 2005, *AJ*, 130, 387
- Sulentic, J.W., Zwitter, T., Marziani, P., & Dultzin-Hacyan, D., 2000, *ApJ*, 536, L5
- Tananbaum, H., et al., 1979, *ApJ*, 234, L9
- Thomas, H.-C., Beuermann, K., Reinsch, K., et al., 1998, *A&A*, 335, 467
- Tueller, J., et al., 2009, *ApJS*, accepted, arXiv:0903.3037v1
- Turner, M.J.L., Abbey, A., Arnaud, M., et al., 2001, *A&A*, 365, L27
- Turner, T.J., & Miller, L., 2009, *A&ARv*, 17, 47
- Vasudevan, R.V., & Fabian, A.C., 2009, *MNRAS*, 392, 1124
- Vasudevan, R.V., Mushotzky, R.F., Winter, L.M., & Fabian, A.C., 2009, *MNRAS*, 399, 1553
- Véron-Cetty, M.-P., Véron, P., Joly, M., & Kol-latschny, W., 2007, *A&A*, 475, 487
- Voges, W., Aschenbach, B., Boller, T., et al., 1999, *A&A*, 349, 389
- Walter, R., & Fink, H.H., 1993, *A&A*, 274, 105
- Walter, R., Orr, A.; Courvoisier, T. J.-L.; Fink, H. H.; Makino, F.; Otani, C.; Wamsteker, W., 1994, *A&A*, 285, 119
- Wandel, A., & Petrosian, V., 1988, *ApJ*, 329, L11
- Williams, R.J., Pogge, R.W., & Mathur, S., 2004, *ApJ*, 610, 737
- Wills, B.J., Wills, D., Evans, N.J., Natta, A., Thompson, K.L., Breger, M., & Sitko, M.L., 1992, *ApJ*, 400, 96
- Winter, L.M., Mushotzky, R.F., Reynolds, C.S., & Tueller, J., 2009, *ApJ*, 690, 1322
- Yuan, W., Siebert, J., Brinkmann, W., 1998, *A&A*, 334, 498
- Young, M., Elvis, M., & Risaliti, G., 2009, *ApJS*, 183, 17
- Zhou, H., Wang, T., Yuan, W., Lu, H., Dong, X., Wang, J., & Lu, Y., 2006, *ApJS*, 166, 128

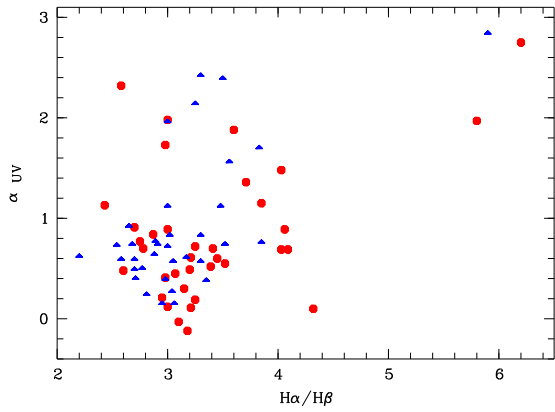


Fig. 2.— Relation between the optical/UV slope  $\alpha_{UV}$  corrected for Galactic reddening and Balmer decrement  $H\alpha/H\beta$ . NLS1s are displayed as blue triangles and BLS1s as filled red circles.

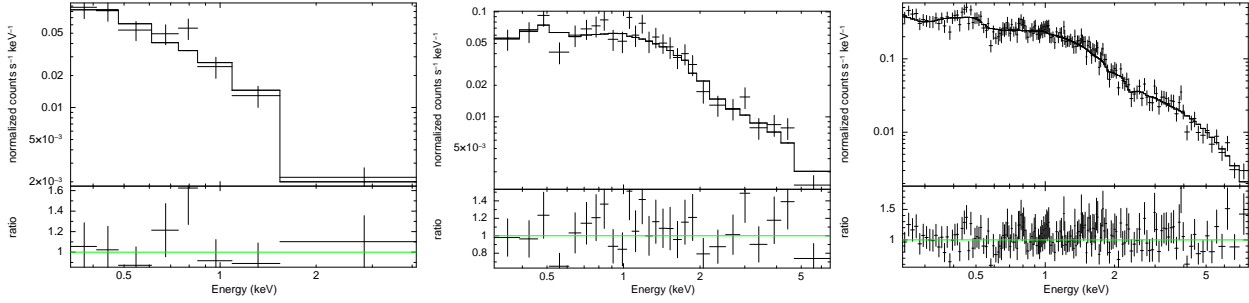


Fig. 1.— Examples of XRT spectra, from the left to the right, RX J0117.5–3826, Fairall 1119, and RX J0128.1–1848. All these spectra were fitted by an absorbed single power law model.

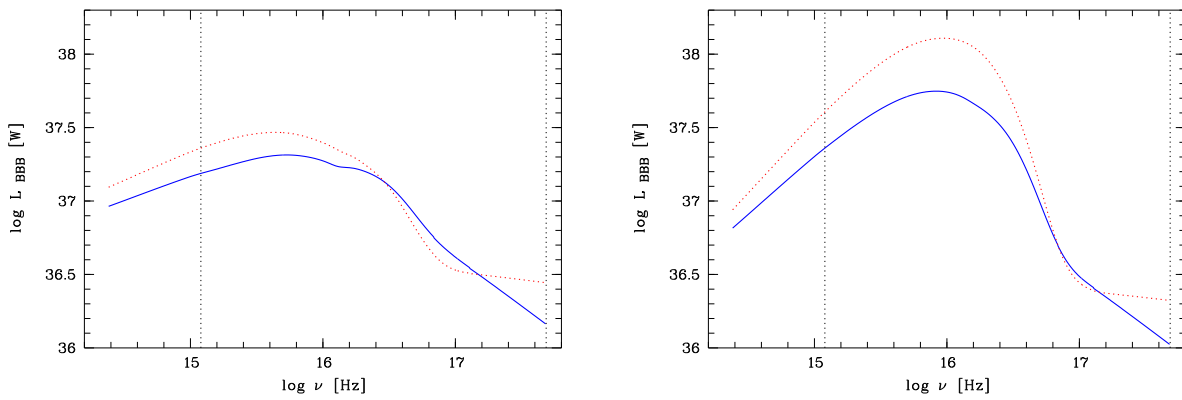


Fig. 3.— Average SEDs of NLS1s (solid blue line) and BLS1s (dotted red line). The left panel displays the SED uncorrected for intrinsic reddening and the right panel shows the SED corrected for intrinsic reddening. The vertical dotted lines mark the frequencies at  $2500 \text{ \AA}$  and  $2 \text{ keV}$ , which are used to determine  $\alpha_{\text{ox}}$ .



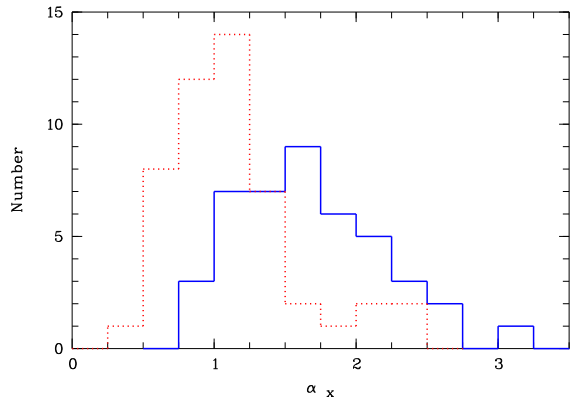


Fig. 4.— Distributions of the 0.3-10.0 keV X-ray energy spectral slope  $\alpha_X$  for NLS1s (solid blue line) and BLS1s (dotted red line).

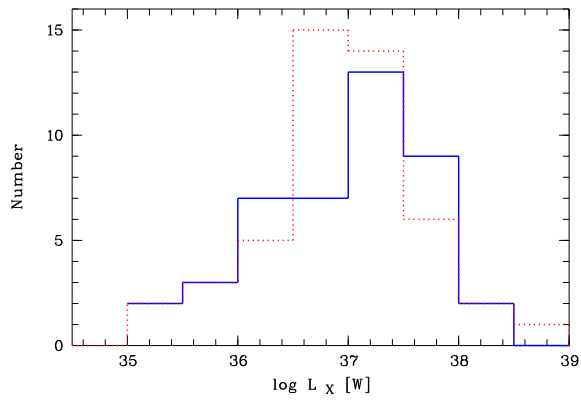


Fig. 8.— Distributions of the 0.3-10.0 keV X-ray luminosity  $\log L_X$  for NLS1s (solid blue line) and BLS1s (dotted red line).

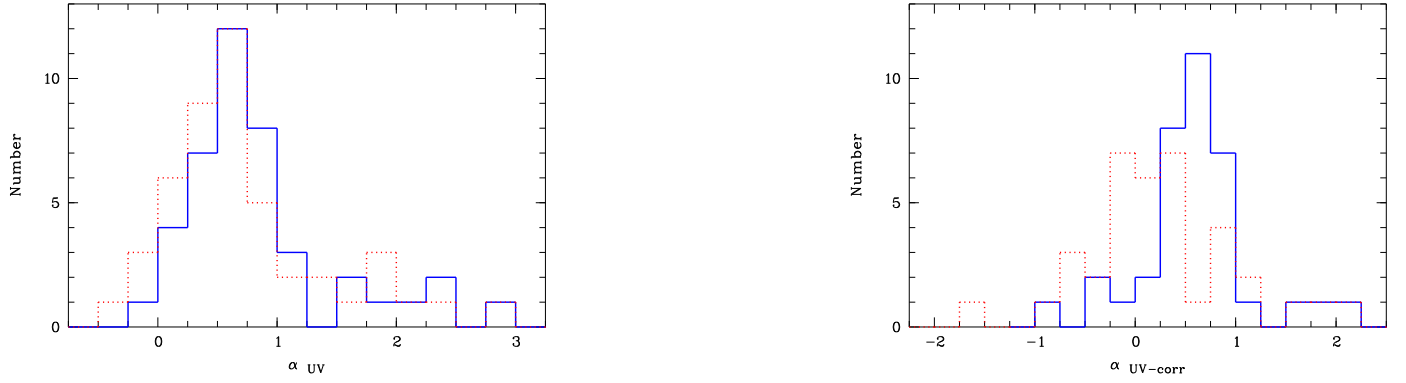


Fig. 5.— Distributions of the optical/UV spectral slope  $\alpha_{UV}$  uncorrected and corrected for intrinsic reddening (left and right panels, respectively). The coding for the lines is given in Figure 3.

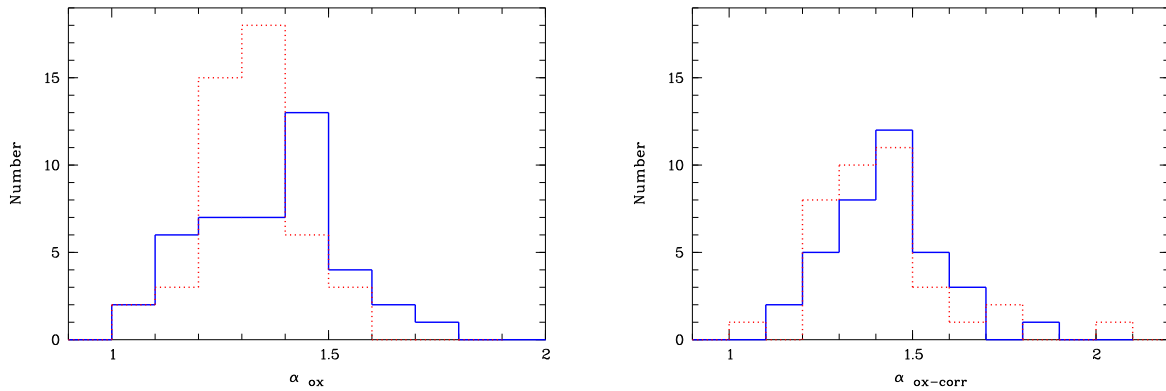


Fig. 6.— Distributions of the optical-to-X-ray spectral slope  $\alpha_{ox}$  uncorrected and corrected for intrinsic reddening (left and right panels, respectively). The coding for the lines is given in Figure 3.

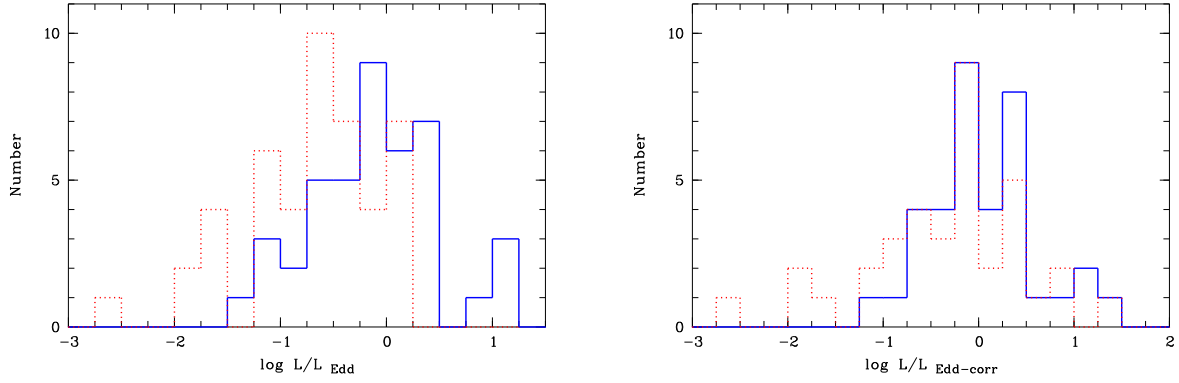


Fig. 7.— Distributions of the Eddington ratios  $L/L_{\text{Edd}}$ , uncorrected and corrected for intrinsic reddening (left and right panels, respectively). The coding for the lines is given in Figure 3.

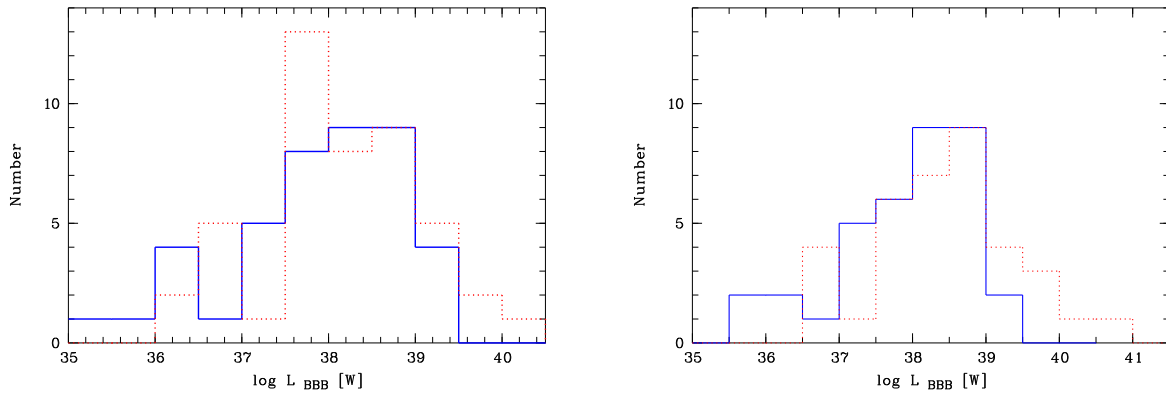


Fig. 9.— Distributions of the Big-Blue-Bump luminosity  $\log L_{\text{BBB}}$  uncorrected and corrected for intrinsic reddening (left and right panels, respectively) for NLS1s (solid blue line) and BLS1s (dotted red line).

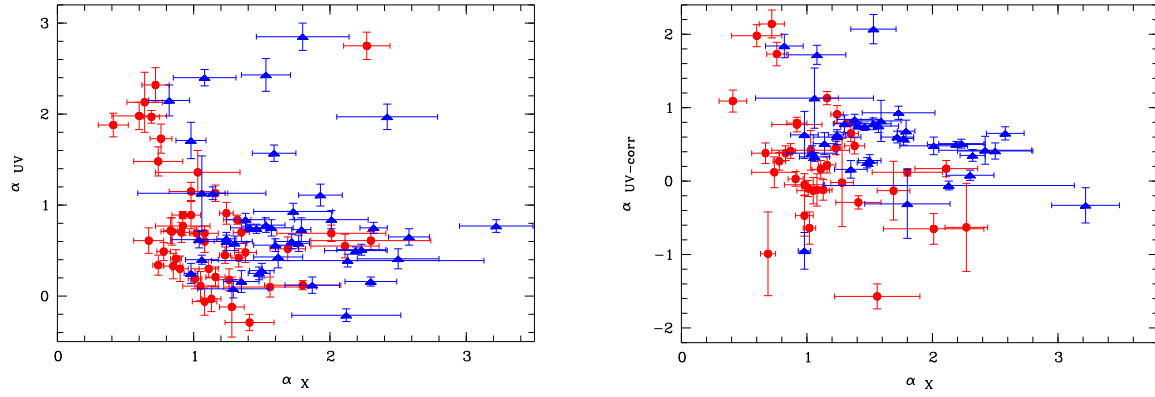


Fig. 10.— 0.3-10 keV X-ray energy spectral slope  $\alpha_X$  and optical/UV spectral slope  $\alpha_{UV}$ . The left panel displays the  $\alpha_{UV}$  value only corrected for Galactic reddening and the right panel the  $\alpha_{UV}$  value corrected for intrinsic and Galactic reddening, determined from the Balmer decrement given in Table 1. NLS1s are displayed as blue triangles and BLS1s as red circles.

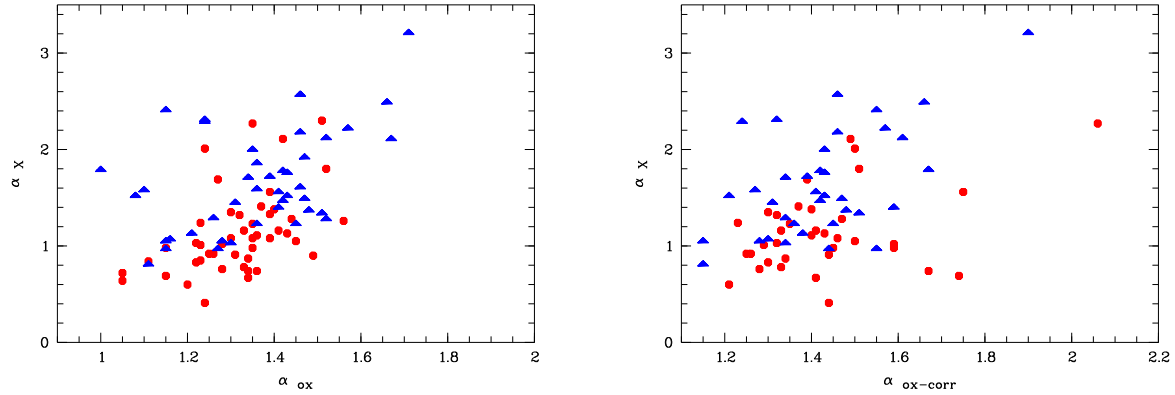


Fig. 11.— Optical-to-X-ray spectral slope  $\alpha_{ox}$  vs. X-ray spectral slope  $\alpha_X$ . The left panel displays  $\alpha_{ox}$  only corrected for Galactic reddening and the right panel corrected for intrinsic and galactic reddening, NLS1s are displayed as blue triangles and BLS1s as red circles.

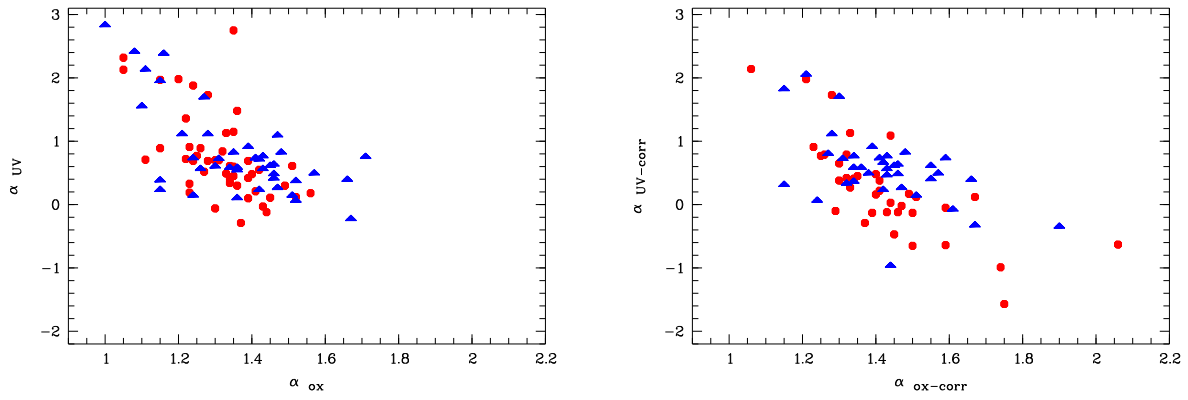


Fig. 12.— Optical-to-X-ray spectral slope  $\alpha_{\text{ox}}$  vs. UV/optical spectral slope  $\alpha_{\text{UV}}$ . The left panel displays the spectral slopes only corrected for Galactic reddening and the right panel corrected for intrinsic and Galactic reddening, NLS1s are displayed as blue triangles and BLS1s as red circles.

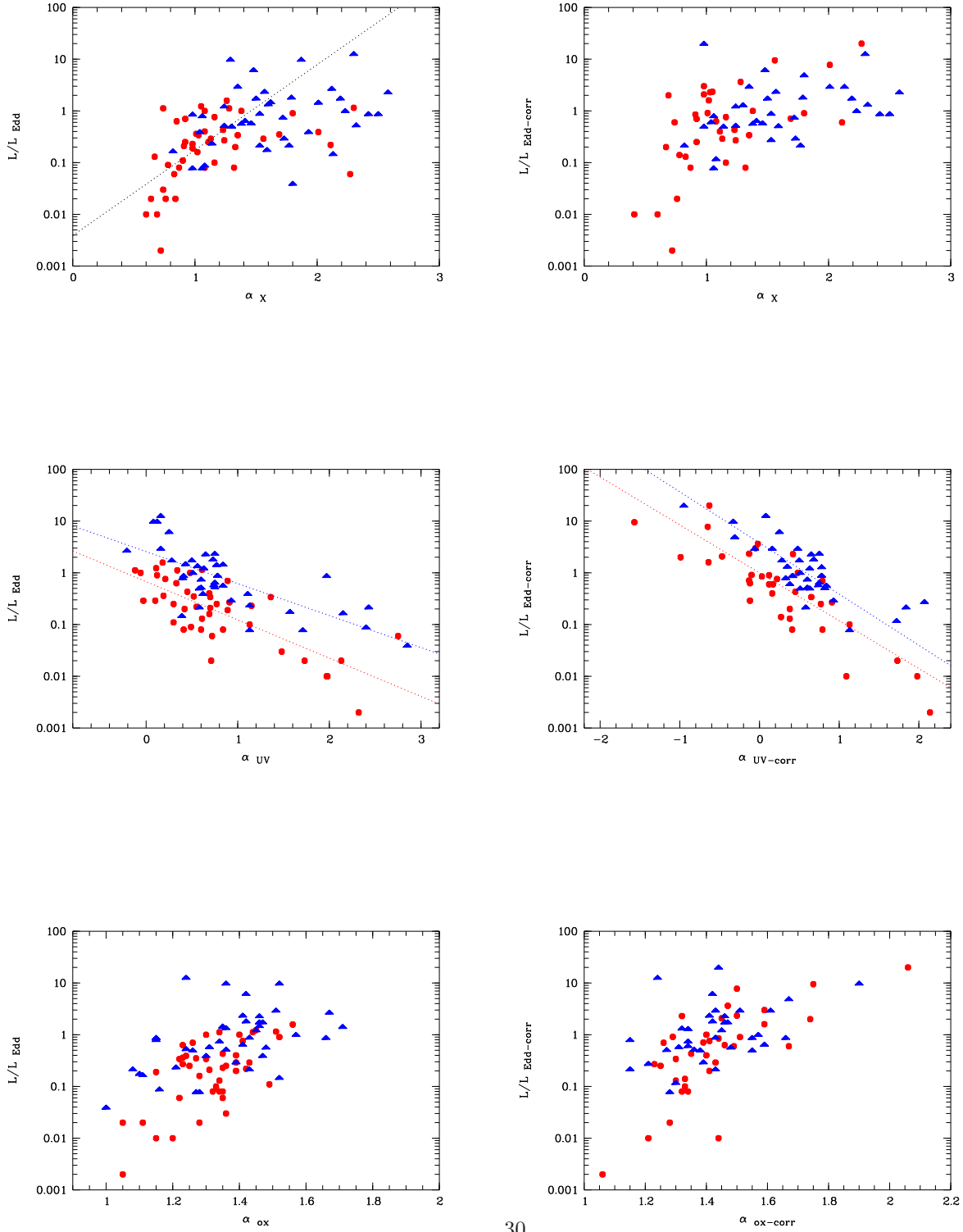


Fig. 13.— 0.2-2.0 keV X-ray energy spectral slope  $\alpha_X$ , optical/UV spectral slope  $\alpha_{\text{UV}}$ , and optical-to-X-ray spectral slope  $\alpha_{\text{ox}}$  vs. the Eddington ratio  $L/L_{\text{Edd}}$ .

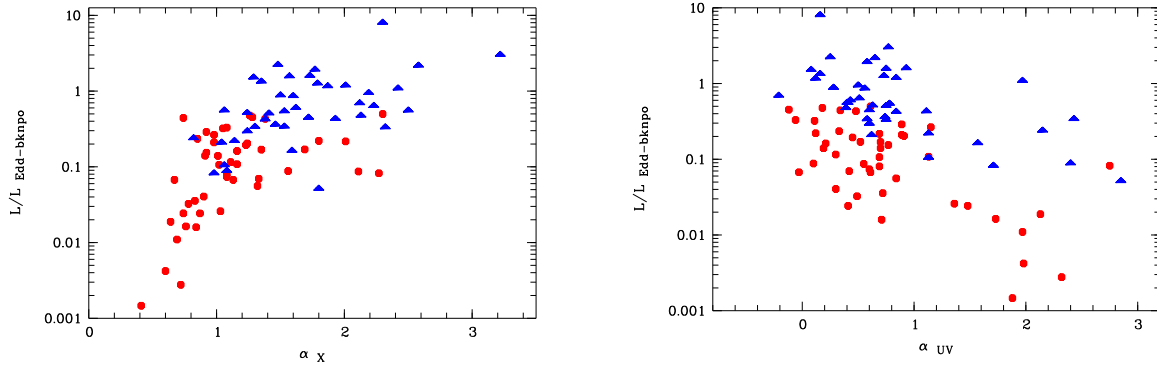


Fig. 14.— 0.2-2.0 keV X-ray energy spectral slope  $\alpha_X$  and optical/UV spectral slope  $\alpha_{UV}$  vs. the Eddington ratio  $L/L_{\text{Edd-bknp0}}$  using the double broken power law mode to fit the SED.

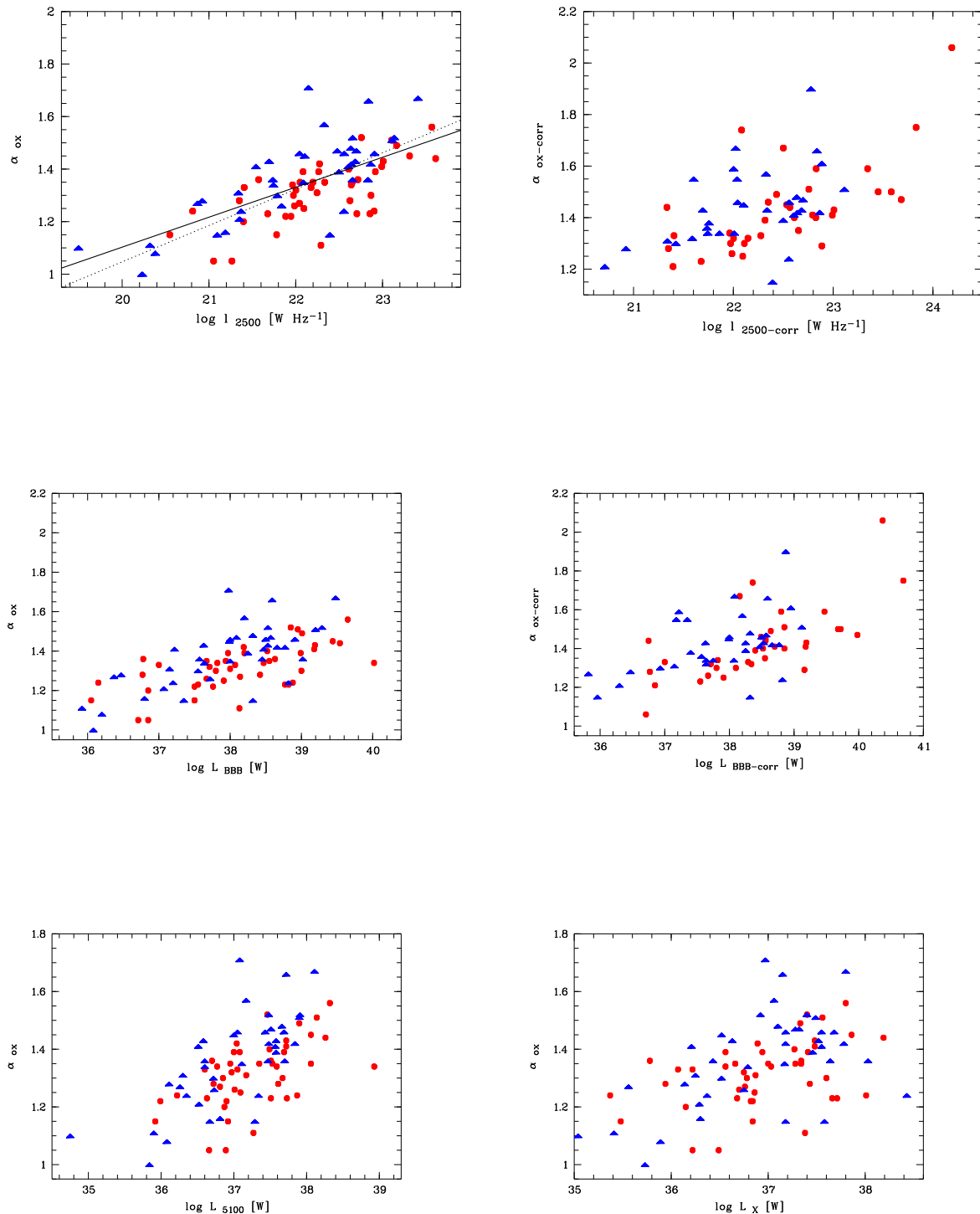


Fig. 15.— Optical-to-X-ray spectral slope  $\alpha_{\text{ox}}$  vs. luminosity density at  $2500\text{\AA}$   $l_{2500}$ , the BBB luminosity  $L_{\text{BBB}}$ , luminosity at  $5100\text{\AA}$   $L_{5100\text{\AA}}$ , and rest-frame 0.2-2.0 keV X-ray luminosity  $L_X$ . The solid line in the  $\alpha_{\text{ox}}\text{-}\log l_{2500\text{\AA}}$  plot displays the relation between  $\alpha_{\text{ox}}$  and the luminosity density at  $2500\text{\AA}$  as given in equation (1). The dashed line displays the same relation reported by Strateva et al. (2005)



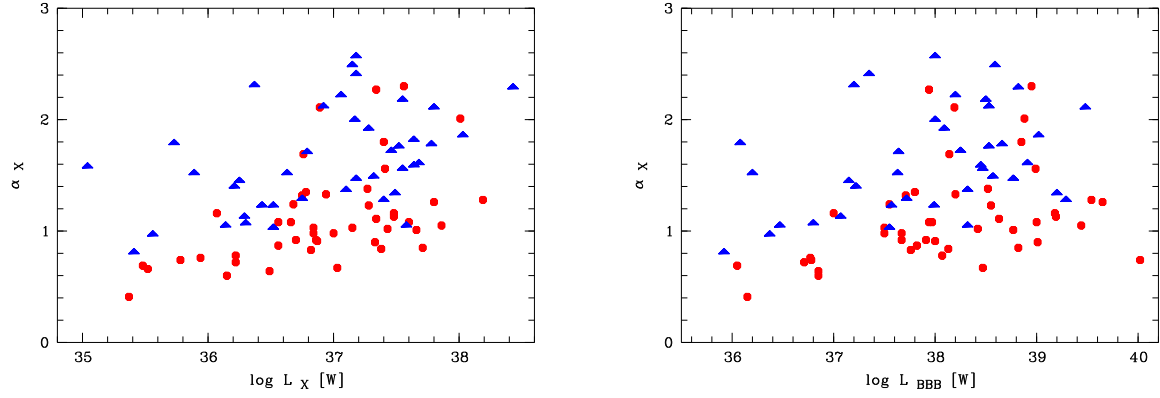


Fig. 16.— X-ray spectral slope  $\alpha_X$  vs. luminosities in the rest-frame 0.2-2.0 keV band and the BBB.

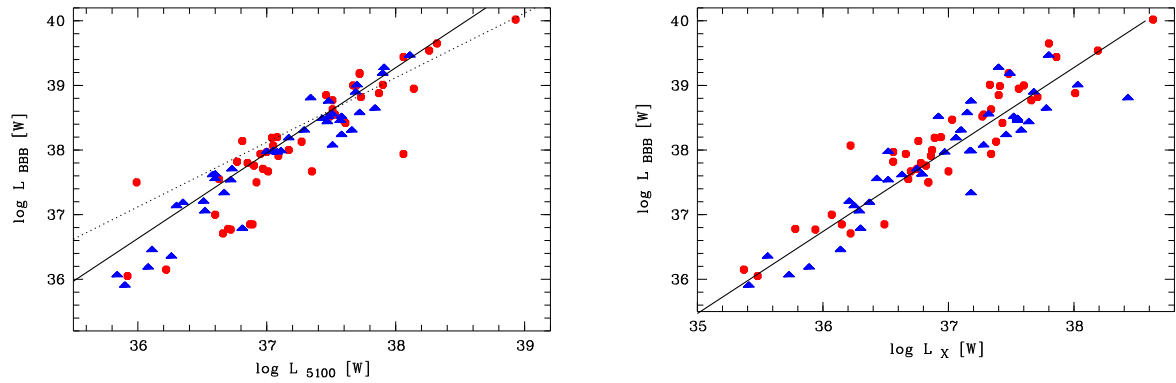


Fig. 17.— Luminosity at  $5100\text{\AA}$  and in the 0.2-2.0 keV band vs. the luminosity in the Big-Blue-Bump. The solid and dashed lines in the left panel display our relation given in equation (12) and that given by Elvis et al. (1994). The solid line in the right panel display equation (13).

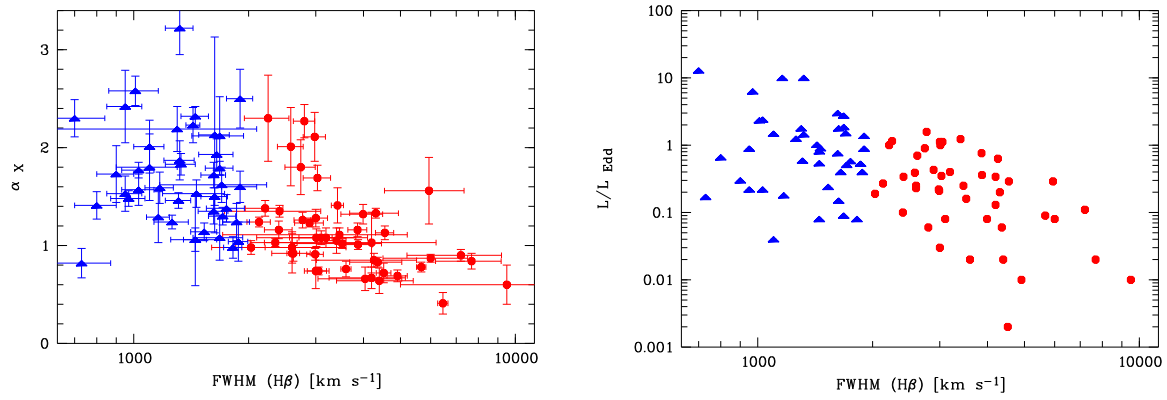


Fig. 18.— FWHM(H $\beta$ ) vs. 0.2-2.0 keV X-ray energy spectral slope  $\alpha_X$  (left) and  $L/L_{\text{Edd}}$  (right).

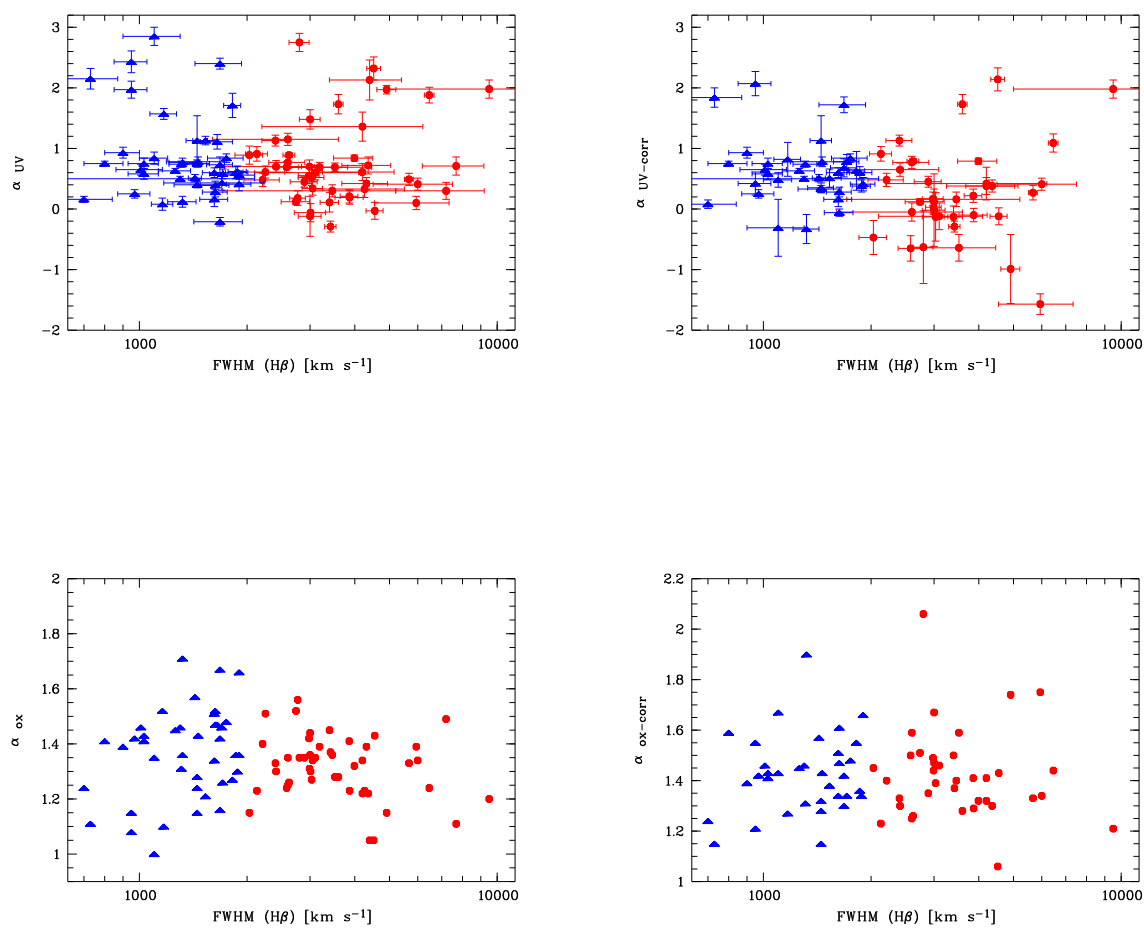


Fig. 19.— FWHM(H $\beta$ ) vs. optical/UV spectral slope  $\alpha_{UV}$  and the optical-to-X-ray spectral slope  $\alpha_{ox}$ , both uncorrected and corrected for intrinsic reddening.

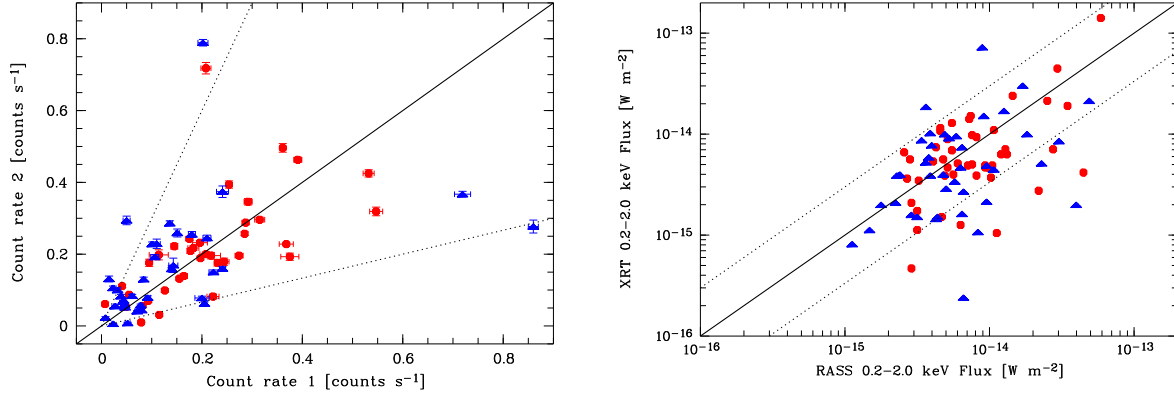


Fig. 20.— Short and long term X-ray flux variability in the soft X-ray selected AGN sample observed by *Swift*. The left panel shows the count rate variability of two *Swift* observations of the same AGN, the right panel the rest frame 0.2-2.0 keV fluxes of the *Swift* XRT and ROSAT All-Sky Survey observations.

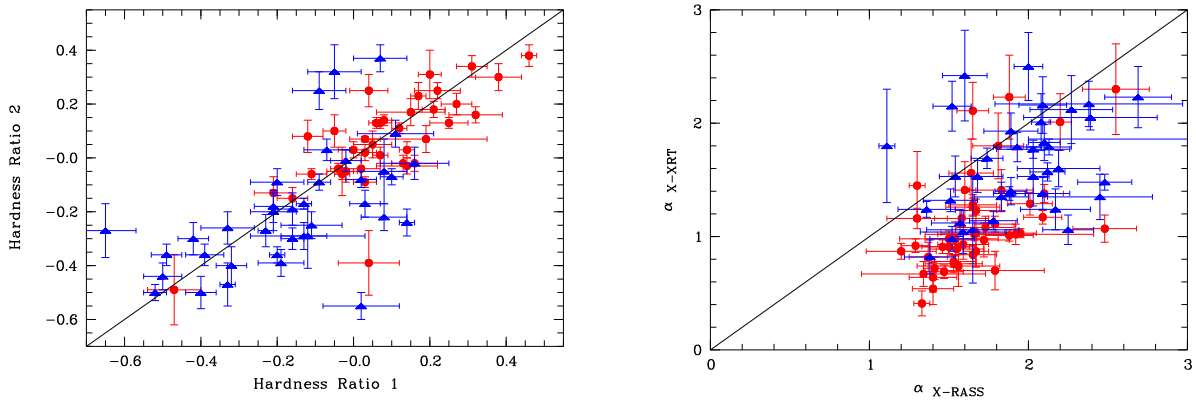


Fig. 21.— Short and long term X-ray spectral variability in the soft X-ray selected AGN sample observed by *Swift*. The left panel shows the Hardness ratio variability of two *Swift* observations of the same AGN, the right panel the X-ray spectral slopes  $\alpha_X$  the *Swift* XRT and ROSAT All-Sky Survey observations.

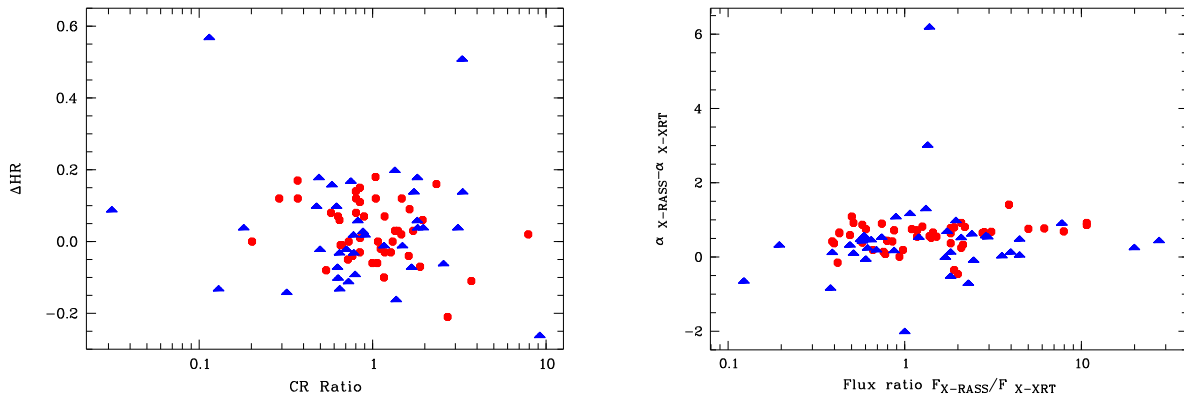


Fig. 22.— Short term and long term X-ray variabilities. The left panel displays the Count rate ratio vs. the difference in the hardness ratios in the *Swift* data, and the right panel shows the flux ratio between the RASS and the *Swift* observations vs. the differences in the X-ray spectral slopes  $\alpha_X$ .

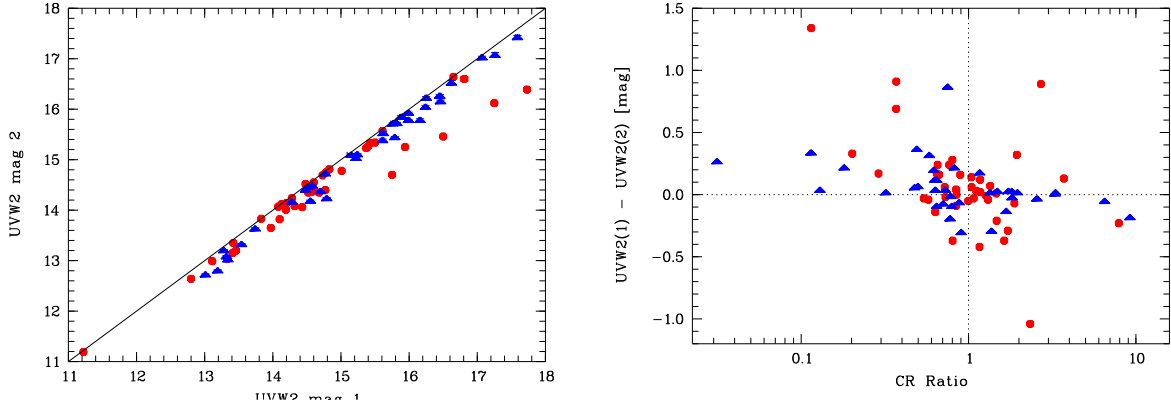


Fig. 23.— UVOT W2 variability. The left panel displays the UVW2 magnitudes of the observations with the largest differences and the right panel shows the difference between the X-ray flux ratio and the difference between the UVW2 magnitudes simultaneously taken with the X-ray data.

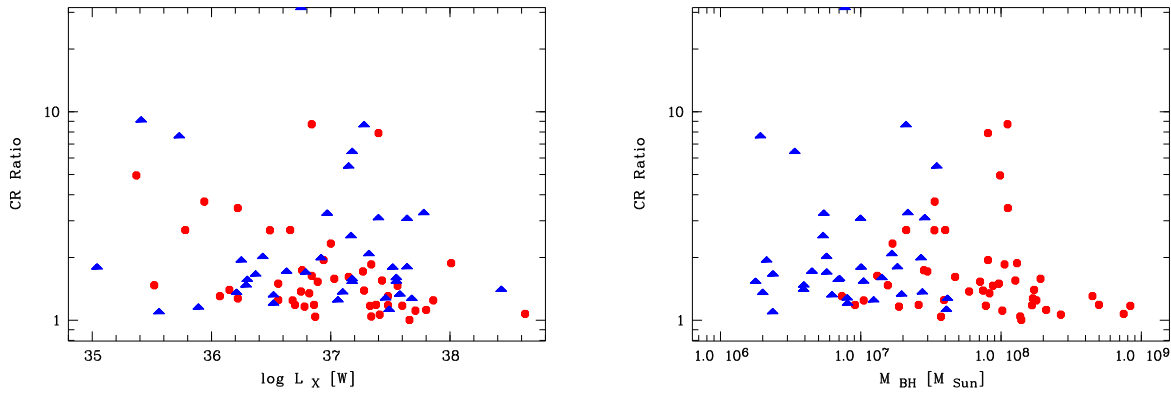


Fig. 24.— Ratio of the *Swift*-XRT count rates of two epochs vs. 0.2-2.0 keV X-ray luminosity  $L_X$  (left panel) and the mass of the central black hole (right panel).



TABLE 1—*Continued*

#	Object	$\alpha_{2000}$	$\delta_{2000}$	z	$N_{\text{H,gal}}^1$	$\alpha_{\text{X}}^2$	$\log F_{\text{X}}^3$	$E_{\text{B-V}}^4$	FWHM(H $\beta$ ) <sup>5</sup>	$M_{\text{BH}}^6$	H $\alpha$ /H $\beta$	$E_{\text{B-V}}^{\text{intr}}^7$
87	RX J2317.8-4422	23 17 49.9	-44 22 28	0.132	1.89	$2.87 \pm 0.44$	-14.41	0.010	1010	3.4	2.88	0.000
88	RX J2325.2-3236	23 25 11.9	-32 36 35	0.216	1.33	$1.92 \pm 0.49$	-14.57	0.014	3010	77.8	...	...
89	IRAS23226-3843	23 25 24.2	-38 26 49	0.036	1.59	$1.20 \pm 0.22$	-13.98	0.025	9500	170.0	3.00	0.000
90	MS 23409-1511	23 43 28.6	-14 55 30	0.137	2.20	$2.03 \pm 0.23$	-14.23	0.030	1030	10.0	3.05	0.000
91	RX J2349.4-3126	23 49 24.1	-31 26 03	0.135	1.23	$1.67 \pm 0.22$	-14.50	0.016	4200	111.2	3.71	0.181
92	AM 2354-304	23 57 28.0	-30 27 40	0.033	1.37	$1.30 \pm 0.19$	-14.39	0.017	2400	7.3	2.43	0.000

<sup>1</sup>Galactic column density from Dickey & Lockman (1990) in units of  $10^{20} \text{ cm}^{-2}$ .

<sup>2</sup>X-ray energy spectral  $\alpha_{\text{X}}$  in the 0.2-2.0 keV band during the RASS as given in Grupe et al. (2001a).

<sup>3</sup>Rest frame 0.2-2.0 keV X-ray flux during the RASS as given in Grupe et al. (2001a) in units of  $\text{W m}^{-2}$ .

<sup>4</sup>Galactic reddening  $E_{\text{B-V}}$  from Schlegel et al. (1998).

<sup>5</sup>FWHM(H $\beta$ ) is given in units of  $\text{km s}^{-1}$  and the values were taken from Grupe et al. (2004a). We separated NLS1s and BLS1s by the common criterion of 2000  $\text{km s}^{-1}$ .

<sup>6</sup>Black hole mass  $M_{\text{BH}}$  in units of  $10^6 M_{\odot}$  determined by the method described in Kaspi et al. (2000) using FWHM(H $\beta$ ) and  $L_{5100\text{\AA}}$  as given in Grupe et al. (2004a).

<sup>7</sup>Intrinsic reddening  $E_{\text{B-V}} - \text{intr}$  derived from the Balmer decrement.

<sup>8</sup>Taken from Lira et al. (1999).



TABLE 2  
OBSERVATION SUMMARY OF THE *Swift*-XRT AND UVOT OBSERVATIONS.

#	Object	Target ID	segment	T <sub>start</sub>	T <sub>stop</sub>	T <sub>XRT</sub> <sup>1</sup>	T <sub>V</sub> <sup>1</sup>	T <sub>B</sub> <sup>1</sup>	T <sub>U</sub> <sup>1</sup>	T <sub>W1</sub> <sup>1</sup>	T <sub>M2</sub> <sup>1</sup>	T <sub>W2</sub> <sup>1</sup>
1	Mkn 335 <sup>2</sup>	90006	003	2008-06-15 00:48	2008-06-15 02:45	2323	200	200	200	401	447	803
2	ESO 242-G008	35756	001	2006-08-16 14:13	2006-08-16 20:52	3886	324	324	324	644	821	1293
			002	2006-08-17 00:03	2006-08-17 16:13	4375	470	470	470	939	1266	1881
			003	2006-11-05 09:47	2006-11-05 18:16	7703	632	632	632	1264	1776	2536
3	Ton S 180	35757	001	2006-09-12 02:33	2006-09-12 13:51	862	92	92	92	185	38	372
			003	2007-05-16 02:15	2007-05-16 16:54	4994	506	506	506	1020	1370	2035
			004	2007-09-27 00:54	2007-09-27 04:20	2248	...	...	...	...	...	...
			005	2007-12-30 21:22	2007-12-31 23:16	10953	900	900	900	1787	2346	3585
4	QSO 0056-36	35301	001	2006-01-06 00:56	2006-01-06 18:48	5282	985	...	...	...	87	4506
			002	2006-05-18 21:00	2006-05-18 23:03	2977	252	253	253	507	728	1030
			003	2006-05-23 04:13	2006-05-23 23:35	7691	643	643	643	1291	1383	2632
			004	2007-09-27 05:46	2007-09-27 09:10	1895	...	...	...	3637	...	...
5	RX J0100.4-5113	36525	001	2007-12-20 01:07	2007-12-20 23:47	4438	360	360	360	723	928	1455
			002	2008-09-13 00:11	2008-09-13 06:47	3938	283	353	353	708	703	1390
			003	2008-11-06 00:29	2008-11-06 21:22	2974	255	255	255	511	537	1023
			004	2008-11-23 16:31	2008-11-24 18:17	7805	458	802	802	1608	1281	2400
6	RX J0105.6-1416	36526	001	2008-01-10 11:19	2008-01-10 22:44	5437	445	445	445	891	1191	1788
			002	2008-05-13 17:17	2008-05-13 23:52	2507	220	220	220	442	280	885
			003	2008-06-16 01:21	2008-06-16 17:38	4754	383	383	383	768	1103	1538
			004	2008-06-26 05:33	2008-06-26 17:00	3718	306	306	306	613	802	1227
7	RX J0117.5-3826	56500	002	2005-05-20 10:48	2005-05-20 12:55	3541	...	...	...	3637	...	...
			004	2005-09-30 07:53	2005-09-30 11:32	3352	...	...	...	3236	...	...
			006	2005-10-14 14:21	2005-10-14 17:53	3426	...	...	...	3445	...	...
		37554	001	2008-06-29 00:55	2008-06-30 07:44	4025	332	332	332	666	825	1333
			002	2009-04-28 01:22	2009-04-28 24:00	3414	309	309	309	620	619	1242
			003	2009-11-10 00:15	2009-11-10 23:07	6678	531	577	620	1279	943	2131
8	MS 0117-28	35758	002	2006-11-04 06:34	2006-11-06 08:43	16192	1333	1333	1333	2666	3730	5343
9	RX J0128.1-1848	36527	001	2007-06-24 06:15	2007-06-24 19:21	2402	203	203	203	421	602	842
			002	2008-02-05 00:55	2008-02-05 23:44	5898	345	573	573	1241	927	2038
			003	2008-02-06 09:05	2008-02-06 12:34	2243	...	344	345	690	...	763
			004	2008-02-07 01:09	2008-02-07 24:00	9883	795	951	951	1905	1176	3729
10	RX J0134.2-4258	36528	001	2007-11-29 07:06	2007-11-29 16:50	2278	160	160	160	323	383	650
11	RX J0136.9-3510	35507	001	2006-01-31 00:11	2006-02-01 22:55	6385	527	283	527	1065	1577	2149
12	RX J0148.3-2758	35075 <sup>3</sup> 35759	001	2006-09-04 19:39	2006-09-05 03:34	999	82	117	199	520	216	331
			002	2006-10-29 01:11	2006-10-29 12:29	953	...	12	12	1112	...	16
			004	2007-05-12 03:28	2007-05-12 06:48	1945	150	150	150	301	411	644
			005	2007-11-25 13:10	2007-11-25 16:43	1448	118	118	118	235	293	474
			006	2008-05-07 02:19	2008-05-07 08:50	362	...	41	41	156	...	100
			007	2008-06-16 19:01	2008-06-16 24:00	4137	342	342	342	684	915	1369
			008	2008-06-27 00:54	2008-06-27 10:48	4561	381	381	381	764	925	1530
13	RX J0152.4-2319	36529	001	2008-01-02 10:30	2008-01-02 23:30	3379	273	273	273	550	619	1103
			002	2008-02-12 19:24	2008-02-12 22:49	1660	138	138	138	277	320	554
			003	2008-02-18 05:29	2008-02-18 23:34	12845	1074	1074	1074	2150	2822	4301
14	Mkn 1044	35760	001	2007-07-25 04:42	2007-07-25 22:32	3069	240	276	276	548	505	978
			002	2007-08-01 00:25	2007-08-01 23:14	7624	636	636	636	1270	1734	2546
			003	2008-03-02 06:55	2008-03-02 15:11	5467	453	453	453	908	1168	1818
15	Mkn 1048	36530	001	2007-07-23 15:44	2007-07-23 22:17	2083	28	284	284	568	...	808
			002	2007-07-29 00:16	2007-07-29 00:26	604	53	53	53	107	94	214
			003	2007-12-17 13:45	2007-12-17 23:36	2918	239	239	239	480	624	964
			004	2008-03-04 05:32	2008-03-04 12:08	2075	215	215	215	432	305	865
			005	2008-06-06 14:43	2008-06-07 23:25	9540	788	788	788	1579	2101	3159
16	RX J0311.3-2046	37555	001	2009-03-26 07:40	2009-03-26 23:51	8417	682	682	682	1366	1887	2734
			002	2009-05-31 04:18	2009-05-31 23:59	7294	601	601	601	1203	1668	2408
17	RX J0319.8-2627	35761	001	2007-03-07 01:29	2007-03-07 24:00	4543	218	218	218	437	430	870
			002	2007-03-10 00:07	2007-03-10 11:27	5786	487	487	487	975	1278	1949
			003	2007-03-15 00:39	2007-03-15 23:33	1888	357	372	372	759	444	1503
			004	2007-03-16 00:49	2007-03-16 04:18	3172	260	260	260	524	723	1049
		36531	001	2008-03-21 00:38	2008-03-22 12:13	9252	743	743	743	1516	1998	3035
			002	2008-04-03 11:38	2008-04-03 13:29	1768	151	151	151	303	304	606
			003	2008-11-28 02:37	2008-11-28 10:57	2259	132	131	136	898	386	527
			004	2009-03-20 21:34	2009-03-21 23:44	14810	1233	1233	1230	2467	3350	4942
18	RX J0323.2-4931	36532	001	2007-12-07 01:30	2007-12-08 16:22	7245	617	619	619	1235	1688	2475
			002	2007-12-15 00:53	2007-12-15 15:23	8832	727	727	727	1452	1950	2911
19	ESO 301-G13	37349	001	2008-10-29 06:29	2008-10-29 16:23	7302	...	...	6221	...	...	...
			002	2008-11-09 01:14	2008-11-10 03:15	10748	789	874	874	1752	2465	3484
		37556	001	2008-12-10 08:59	2008-12-10 20:17	5556	442	442	442	886	1314	1774
			002	2009-10-18 03:32	2009-10-18 16:27	1191	88	88	87	176	275	353
			003	2009-12-29 14:40	2009-12-29 23:10	8782	698	698	813	1676	1868	2794
20	VCV 0331-37	37557	001	2008-07-03 14:09	2008-07-03 19:00	1921	143	193	194	389	298	581
			002	2008-07-04 15:50	2008-07-04 15:57	422	36	36	36	72	69	145
			003	2008-10-26 09:28	2008-10-27 19:23	9967	494	994	994	1990	1357	3477
			004	2009-02-23 02:34	2009-03-23 23:42	8688	700	733	733	1468	1763	2938
			005	2009-03-25 00:58	2009-03-25 14:17	11980	1098	1094	1098	2199	1763	4398
21	RX J0349.1-4711	35762	001	2006-08-26 10:33	2006-08-28 12:34	7829	653	653	654	1308	1524	2614
			002	2007-03-13 21:21	2007-03-13 23:07	1174	97	97	97	194	243	390
			003	2007-03-26 17:54	2007-03-26 23:00	5935	494	494	494	987	1381	1979
22	Fairall 1116	35303	001	2006-01-13 03:11	2006-01-13 14:28	462	...	...	...	...	...	208
			002	2006-01-17 00:17	2006-01-17 02:14	1216	80	58	80	159	243	588
			003	2006-04-08 01:00	2006-04-09 02:51	9784	525	525	525	1045	1334	2132
			004	2006-05-02 03:34	2006-05-02 22:53	2055	161	167	210	416	340	654
			005	2007-09-26 01:11	2007-09-26 03:05	1927	...	...	...	...	...	...
23	Fairall 1119	37558	001	2008-10-12 00:17	2008-10-13 16:30	4746	189	471	657	1464	563	1054
			002	2008-10-26 01:27	2008-10-26 08:04	4327	307	383	383	766	870	1466
24	RX J0412.7-4712	36534	001	2007-12-25 00:29	2007-12-25 15:21	12199	1002	1002	1002	1996	2789	4004
			002	2008-01-01 23:57	2008-01-02 12:59	4222	297	350	450	979	822	1199



TABLE 2—Continued

#	Object	Target ID	segment	$T_{\text{start}}$	$T_{\text{stop}}$	$T_{\text{XRT}}^1$	$T_{\text{V}}^1$	$T_{\text{B}}^1$	$T_{\text{U}}^1$	$T_{\text{W1}}^1$	$T_{\text{M2}}^1$	$T_{\text{W2}}^1$	
58	RX J1355.2+5612	36547	001	2007-05-13 00:46	2007-05-13 21:49	4404	357	357	357	725	943	1451	
			002	2007-05-21 20:53	2007-05-21 22:36	967	...	155	155	311	...	308	
			003	2007-06-21 00:05	2007-06-21 19:35	3380	296	296	296	591	775	1185	
			004	2007-06-26 16:32	2007-06-26 23:09	3972	324	324	324	648	875	1301	
			005	2007-06-28 00:44	2007-06-28 23:27	1069	64	64	65	402	171	256	
59	PG 1402+261	35077	001	2006-07-07 02:59	2006-07-07 09:41	4063	309	309	314	644	898	1338	
			002	2006-08-01 04:08	2006-08-01 12:16	2060	199	200	200	397	431	796	
			003	2006-08-13 19:42	2006-08-13 23:12	2792	195	282	282	562	533	846	
60	RX J1413.6+7029	37573	001	2008-05-14 13:04	2008-05-14 23:03	8336	672	672	672	1345	2041	2691	
			002	2009-03-15 01:06	2009-03-16 06:14	12163	1034	1034	1034	2070	2314	4146	
61	NGC 5548 <sup>9</sup>	30022	059	2007-06-19 07:49	2007-06-19 09:52	2276	186	187	187	373	478	748	
62	Mkn 813	56600	002	2005-05-20 12:14	2005-05-20 13:57	704	...	...	...	722	...	...	
			001	2006-04-14 05:26	2006-04-14 07:06	320	127	45	128	...	...	...	...
			002	2007-01-06 00:59	2007-01-06 03:03	3356	1099	1071	1099	...	...	...	...
			003	2007-01-10 00:02	2007-01-10 13:05	6433	556	556	556	1105	1460	2220	
63	Mkn 684	35078	001	2005-07-14 09:48	2005-07-14 15:02	4740	7	7	7	7	7	7	
			006	2005-09-15 00:39	2005-09-15 10:55	12856	7	7	7	7	7	7	7
			007	2005-09-18 06:13	2005-09-19 20:52	...	...	...	2148	2735	2768	...	...
			008	2006-05-24 06:46	2006-05-24 18:04	1364	110	110	110	221	218	457	
			009	2006-05-25 06:39	2006-05-25 16:33	6538	516	510	524	1049	1461	2158	
			001	2006-08-29 13:30	2006-08-29 22:56	2644	211	211	211	439	554	843	
			002	2006-10-08 16:01	2006-10-09 06:47	4148	369	369	369	741	812	865	
			003	2007-09-26 21:16	2007-09-26 23:06	1517	...	...	...	...	...	...	
65	PG 1448+273	35079	001	2005-09-13 00:54	2005-09-13 23:30	9405	7	7	7	7	7	7	
			003	2007-09-26 14:51	2007-09-26 16:29	866	...	...	...	...	...	...	...
66	Mkn 841	35468 36388	002	2007-01-01 00:40	2007-01-01 23:38	10240	828	828	828	1664	2221	3331	
			001	2007-02-02 00:40	2007-02-02 13:42	5035	419	419	419	841	1066	1680	
			002	2007-02-03 00:51	2007-02-02 17:08	4907	403	403	403	814	1053	1630	
			003	2008-06-04 07:12	2008-06-04 07:28	957	90	90	90	181	68	362	
			001	2005-11-05 00:05	2005-11-06 01:33	6950	656	438	536	1072	1646	2889	
			002	2005-11-08 03:36	2005-11-08 23:13	6490	545	387	545	1088	1634	2165	
			003	2007-09-26 11:38	2007-09-26 13:30	1911	...	...	...	...	...	...	...
			004	2007-10-09 00:01	2007-10-09 22:26	6640	...	...	...	...	...	...	
			005	2007-10-10 00:01	2007-10-10 22:28	6513	...	...	...	...	...	...	
			006	2007-10-11 22:52	2007-10-11 22:52	10555	...	...	...	...	...	...	
			008	2008-06-05 04:34	2008-06-05 18:52	2053	168	168	168	336	434	673	
68	Mkn 876	35308	001	2006-05-30 07:33	2006-05-30 23:52	8396	638	417	666	1337	2079	2770	
			002	2006-06-18 01:14	2006-06-20 24:00	4013	368	352	376	743	1061	1539	
			003	2007-09-25 00:13	2007-09-25 05:13	2207	...	...	...	...	...	...	...
			004	2007-10-02 17:04	2007-10-02 23:37	2582	...	...	...	...	...	...	...
			005	2007-10-04 04:18	2007-10-04 09:20	2876	...	...	...	...	...	...	...
			006	2007-10-04 10:37	2007-10-04 23:38	5904	...	...	...	...	...	...	...
			001	2008-05-24 09:33	2008-05-24 12:58	3379	220	325	325	651	610	1151	
			002	2009-01-05 02:42	2009-01-05 23:41	3360	191	307	652	1647	217	763	
			001	2008-01-10 20:39	2007-01-10 24:00	2332	190	190	190	381	515	763	
70	KUG 1618+410	36548	002	2008-01-14 11:16	2008-01-14 22:53	9951	942	942	942	1887	2651	3775	
			003	2009-12-29 04:28	2009-12-29 12:53	2423	...	...	...	...	2410	...	...
			001	2008-05-20 05:42	2008-05-20 10:54	5339	435	435	435	871	1264	1743	
71	PG 1626+554	37576	002	2008-05-21 20:18	2008-05-21 23:35	707	21	35	161	322	48	86	
			003	2008-06-01 04:21	2008-06-02 15:52	9697	743	743	743	1488	2019	2978	
			001	2007-06-26 00:34	2007-06-26 15:12	3032	247	247	247	488	578	986	
72	EXO 1627+40	36549	002	2008-01-08 01:05	2008-01-08 12:34	7629	629	629	629	1255	1683	2514	
			003	2008-01-11 19:11	2008-01-12 06:36	6458	552	553	552	1106	1494	2214	
			004	2008-04-05 01:54	2008-04-05 06:53	2018	149	169	169	340	213	680	
			007	2008-05-03 10:52	2008-05-03 11:10	1034	85	85	85	171	239	342	
73	RX J1702.5+3247	35771	001	2006-08-31 00:45	2006-08-31 23:31	1251	181	181	181	360	473	720	
			002	2006-10-11 00:19	2006-10-11 22:54	9125	754	755	755	1512	1891	3025	
			003	2007-01-19 01:03	2007-01-19 23:46	2914	238	238	238	479	643	960	
			004	2007-01-23 01:14	2007-01-23 16:06	6945	585	586	586	1170	1627	2343	
74	II Zw 136	37577	003	2008-07-18 10:18	2008-07-18 10:32	815	66	66	66	132	194	264	
			004	2008-07-19 10:31	2008-07-19 15:26	3463	351	352	352	704	1012	1409	
			005	2008-08-06 00:51	2008-08-06 05:52	2410	204	204	204	409	465	818	
			006	2008-11-20 01:58	2008-11-20 20:48	2120	182	182	182	393	132	789	
			001	2008-06-24 13:15	2008-06-24 16:31	400	...	...	...	13	231	238	
75	RX J2146.6-3051	37578	002	2008-06-27 00:40	2007-06-27 11:57	2692	...	...	...	801	1032	1032	
			003	2008-07-22 04:39	2008-07-22 12:47	1127	...	...	...	234	436	436	
			004	2008-10-01 17:50	2008-10-01 22:44	2158	...	...	...	705	704	704	
			005	2008-11-20 00:03	2008-11-20 22:37	10012	...	...	...	3080	3373	3373	
76	RX J2216.8-4451	35081 37579	001	2005-07-09 00:24	2005-07-10 21:31	18944	...	...	...	...	...	19529	
			001	2008-07-11 22:55	2008-07-12 19:58	6972	602	602	602	1206	1216	2415	
			002	2008-07-14 08:48	2008-07-14 18:34	3364	283	283	283	567	435	1136	
			003	2008-07-24 04:47	2008-07-24 09:48	2372	204	204	204	409	474	818	
			004	2008-07-26 00:09	2008-07-26 13:10	5577	468	468	468	934	1076	1880	
77	RX J2217.9-5941	35772	001	2006-11-01 17:27	2006-11-01 23:52	2657	215	215	215	437	559	871	
			002	2006-11-02 17:34	2006-11-03 11:11	8970	744	744	744	1485	1996	2981	
			003	2007-04-30 00:21	2007-04-30 04:00	4370	359	359	359	719	1021	1439	
			008	2007-09-12 00:41	2007-09-12 23:14	7230	...	...	...	...	...	...	...
			009	2007-09-13 01:05	2007-09-13 23:40	5631	...	...	...	...	...	...	...
			010	2007-09-14 01:07	2007-09-14 23:45	5631	...	...	...	...	...	...	
78	RX J2242.6-3845	37580	001	2008-07-18 12:06	2008-07-19 07:49	4654	609	625	625	1251	1477	2505	
			002	2008-07-21 17:16	2008-07-21 24:00	4063	347	347	347	694	832	1388	
			003	2008-07-25 03:13	2008-07-25 08:12	2739	233	233	233	468	528	936	
79	RX J2245.3-4652	35309	001	2006-04-14 16:06	2006-04-14 16:12	327	...	22	97	195	...	...	
			002	2006-04-21 21:47	2006-04-21 23:28	562	...	48	158	342	...	...	...
			003	2006-06-11 23:46	2006-06-12 24:00	8905	658	670	696	1402	1948	2959	
			004	2006-06-15 16:11	2006-06-15 22:45	2233	165	160	161	346	447	737	

TABLE 2—*Continued*

#	Object	Target ID	segment	$T_{\text{start}}$	$T_{\text{stop}}$	$T_{\text{XRT}}^1$	$T_{\text{V}}^1$	$T_{\text{B}}^1$	$T_{\text{U}}^1$	$T_{\text{W1}}^1$	$T_{\text{M2}}^1$	$T_{\text{W2}}^1$	
80	RX J2248.6–5109	35773	001	2006-09-21 00:20	2006-09-22 23:22	9759	11	11	11	11	11	11	
			002	2006-11-01 07:37	2006-11-01 16:01	5769	11	11	11	11	11	11	11
			004	2007-09-15 09:23	2007-09-17 22:41	22550	...	...	...	...	...	...	...
			005	2007-09-26 00:57	2007-09-26 04:12	1918	...	...	...	...	...	...	...
81	MS 2254-36	36551	001	2007-06-23 17:27	2007-06-23 23:54	3169	207	278	300	655	563	1037	
			002	2007-08-04 05:09	2007-08-04 22:52	6480	523	523	523	1059	1365	2127	
			004	2007-12-07 01:20	2007-12-08 00:03	5634	514	514	514	1029	1325	2056	
			005	2007-12-11 04:55	2007-12-11 10:08	6112	505	505	505	1011	1407	2019	
82	RX J2258.7–2609	37581	001	2008-07-24 00:03	2008-07-24 03:18	1033	104	104	104	208	146	417	
			002	2008-08-02 13:42	2008-08-02 23:42	7218	608	607	608	1217	1349	2435	
			003	2008-09-16 19:45	2008-09-16 19:58	709	61	61	61	122	134	244	
			004	2008-11-23 00:19	2008-11-24 23:04	18563	1519	1519	1519	3044	3926	6096	
83	RX J2301.6–5913	37582	001	2008-07-26 06:20	2008-07-26 08:09	1597	131	131	131	263	358	527	
			002	2008-08-03 00:59	2008-08-03 09:15	6167	562	562	562	1125	900	2251	
			004	2009-07-20 13:38	2009-07-20 17:07	3839	320	320	320	641	845	1283	
			005	2009-09-24 13:39	2009-09-24 23:34	7252	588	588	588	1178	1700	2357	
84	RX J2301.8–5508	35082	001	2005-11-26 07:49	2005-11-26 22:28	3704	315	209	315	631	965	1287	
			002	2005-12-08 00:31	2005-12-08 10:25	5756	497	248	495	935	1522	2033	
85	RX J2304.6–3501	36087	001	2006-09-19 00:05	2006-09-19 00:19	821	...	...	93	188	281	349	
86	RX J2312.5–3404	36552	001	2007-08-08 00:36	2007-08-08 21:45	11630	1031	1119	1119	2240	2637	4403	
			002	2007-12-23 09:19	2007-12-24 00:02	7885	560	561	561	1125	1454	2257	
87	RX J2317.8–4422	56630	003	2005-05-26 08:08	2005-05-26 10:09	3604	...	...	...	2445	...	...	
			001	2006-04-18 00:18	2006-04-18 23:02	7072	677	677	673	1343	1746	2745	
88	RX J2325.2–3236	35774	002	2006-04-20 05:18	2006-04-20 23:04	3212	264	264	264	529	717	1075	
			001	2006-09-23 00:53	2006-09-25 05:51	5555	260	846	846	1736	127	2490	
			002	2006-11-06 14:53	2006-11-06 23:09	7999	657	657	657	1320	1852	2640	
			003	2008-08-29 00:21	2008-08-30 22:59	4108	311	319	319	641	634	1285	
89	IRAS 23226–3643	36642	001	2007-06-15 00:06	2007-06-15 08:21	5037	...	...	...	...	4970	...	
			002	2007-07-31 01:46	2007-07-31 21:19	6213	...	...	...	6129	...	...	
			001	2008-07-29 05:34	2008-07-29 08:54	1095	104	104	104	208	114	417	
			002	2009-09-18 00:03	2009-09-18 22:35	17423	...	...	...	...	...	...	
90	MS 23409–1511	36554	001	2007-11-25 19:28	2007-11-26 22:56	2997	242	242	242	484	603	978	
			002	2008-01-16 02:10	2008-01-16 23:19	7843	678	678	678	1358	1366	2714	
			003	2008-01-19 13:44	2008-01-19 23:40	4657	401	401	401	804	966	1609	
			004	2008-01-20 09:04	2008-01-21 09:22	5383	486	520	520	1041	878	2023	
91	RX J2349.4–3126	35775	005	2008-06-04 12:52	2008-06-04 14:40	1608	132	132	132	263	356	527	
			001	2006-09-19 06:29	2006-09-19 21:09	2429	135	322	495	1025	382	1022	
			003	2007-05-11 17:47	2007-05-12 02:00	3746	311	311	311	617	805	1335	
			006	2008-11-22 13:06	2008-11-22 22:57	4162	332	332	332	666	969	1333	
92	AM 2354-304	37584	007	2009-09-24 00:54	2009-09-24 24:00	6338	515	515	514	1031	1403	2065	
			001	2009-01-18 23:25	2009-01-19 23:38	6050	494	494	494	990	1231	1985	
			003	2009-06-12 00:29	2009-06-13 12:01	10630	916	916	916	1835	2294	3671	

<sup>1</sup>XRT and UVOT exposure times are given in s.

<sup>2</sup>*Swift* observed Mkn 335 several times as a monitoring project Grupe et al. (2007b); Grupe et al. (2008a). Here we used one of the observations during the more typical high-state.

<sup>3</sup>The Narrow Line Seyfert 1 galaxy RX J0148.3–2758 has been observed by *Swift* multiple times and the results of the observations obtained in 2005 have already been published in (Grupe et al. 2006a). Therefore here we only list the new, previously unpublished observations.

<sup>4</sup>PG 1211+143 was monitored by *Swift* for more than a month (Bachev et al. 2009). Here we picked only one of the observations during high state

<sup>5</sup>Mkn 766 has been observed through a monitoring campaign by *Swift*(Grupe et al. in prep). Here we only present the first segment of data as a representative observation.

<sup>6</sup>3C 273 has been observed by *Swift* many times as a calibration target as well as a science target. Here we only picked two recent observations in 2009 which were observed in 5 UVOT filters in the  $5' \times 5'$  UVOT hardware window.

<sup>7</sup>UVOT observations done with the grisms.

<sup>8</sup>MCG+08-23-067 was previously observed in 2005. However, these observations were all performed with the UV grism

<sup>9</sup>The data of NGC 5548 are from an observing campaign in 2007 with simultaneous observations with Suzaku (Krongold et al. 2010).

<sup>10</sup>Mkn 684 has been observed a few times before the listed observations. However, for these observation the UVOT was using the grisms.

<sup>11</sup>Due to a bright star  $3'$  away from the position of RX J2248.6–5109 UVOT could not observe the field in order to avoid damaging the instrument.

TABLE 3  
RESULTS OF THE *Swift*-UVOT PHOTOMETRY

#	Object	segment(s)	V <sup>1</sup>	B <sup>1</sup>	U <sup>1</sup>	UVW1 <sup>1</sup>	UVM2 <sup>1</sup>	UVW2 <sup>1</sup>
1	Mkn 335	003	14.20±0.01	14.45±0.01	13.27±0.01	13.11±0.01	12.97±0.01	13.01±0.01
2	ESO 242-G008	001+002	16.09±0.02	16.70±0.02	16.01±0.01	15.97±0.01	15.97±0.02	15.94±0.01
		003	15.93±0.02	16.44±0.02	15.54±0.01	15.42±0.01	15.32±0.01	15.25±0.01
3	Ton S 180	001	14.46±0.02	14.58±0.01	13.39±0.01	13.09±0.01	13.12±0.03	12.85±0.01
		003	14.56±0.01	14.70±0.01	13.49±0.01	13.22±0.01	13.01±0.01	13.02±0.01
		005	14.29±0.01	14.44±0.00	13.23±0.00	12.94±0.00	12.71±0.00	12.73±0.00
4	QSO 0056-36	001	15.76±0.01	...	...	...	14.26±0.04	14.10±0.01
		002	15.55±0.05	15.65±0.02	14.30±0.02	14.05±0.01	13.82±0.01	13.80±0.01
		003	15.59±0.02	15.64±0.01	14.30±0.01	14.06±0.01	13.87±0.01	13.82±0.01
5	RX J0100.4-5113	001	15.24±0.02	15.72±0.01	14.61±0.01	14.39±0.01	14.21±0.01	14.24±0.01
		002	15.23±0.02	15.70±0.01	14.62±0.01	14.41±0.01	14.26±0.01	14.28±0.01
		003	15.19±0.02	15.62±0.01	14.51±0.01	14.23±0.01	14.02±0.01	14.00±0.01
		004	15.16±0.01	15.60±0.01	14.44±0.01	14.17±0.01	13.96±0.01	13.92±0.01
6	RX J0105.6-1416	001	15.35±0.02	15.92±0.01	14.74±0.01	14.57±0.01	14.46±0.01	14.43±0.01
		002	15.29±0.02	15.73±0.02	14.48±0.01	14.29±0.01	14.15±0.02	14.08±0.01
		003	15.22±0.02	15.65±0.01	14.46±0.01	14.30±0.01	14.14±0.01	14.06±0.01
		004	15.27±0.02	15.78±0.01	14.55±0.01	14.37±0.01	14.27±0.01	14.21±0.01
7	RX J0117.5-3826	002	...	...	...	15.85±0.01	...	...
		004	...	...	...	15.93±0.01	...	...
		006	...	...	...	15.93±0.01	...	...
		001	16.90±0.05	17.17±0.03	16.15±0.02	16.15±0.02	15.97±0.03	16.05±0.02
		002	17.05±0.06	17.33±0.04	16.28±0.03	16.32±0.03	16.16±0.03	16.24±0.02
		003	17.24±0.04	17.43±0.02	16.37±0.02	16.36±0.02	16.21±0.03	16.22±0.01
8	MS 0117-28	002	16.20±0.02	16.29±0.01	15.19±0.01	14.96±0.01	14.66±0.01	14.69±0.01
9	RX J0128.1-1848	001	14.79±0.02	15.15±0.02	14.21±0.01	14.12±0.01	14.01±0.01	14.13±0.01
		002	14.78±0.01	15.21±0.01	14.25±0.01	14.26±0.01	14.19±0.01	14.24±0.01
		003	...	15.22±0.01	14.22±0.01	14.22±0.01	...	14.20±0.01
		004	14.79±0.01	15.23±0.01	14.23±0.01	14.23±0.01	14.16±0.01	14.18±0.01
10	RX J0134.2-4258	001	16.17±0.04	16.33±0.03	15.01±0.02	14.67±0.02	14.38±0.02	14.47±0.01
11	RX J0136.9-3510	001	17.41±0.06	17.47±0.04	16.31±0.02	16.11±0.02	16.11±0.02	16.17±0.01
12	RX J0148.3-2758	001	15.56±0.05	15.88±0.03	14.74±0.02	14.72±0.01	14.87±0.03	14.79±0.02
		002	...	15.66±0.07	14.51±0.05	14.37±0.01	...	14.48±0.08
		004	15.28±0.03	15.59±0.02	14.47±0.02	14.36±0.02	14.25±0.02	14.24±0.01
		005	15.54±0.04	15.72±0.02	14.58±0.02	14.44±0.02	14.36±0.02	14.33±0.01
		006	...	15.69±0.04	14.53±0.03	14.51±0.02	...	14.28±0.03
		007	15.47±0.02	15.73±0.01	14.55±0.01	14.42±0.01	14.27±0.01	14.28±0.01
		008	15.49±0.02	15.75±0.01	14.62±0.01	14.56±0.01	14.44±0.01	14.43±0.01
13	RX J0152.4-2319	001	15.43±0.02	15.78±0.01	14.54±0.01	14.37±0.01	14.16±0.01	14.15±0.01
		002	15.42±0.03	15.78±0.02	14.55±0.02	14.40±0.02	14.16±0.01	14.17±0.01
		003	15.42±0.01	15.76±0.01	14.49±0.01	14.33±0.01	14.11±0.01	14.09±0.01
14	Mkn 1044	001	14.34±0.02	14.67±0.01	13.61±0.01	13.44±0.01	13.29±0.01	13.34±0.01
		002	14.34±0.01	14.63±0.01	13.57±0.01	13.43±0.01	13.27±0.01	13.32±0.01
		003	14.16±0.01	14.43±0.01	13.34±0.01	13.16±0.01	12.97±0.01	13.03±0.01
15	Mkn 1048	001	14.53±0.05	14.93±0.01	13.66±0.01	13.39±0.01	...	13.36±0.01
		002	14.49±0.03	14.95±0.02	13.64±0.02	13.42±0.02	13.64±0.02	13.41±0.01
		003	14.42±0.01	14.84±0.01	13.51±0.01	13.27±0.01	13.15±0.01	13.19±0.01
		004	14.45±0.02	14.86±0.01	13.54±0.01	13.32±0.01	13.21±0.01	13.26±0.01
		005	14.47±0.01	14.85±0.01	13.54±0.01	13.32±0.01	13.20±0.01	13.24±0.01
16	RX J0311.3-2046	001	15.83±0.02	16.26±0.01	15.05±0.01	14.92±0.01	14.84±0.01	14.80±0.01
		002	15.79±0.02	16.22±0.01	15.00±0.01	14.85±0.01	14.76±0.01	14.73±0.01
17	RX J0319.8-2627	001	15.80±0.03	16.62±0.03	15.75±0.03	15.65±0.03	15.62±0.03	15.49±0.02
		002	15.87±0.02	16.64±0.02	15.81±0.02	15.82±0.02	15.71±0.02	15.75±0.01
		003	15.86±0.03	16.60±0.02	15.77±0.02	15.67±0.02	15.61±0.03	15.59±0.01
		004	15.88±0.03	16.60±0.02	15.84±0.02	15.54±0.02	15.65±0.03	15.64±0.02
		001	15.63±0.02	16.31±0.01	15.30±0.01	15.15±0.01	14.88±0.01	14.85±0.01
		002	15.64±0.04	16.25±0.03	15.22±0.02	15.01±0.02	14.75±0.03	14.70±0.01
		003	15.86±0.04	16.62±0.03	15.98±0.03	15.94±0.02	15.82±0.04	15.91±0.03
		004	15.84±0.01	16.54±0.01	15.72±0.01	15.64±0.01	15.50±0.01	15.50±0.01
18	RX J0323.2-4931	001	16.24±0.02	16.92±0.02	16.49±0.02	16.80±0.03	16.88±0.03	17.07±0.02
		002	16.29±0.02	16.94±0.02	16.46±0.02	16.79±0.02	16.94±0.03	17.03±0.02
19	ESO 301-G13	001	...	...	14.74±0.01	...	...	...
		002	15.44±0.01	15.95±0.01	14.78±0.01	14.63±0.01	14.48±0.01	14.45±0.01
		001	15.58±0.02	16.14±0.01	15.05±0.01	14.97±0.01	14.88±0.01	14.87±0.01
		002	15.47±0.04	16.02±0.02	14.81±0.02	14.66±0.02	14.54±0.02	14.57±0.02
		003	15.49±0.01	15.99±0.01	14.81±0.01	14.66±0.01	14.54±0.01	14.50±0.01
20	VCV 0331-37	001	16.32±0.05	16.57±0.03	15.33±0.02	15.23±0.02	15.12±0.03	15.10±0.02
		002	16.07±0.09	16.55±0.06	15.33±0.05	15.33±0.05	15.25±0.05	15.15±0.06
		003	16.27±0.03	16.56±0.01	15.35±0.01	15.27±0.01	15.15±0.01	15.10±0.01
		004	16.18±0.02	16.57±0.01	15.21±0.01	15.09±0.01	14.94±0.01	14.90±0.01
		005	16.14±0.02	16.46±0.01	15.21±0.01	15.08±0.01	14.93±0.01	14.88±0.01
21	RX J0349.1-4711	001	17.04±0.04	17.07±0.02	16.08±0.02	15.98±0.02	15.70±0.02	15.71±0.01
		002	17.07±0.11	16.97±0.06	16.09±0.05	16.02±0.05	15.76±0.05	15.76±0.03
		003	16.99±0.05	17.11±0.03	16.06±0.02	15.96±0.02	15.64±0.02	15.72±0.01
22	Fairall 1116	001	...	...	...	...	...	13.91±0.02
		002	14.91±0.04	15.37±0.04	14.33±0.03	14.14±0.02	14.01±0.02	13.97±0.01
		003	14.91±0.01	15.27±0.01	14.15±0.01	13.92±0.01	13.74±0.01	13.67±0.01
		004	14.89±0.03	15.21±0.02	14.10±0.01	13.90±0.01	13.72±0.02	13.65±0.01
23	Fairall 1119	001	15.92±0.04	16.75±0.02	16.41±0.02	16.50±0.02	16.65±0.04	16.64±0.03
		002	15.86±0.03	16.78±0.02	16.36±0.02	16.45±0.03	16.64±0.04	16.65±0.02
24	RX J0412.7-4712	001	15.60±0.01	16.01±0.01	14.89±0.01	14.73±0.01	14.60±0.01	14.52±0.01
		002	15.58±0.02	15.98±0.01	14.82±0.01	14.61±0.01	14.44±0.01	14.35±0.01
25	1H 0419-577	001	14.47±0.01	14.80±0.01	13.60±0.01	13.52±0.01	13.43±0.01	13.35±0.01
		002	14.52±0.01	14.85±0.01	13.64±0.01	13.59±0.01	13.48±0.01	13.42±0.01
26	Fairall 303	001	...	16.46±0.02	15.46±0.01	15.25±0.01	...	...
		002	16.04±0.03	16.43±0.02	15.39±0.02	15.22±0.02	15.10±0.02	15.11±0.01
		003	16.08±0.02	16.49±0.01	15.48±0.01	15.31±0.01	15.23±0.02	15.24±0.01

TABLE 3—Continued

#	Object	segment(s)	V <sup>1</sup>	B <sup>1</sup>	U <sup>1</sup>	UVW1 <sup>1</sup>	UVM2 <sup>1</sup>	UVW2 <sup>1</sup>
27	RX J0437.4–4711	004	...	16.64±0.02	15.77±0.02	15.67±0.02	...	15.80±0.04
		001	15.01±0.01	15.37±0.01	14.37±0.01	14.22±0.01	14.07±0.01	14.10±0.00
		002	15.00±0.02	15.39±0.01	14.35±0.01	14.23±0.01	14.08±0.01	14.12±0.01
28	RX J0439.6–5311	001	17.39±0.05	17.61±0.03	16.52±0.02	16.18±0.02	15.87±0.02	15.93±0.01
		002	17.60±0.11	17.64±0.06	16.53±0.04	...	...	...
		003	17.47±0.07	17.64±0.04	16.41±0.03	16.15±0.02	15.90±0.03	15.91±0.02
29	RX J0859.0+4846	004	17.49±0.07	17.57±0.04	16.45±0.03	16.15±0.02	15.91±0.03	15.92±0.02
		005	17.37±0.09	17.66±0.05	16.46±0.03	16.18±0.03	15.95±0.03	15.99±0.02
		001	15.48±0.01	15.91±0.01	14.74±0.01	14.67±0.01	14.61±0.01	14.58±0.01
		002	15.42±0.03	15.81±0.02	14.65±0.02	14.57±0.01	14.62±0.02	14.51±0.01
		003	15.35±0.02	15.78±0.01	14.59±0.01	14.49±0.01	14.37±0.01	14.37±0.01
30	RX J0902.5–0700	001	17.08±0.06	17.60±0.04	16.46±0.03	16.41±0.03	16.43±0.09	16.16±0.02
		002	17.05±0.06	17.41±0.03	16.25±0.02	16.16±0.02	15.89±0.03	15.87±0.01
		003	16.98±0.05	17.42±0.03	16.27±0.02	16.11±0.02	15.82±0.03	15.79±0.02
31	Mkn 110	001	14.70±0.01	14.88±0.01	13.53±0.01	13.28±0.01	13.14±0.01	13.12±0.01
		002	14.64±0.01	14.86±0.01	13.49±0.01	13.22±0.01	13.08±0.01	13.06±0.01
32	PG 0953+414	001	...	...	...	13.46±0.01	13.21±0.01	13.18±0.01
33	RX J1005.7+4332	001	16.37±0.04	16.54±0.09	15.37±0.02	15.07±0.02	15.03±0.02	14.78±0.01
		002	16.54±0.05	16.68±0.03	15.43±0.02	15.19±0.02	15.01±0.02	14.96±0.01
		003	16.37±0.03	16.70±0.02	15.44±0.01	15.25±0.01	14.96±0.01	15.01±0.01
34	RX J1007.1+2203	001	16.95±0.09	17.20±0.05	16.07±0.03	16.10±0.03	15.89±0.04	15.88±0.02
		002	16.87±0.04	17.23±0.03	16.12±0.02	16.06±0.02	15.88±0.02	15.85±0.02
35	CBS 126	001	15.37±0.02	15.78±0.01	14.52±0.01	14.47±0.01	14.38±0.01	14.32±0.01
		002	15.38±0.02	15.69±0.01	14.45±0.01	14.30±0.01	14.20±0.02	14.08±0.01
36	Mkn 141	001	15.25±0.01	15.84±0.01	15.25±0.01	15.34±0.01	15.41±0.01	15.40±0.01
		002	15.24±0.02	15.82±0.01	15.19±0.02	15.20±0.02	15.19±0.02	15.27±0.01
		003	15.23±0.03	15.79±0.03	15.19±0.03	15.19±0.02	15.28±0.04	15.29±0.02
37	Mkn 142	001	15.73±0.01	16.08±0.01	15.08±0.01	14.91±0.01	14.71±0.01	14.70±0.01
		002	15.55±0.03	15.91±0.02	14.83±0.01	14.64±0.01	14.39±0.02	14.38±0.01
		003	16.01±0.02	16.40±0.01	15.43±0.01	15.50±0.01	15.45±0.02	15.59±0.01
38	RX J1117.1+6522	002	16.19±0.02	16.55±0.01	15.60±0.01	15.76±0.02	15.63±0.02	15.79±0.01
		003	16.06±0.03	16.45±0.02	15.50±0.02	15.52±0.02	15.36±0.02	15.45±0.01
		004	16.01±0.02	16.42±0.01	15.43±0.01	15.53±0.01	15.50±0.02	15.56±0.01
		001	14.46±0.01	14.56±0.01	13.24±0.01	13.04±0.01	12.78±0.01	12.80±0.01
39	Ton 1388	002	14.43±0.03	14.51±0.01	13.28±0.01	12.94±0.01	12.67±0.01	12.64±0.01
		002	...	...	...	14.77±0.01	...	...
40	EXO 1128+6908	001	15.30±0.01	15.83±0.01	14.98±0.01	14.80±0.01	14.83±0.01	14.62±0.01
41	B2 1128+31	001	16.23±0.04	16.09±0.01	14.96±0.01	14.93±0.01	14.35±0.01	14.40±0.01
		002	16.30±0.04	16.17±0.02	15.13±0.04	14.95±0.02	14.55±0.02	14.77±0.01
		003	16.34±0.03	16.21±0.01	15.15±0.01	15.09±0.01	14.72±0.01	14.87±0.01
42	SBS 1136+579	001	...	...	15.74±0.01	15.52±0.01	...	...
		002	16.56±0.03	...	15.95±0.02	15.78±0.02	15.65±0.02	15.46±0.01
		003	16.95±0.04	...	16.72±0.03	16.63±0.03	16.57±0.03	16.50±0.02
43	CASG 855	001	...	...	...	...	...	16.60±0.05
44	NGC 4051	001	15.92±0.04	16.84±0.04	16.50±0.05	16.59±0.05	16.79±0.09	16.81±0.04
		002	...	14.04±0.01	13.28±0.01	13.30±0.01	13.24±0.05	13.46±0.06
45	GQ Comae	001	...	...	13.56±0.01	13.94±0.01	...	...
		001	16.30±0.03	16.46±0.02	15.20±0.01	15.01±0.01	14.75±0.01	14.55±0.01
		002	16.35±0.03	16.49±0.01	15.23±0.01	15.06±0.01	14.80±0.01	14.60±0.01
		001	17.11±0.05	17.47±0.03	16.44±0.02	16.36±0.02	16.15±0.02	16.23±0.02
		002	17.12±0.09	17.52±0.06	16.39±0.04	16.44±0.04	16.24±0.05	16.25±0.03
46	RX J1209.7+3217	003	...	17.82±0.11	16.53±0.07	16.39±0.05	...	16.26±0.09
		004	17.14±0.07	17.53±0.05	16.41±0.03	16.35±0.03	16.23±0.04	16.25±0.02
		005	17.01±0.07	17.32±0.04	16.28±0.03	16.14±0.03	15.93±0.03	15.97±0.02
		006	16.95±0.03	17.32±0.02	16.24±0.01	16.14±0.01	15.93±0.01	16.96±0.01
		014	14.27±0.01	14.57±0.01	13.30±0.02	13.24±0.01	13.10±0.02	13.11±0.01
47	PG 1211+143	001	14.28±0.01	14.94±0.01	14.66±0.01	15.17±0.01	15.40±0.03	15.48±0.01
48	Mkn 766	021	12.77±0.01	...	...	11.44±0.01	11.19±0.01	11.19±0.01
49	3C 273	039	12.73±0.01	...	11.63±0.01	11.42±0.01	11.19±0.01	11.22±0.01
50	RX J1231.6+7044	001	16.27±0.09	16.46±0.06	15.33±0.05	15.29±0.05	15.03±0.04	14.78±0.02
		002	16.39±0.04	16.43±0.03	15.33±0.02	15.18±0.02	14.96±0.02	14.75±0.01
		003	16.45±0.04	16.42±0.03	15.37±0.02	15.23±0.01	14.99±0.01	14.77±0.01
		004	16.44±0.04	16.47±0.02	15.29±0.02	15.21±0.01	15.00±0.02	14.78±0.01
		001	15.62±0.02	16.38±0.02	16.08±0.02	16.24±0.02	16.25±0.03	16.34±0.02
51	MCG+08-23-067	001	13.80±0.01	14.55±0.01	13.86±0.01	13.89±0.01	14.03±0.01	14.45±0.01
52	NGC 4593	002	17.34±0.06	17.47±0.03	16.38±0.02	16.18±0.02	15.89±0.02	15.99±0.01
53	RX J1304.2+0205	003	17.22±0.14	17.31±0.03	16.23±0.02	15.98±0.02	15.80±0.06	15.79±0.02
		001	15.50±0.02	15.64±0.01	14.31±0.01	14.15±0.01	13.91±0.01	13.83±0.01
		002	15.54±0.02	15.66±0.01	14.30±0.01	14.15±0.01	13.89±0.01	13.83±0.01
55	RX J1319.9+5235	001	17.32±0.06	17.97±0.04	17.34±0.04	17.50±0.04	17.44±0.04	17.59±0.03
		002	17.30±0.05	17.89±0.04	17.36±0.04	17.44±0.04	17.29±0.04	17.43±0.03
		003	17.30±0.05	17.93±0.04	17.36±0.04	17.51±0.04	17.46±0.05	17.47±0.03
		004	17.23±0.04	17.93±0.03	17.35±0.03	17.43±0.03	17.36±0.04	17.53±0.02
		001	14.20±0.01	14.77±0.01	14.13±0.01	14.76±0.01	15.05±0.01	15.33±0.01
56	IRAS 1334+24	002	...	...	14.17±0.01	14.80±0.01	15.07±0.02	15.39±0.01
		003	...	...	14.23±0.01	14.82±0.02	15.14±0.02	15.43±0.02
		004	...	...	14.18±0.01	14.86±0.02	15.13±0.02	15.42±0.02
		001	15.96±0.07	16.30±0.03	15.05±0.02	14.81±0.01	14.52±0.03	14.45±0.01
57	Ton 730	001	16.39±0.03	16.94±0.03	15.87±0.02	15.81±0.02	15.61±0.02	15.68±0.01
		002	...	16.93±0.04	15.87±0.03	15.79±0.03	...	15.76±0.03
		003	16.50±0.04	16.98±0.03	15.89±0.02	15.85±0.02	15.75±0.02	15.79±0.02
58	RX J1355.2+5612	004	16.41±0.03	16.96±0.03	15.90±0.02	15.83±0.02	15.66±0.02	15.73±0.01
		005	16.53±0.08	17.04±0.06	15.92±0.05	15.86±0.03	15.71±0.05	15.80±0.03
		001	15.27±0.02	15.36±0.02	14.09±0.01	14.16±0.01	13.71±0.01	13.68±0.01
		002	15.30±0.03	15.48±0.01	14.22±0.01	13.97±0.01	13.76±0.01	13.74±0.01
59	PG 1402+261	003	15.34±0.03	15.48±0.01	14.18±0.01	13.91±0.01	13.64±0.01	13.64±0.01

TABLE 3—Continued

#	Object	segment(s)	V <sup>1</sup>	B <sup>1</sup>	U <sup>1</sup>	UVW1 <sup>1</sup>	UVM2 <sup>1</sup>	UVW2 <sup>1</sup>
60	RX J1413.6+7029	001	16.82±0.03	17.82±0.03	17.34±0.03	17.55±0.04	17.49±0.04	17.25±0.02
		002	16.63±0.02	17.44±0.02	16.60±0.02	16.53±0.02	16.34±0.02	16.12±0.01
61	NGC 5548	059	14.32±0.02	15.02±0.02	14.52±0.02	14.39±0.02	14.51±0.02	14.68±0.01
62	Mkn 813	002	...	...	...	14.18±0.01	...	...
		001	15.16±0.03	15.36±0.03	14.02±0.01	...	...	...
		002	14.87±0.01	15.04±0.01	13.70±0.01	...	...	...
		003	14.87±0.01	15.03±0.01	13.70±0.01	13.49±0.01	13.32±0.01	13.33±0.01
		007	...	...	...	14.24±0.01	14.44±0.01	14.54±0.01
63	Mkn 684	008	14.64±0.02	15.06±0.02	13.95±0.01	13.77±0.01	13.54±0.02	13.72±0.01
		009	14.57±0.01	14.97±0.01	13.92±0.01	13.73±0.01	13.58±0.01	13.67±0.01
64	Mkn 478	001	14.57±0.02	14.83±0.01	13.63±0.01	13.44±0.01	13.26±0.01	13.28±0.01
		002	14.54±0.02	14.83±0.01	13.66±0.01	13.46±0.01	13.30±0.01	13.21±0.01
66	Mkn 841	002	14.67±0.01	15.03±0.01	13.73±0.01	13.53±0.01	13.45±0.01	13.46±0.01
		001	14.64±0.01	14.98±0.01	13.65±0.01	13.45±0.01	13.38±0.01	13.38±0.01
		002	14.66±0.01	14.99±0.01	13.65±0.01	13.45±0.01	13.33±0.01	13.36±0.01
		003	14.59±0.03	14.82±0.02	13.53±0.01	13.29±0.01	13.20±0.03	13.22±0.01
67	Mkn 493	001	15.03±0.01	15.37±0.01	14.37±0.01	14.23±0.01	14.10±0.01	14.19±0.01
		002	15.45±0.02	15.78±0.01	14.69±0.01	14.57±0.01	14.45±0.01	14.55±0.01
		008	15.12±0.02	15.59±0.02	14.61±0.02	14.51±0.02	14.38±0.02	14.48±0.01
68	Mkn 876	001	14.48±0.01	14.72±0.01	13.43±0.01	13.29±0.01	13.10±0.01	13.11±0.01
		002	14.50±0.01	14.66±0.01	13.43±0.01	13.21±0.01	13.02±0.01	12.99±0.01
69	RX J1618.1+3619	001	16.47±0.04	17.14±0.03	16.89±0.03	17.14±0.04	17.14±0.06	17.26±0.03
		002	16.35±0.05	17.05±0.03	16.77±0.02	17.03±0.02	16.95±0.09	17.08±0.04
		003	...	...	...	...	17.07±0.03	...
70	KUG 1618+410	001	16.12±0.04	16.81±0.03	16.32±0.03	16.33±0.03	16.17±0.04	16.16±0.02
		002	16.14±0.02	16.91±0.01	16.47±0.02	16.45±0.02	16.43±0.02	16.46±0.01
71	PG 1626+554	001	15.78±0.02	15.89±0.01	14.59±0.01	14.46±0.01	14.28±0.01	14.20±0.01
		002	15.90±0.10	15.96±0.04	14.62±0.01	14.48±0.01	14.47±0.05	14.40±0.03
		003	15.69±0.02	15.86±0.01	14.56±0.01	14.41±0.01	14.22±0.01	14.14±0.01
72	EXO 1627+40	001	17.99±0.10	18.06±0.06	17.07±0.05	16.89±0.04	16.55±0.04	16.57±0.03
		002	18.03±0.07	18.22±0.04	17.18±0.03	16.89±0.02	16.66±0.03	16.60±0.02
		003	17.94±0.09	18.16±0.04	17.12±0.03	16.98±0.03	16.52±0.03	16.58±0.02
		004	18.10±0.21	18.12±0.09	17.15±0.06	16.88±0.05	16.60±0.07	16.62±0.03
		007	17.79±0.15	18.15±0.10	17.15±0.08	16.91±0.07	16.71±0.07	16.53±0.04
73	RX J1702.5+3247	001	15.54±0.03	15.73±0.02	14.55±0.02	14.49±0.02	14.34±0.02	14.41±0.01
		002	15.47±0.01	15.72±0.01	14.54±0.01	14.50±0.01	14.35±0.01	14.47±0.01
		003	15.50±0.03	15.74±0.02	14.55±0.01	14.49±0.01	14.36±0.02	14.45±0.01
		004	15.49±0.02	15.73±0.01	14.60±0.01	14.55±0.01	14.38±0.01	14.48±0.01
74	II Zw 136	003	14.33±0.03	14.60±0.02	13.31±0.01	13.20±0.01	12.97±0.02	13.03±0.01
		004	14.34±0.01	14.57±0.01	13.31±0.01	13.20±0.01	12.98±0.01	13.04±0.01
		005	14.45±0.02	14.41±0.02	13.49±0.01	13.38±0.01	13.23±0.01	13.33±0.01
		006	14.48±0.02	14.73±0.01	13.45±0.01	13.29±0.01	13.08±0.02	13.17±0.01
75	RX J2146.6–3051	001	...	...	...	14.74±0.09	14.72±0.03	14.69±0.02
		002	...	...	...	14.84±0.01	14.72±0.01	14.70±0.01
		003	...	...	...	14.84±0.02	14.76±0.02	14.73±0.02
		004	...	...	...	14.75±0.01	14.65±0.02	14.61±0.01
		005	...	...	...	14.90±0.01	14.79±0.01	14.77±0.01
76	RX J2216.8–4451	001	...	...	...	...	...	14.28±0.01
		001	15.80±0.02	16.08±0.01	14.79±0.01	14.58±0.01	14.31±0.01	14.26±0.01
		002	15.84±0.03	16.09±0.02	14.77±0.01	14.56±0.01	14.30±0.02	14.27±0.01
		003	15.89±0.03	16.01±0.02	14.75±0.01	14.54±0.01	14.26±0.02	14.21±0.01
		004	15.76±0.02	16.01±0.01	14.74±0.01	14.50±0.01	14.23±0.01	14.17±0.01
77	RX J2217.9–5941	001	16.64±0.05	17.11±0.04	15.94±0.03	15.78±0.03	15.52±0.03	15.53±0.02
		002	16.70±0.03	17.08±0.02	15.99±0.02	15.80±0.01	15.54±0.01	15.62±0.01
		003	16.79±0.05	17.07±0.03	15.99±0.02	15.84±0.02	15.55±0.02	15.58±0.01
78	RX J2242.6–3845	001	17.24±0.04	17.35±0.02	16.19±0.02	16.07±0.02	15.83±0.02	15.82±0.01
		002	17.02±0.05	17.25±0.03	16.11±0.02	15.96±0.02	15.85±0.03	15.73±0.01
		003	17.08±0.06	17.27±0.04	16.16±0.03	16.04±0.03	15.78±0.03	15.75±0.02
79	RX J2245.3–4652	001	...	15.65±0.05	14.51±0.04	14.38±0.02	...	...
		002	...	15.49±0.03	14.49±0.01	14.36±0.01	...	...
		003	15.19±0.02	15.42±0.01	14.38±0.01	14.29±0.01	14.18±0.01	14.13±0.01
		004	15.24±0.03	15.43±0.03	14.31±0.01	14.27±0.01	14.17±0.02	14.12±0.01
81	MS 2254-36	001	15.65±0.03	16.20±0.02	15.35±0.02	15.23±0.02	15.09±0.02	15.15±0.01
		002	15.63±0.02	16.11±0.01	15.24±0.01	15.16±0.01	15.03±0.01	15.04±0.01
		004	15.69±0.02	16.23±0.01	15.39±0.01	15.30±0.01	15.15±0.01	15.22±0.01
		005	15.66±0.02	16.18±0.01	15.34±0.01	15.22±0.01	15.09±0.01	15.12±0.01
82	RX J2258.7–2609	001	16.03±0.05	16.86±0.05	15.88±0.04	15.63±0.04	15.58±0.06	15.50±0.03
		002	16.16±0.02	16.85±0.02	15.67±0.01	15.58±0.01	15.47±0.02	15.34±0.01
		003	16.07±0.07	16.88±0.06	15.58±0.04	15.33±0.04	15.25±0.05	15.13±0.03
		004	16.17±0.02	16.89±0.01	15.76±0.01	15.68±0.01	15.61±0.01	15.50±0.01
83	RX J2301.6–5913	001	16.74±0.07	17.19±0.05	15.89±0.03	15.99±0.04	15.83±0.04	15.61±0.02
		002	16.71±0.03	17.16±0.02	15.86±0.02	15.93±0.02	15.80±0.03	15.57±0.01
		004	16.67±0.04	17.04±0.03	15.84±0.02	15.95±0.02	15.83±0.03	15.67±0.02
		005	16.60±0.03	16.98±0.02	15.71±0.01	15.71±0.01	15.51±0.02	15.25±0.01
		006	...	16.96±0.04	15.72±0.03	15.69±0.02	...	15.31±0.02
84	RX J2301.8–5508	001	15.47±0.02	15.80±0.02	14.76±0.01	14.76±0.01	14.67±0.01	14.77±0.01
		002	15.48±0.02	15.80±0.02	14.75±0.01	14.73±0.01	14.61±0.01	14.73±0.01
85	RX J2304.6–3501	001	...	...	16.41±0.05	16.54±0.06	16.44±0.06	16.43±0.04
86	RX J2312.5–3404	001	16.57±0.02	16.67±0.01	15.57±0.01	15.57±0.01	15.38±0.01	15.23±0.01
		002	16.60±0.03	16.84±0.02	15.72±0.02	15.68±0.02	15.54±0.04	15.37±0.01
87	RX J2317.8–4422	003	...	...	...	15.60±0.01	...	...
		001	16.80±0.04	17.15±0.02	16.16±0.02	16.06±0.02	15.83±0.02	15.85±0.01
		002	16.70±0.05	17.14±0.04	16.10±0.03	16.07±0.03	15.87±0.03	15.90±0.02
88	RX J2325.2–3236	001	16.73±0.05	16.58±0.01	15.40±0.01	15.20±0.01	15.22±0.05	14.83±0.01
		002	16.62±0.03	16.57±0.02	15.38±0.01	15.19±0.01	14.96±0.01	14.81±0.01
		003	16.81±0.05	16.77±0.02	15.54±0.02	15.39±0.02	15.19±0.02	14.97±0.01

TABLE 3—*Continued*

#	Object	segment(s)	V <sup>1</sup>	B <sup>1</sup>	U <sup>1</sup>	UVW1 <sup>1</sup>	UVM2 <sup>1</sup>	UVW2 <sup>1</sup>
89	IRAS 23226–3826	001	...	...	...	...	15.06±0.01	...
		002	...	...	...	15.00±0.01	...	...
90	MS 23409–1511	001	14.64±0.03	15.24±0.02	14.83±0.02	14.90±0.02	14.82±0.05	14.98±0.02
		002	15.65±0.02	15.93±0.01	14.78±0.01	14.65±0.01	14.38±0.01	14.48±0.01
		003	15.68±0.03	15.93±0.02	14.79±0.01	14.64±0.01	14.53±0.01	14.58±0.01
		004	15.69±0.02	15.96±0.01	14.80±0.01	14.66±0.01	14.40±0.01	14.52±0.01
		005	15.60±0.04	15.88±0.02	14.79±0.02	14.67±0.02	14.41±0.02	14.49±0.01
91	RX J2349.4–3126	001	16.69±0.07	17.83±0.05	17.36±0.04	17.60±0.04	17.65±0.04	17.73±0.04
		003	16.63±0.05	17.43±0.04	16.59±0.03	16.66±0.04	16.49±0.04	16.39±0.02
		006	16.69±0.04	17.41±0.04	16.77±0.04	16.75±0.04	16.63±0.04	16.53±0.02
		007	16.71±0.03	17.50±0.03	16.74±0.03	16.94±0.03	16.81±0.03	16.73±0.02
		001	15.05±0.01	15.56±0.01	14.69±0.01	14.59±0.01	14.45±0.01	14.48±0.01
92	AM 2354–304	003	15.07±0.01	15.53±0.01	14.69±0.01	14.59±0.01	14.45±0.01	14.52±0.01

<sup>1</sup>UVOT magnitudes corrected for Galactic reddening using the  $E_{(B-V)}$  values by Schlegel et al. (1998) as given in Table 1.



TABLE 4  
SPECTRAL ANALYSIS OF THE *Swift* XRT DATA.

#	Object	segment(s)	Model <sup>1</sup>	$\alpha_{X,soft}$	$E_{break}$ <sup>2</sup>	$\alpha_{X,hard}$	$\log F_{0.2-2.0keV}$ <sup>3</sup>	$\chi^2/\nu$	CR <sup>4</sup>	HR <sup>5</sup>
1	Mkn 335	003	(1)	1.31±0.09	—	—	-13.37	34/37	1.237±0.030	+0.03±0.02
2	ESO 242-G008	001-002	(1)	0.74 <sup>+0.18</sup> <sub>-0.17</sub>	—	—	-14.41	14/12	0.041±0.003	+0.14±0.08
		003	(1)	1.17 <sup>+0.11</sup> <sub>-0.10</sub>	—	—	-14.41	37.0/34	0.111±0.004	-0.03±0.03
3	Ton S 180	003	(2)	1.46 <sup>+0.13</sup> <sub>-0.14</sub>	1.35 <sup>+0.24</sup> <sub>-0.23</sub>	0.75 <sup>+0.17</sup> <sub>-0.15</sub>	-14.41	24.5/32	—	—
		001	(1)	1.56±0.17	—	—	-13.72	17/14	0.495±0.026	-0.29±0.05
		003	(1)	1.48±0.06	—	—	-13.66	63/65	0.543±0.011	-0.23±0.02
		004	(1)	1.40±0.12	—	—	-14.07	20/16	0.202±0.010	-0.13±0.06
4	QSO 0056-36	005	(1)	1.58±0.04	—	—	-13.52	122/125	0.789±0.009	-0.22±0.01
		001	(1)	1.17±0.08	—	—	-14.23	40/41	0.187±0.006	-0.05±0.03
		002	(1)	1.06±0.11	—	—	-14.22	23/27	0.244±0.010	-0.01±0.04
		003	(1)	1.13±0.07	—	—	-14.31	62/54	0.195±0.006	+0.02±0.03
5	RX J0100.4-5113	004	(1)	0.97±0.15	—	—	-14.33	7/12	0.179±0.010	+0.10±0.06
		001	(1)	1.08±0.10	—	—	-14.34	28/26	0.164±0.007	+0.05±0.04
		002	(1)	1.19±0.14	—	—	-14.40	15/20	0.139±0.007	+0.05±0.05
		003	(1)	1.36±0.20	—	—	-14.15	20/25	0.205±0.008	-0.09±0.04
6	RX J0105.6-1416	004	(1)	1.36±0.08	—	—	-14.02	44/51	0.189±0.005	-0.06±0.03
		001	(1)	0.92±0.06	—	—	-14.15	65/64	0.292±0.008	+0.13±0.03
		002	(1)	0.99±0.09	—	—	-14.08	28/33	0.322±0.012	+0.08±0.04
		003	(1)	1.14±0.06	—	—	-13.98	66/65	0.346±0.009	-0.02±0.03
7	RX J0117.5-3826	004	(1)	1.02±0.07	—	—	-14.05	55/48	0.326±0.010	+0.09±0.03
		002	(1)	2.16 <sup>+0.26</sup> <sub>-0.24</sub>	—	—	-14.31	6/9	0.069±0.004	-0.48±0.06
		004	(1)	2.13 <sup>+0.36</sup> <sub>-0.33</sub>	—	—	-14.57	7/5	0.039±0.003	-0.50±0.05
		006	(1)	1.98 <sup>+0.18</sup> <sub>-0.18</sub>	—	—	-14.30	11/10	0.083±0.005	-0.44±0.05
8	MS 0117-28	001	(1)	1.73 <sup>+0.29</sup> <sub>-0.28</sub>	—	—	-14.62	3/6	0.045±0.004	-0.42±0.07
		002	(1)	2.14 <sup>+0.28</sup> <sub>-0.26</sub>	—	—	-14.41	5/6	0.058±0.004	-0.44±0.07
		003	(1)	2.09 <sup>+0.26</sup> <sub>-0.25</sub>	—	—	-14.69	8/7	0.033±0.002	-0.44±0.07
		002	(1)	1.60 <sup>+0.16</sup> <sub>-0.15</sub>	—	—	-14.87	26/19	0.030±0.001	-0.20±0.05
9	RX J0128.1-1848	002	(2)	2.12 <sup>+0.60</sup> <sub>-0.33</sub>	0.82±0.22	1.33 <sup>+0.20</sup> <sub>-0.21</sub>	-14.80	18/17	—	—
		001	(1)	0.92 <sup>+0.08</sup> <sub>-0.07</sub>	—	—	-13.93	37/47	0.453±0.014	+0.14±0.03
		002	(1)	0.89 <sup>+0.05</sup> <sub>-0.05</sub>	—	—	-14.02	78/86	0.391±0.008	+0.14±0.02
		003	(1)	1.10±0.08	—	—	-13.89	41/43	0.463±0.015	+0.03±0.03
10	RX J0134.2-4258	004	(1)	1.01±0.04	—	—	-13.91	147/153	0.459±0.007	+0.08±0.02
		001	(1)	1.29 <sup>+0.28</sup> <sub>-0.26</sub>	—	—	-14.77	8/7	0.066±0.006	-0.06±0.08
		001	(1)	1.87±0.16	—	—	-14.33	23/21	0.081±0.004	-0.36±0.04
		002	(1)	1.75 <sup>+0.21</sup> <sub>-0.20</sub>	—	—	-13.78	9/12	0.348±0.019	-0.38±0.05
11	RX J0136.9-3510	004	(1)	1.82±0.16	—	—	-13.95	15/16	0.241±0.012	-0.39±0.05
		005	(1)	1.73±0.13	—	—	-13.77	21/22	0.374±0.016	-0.36±0.04
		006	(1)	1.81 <sup>+0.41</sup> <sub>-0.40</sub>	—	—	-13.82	3/4	0.322±0.031	-0.40±0.09
		007	(1)	1.67±0.08	—	—	-13.82	80/53	0.339±0.009	-0.34±0.03
12	RX J0148.3-2758	008	(1)	1.57 <sup>+0.09</sup> <sub>-0.08</sub>	—	—	-14.09	44/38	0.219±0.007	-0.29±0.03
		001	(1)	1.25±0.11	—	—	-14.35	22/24	0.175±0.007	-0.11±0.04
		002	(1)	1.24±0.16	—	—	-14.21	7/12	0.194±0.011	-0.07±0.06
		003	(1)	1.23±0.04	—	—	-14.16	102/110	0.243±0.005	-0.06±0.02
13	RX J0152.4-2319	001	(1)	1.46±0.08	—	—	-13.51	47/46	0.719±0.016	-0.13±0.02
		002	(1)	1.47±0.06	—	—	-13.84	135/90	0.367±0.008	-0.17±0.02
		002	(2)	1.69 <sup>+0.14</sup> <sub>-0.09</sub>	1.58 <sup>+0.41</sup> <sub>-0.43</sub>	0.86±0.22	-13.81	88/88	—	—
		003	(3)	1.49±0.09	—	—	-14.07	60/47	—	—
14	Mkn 1044	001	(1)	0.61±0.15	—	—	-14.33	33/18	0.208±0.010	+0.25±0.05
		002	(2)	4.44 <sup>+0.66</sup> <sub>-0.57</sub>	1.00 <sup>+0.12</sup> <sub>-0.10</sub>	0.57±0.21	-12.65	13/16	—	—
		003	(1)	1.02±0.08	—	—	-13.62	57/44	0.718±0.016	+0.13±0.02
		004	(1)	0.71±0.12	—	—	-13.89	22/22	0.570±0.018	+0.22±0.03
15	Mkn 1048	005	(1)	0.78±0.05	—	—	-13.84	130/107	0.634±0.009	+0.24±0.01
		001	(1)	0.83±0.05	—	—	-14.19	84/91	0.284±0.006	+0.24±0.02
		002	(1)	0.87±0.07	—	—	-14.25	74/57	0.211±0.006	+0.21±0.03
		001	(1)	0.82±0.11	—	—	-14.60	5/18	0.102±0.005	+0.18±0.05
16	RX J0311.3-2046	002	(1)	0.94±0.14	—	—	-14.65	21/17	0.083±0.004	+0.12±0.05
		003	(1)	0.87 <sup>+0.34</sup> <sub>-0.33</sub>	—	—	-14.63	0.4/4	0.082±0.007	+0.12±0.08
		004	(1)	0.70 <sup>+0.18</sup> <sub>-0.17</sub>	—	—	-14.74	9/9	0.090±0.006	+0.25±0.06
		001	(1)	1.08±0.07	—	—	-14.45	36/48	0.129±0.004	+0.04±0.03
17	RX J0319.8-2627	002	(1)	1.05±0.13	—	—	-14.25	19/15	0.222±0.012	+0.04±0.05
		003	(1)	0.55±0.25	—	—	-14.95	7/3	0.060±0.005	+0.44±0.08
		004	(1)	0.98±0.07	—	—	-14.53	78/63	0.108±0.003	+0.13±0.03
		001	(1)	1.33 <sup>+0.21</sup> <sub>-0.20</sub>	—	—	-14.86	15/12	0.043±0.003	-0.07±0.06
18	RX J0323.2-4931	001	(2)	1.98 <sup>+0.93</sup> <sub>-0.45</sub>	0.89 <sup>+0.45</sup> <sub>-0.33</sub>	0.89 <sup>+0.34</sup> <sub>-0.36</sub>	-14.76	6/10	—	—
		002	(1)	1.08±0.13	—	—	-14.72	40/25	0.068±0.003	+0.03±0.04
		002	(2)	1.53 <sup>+0.27</sup> <sub>-0.26</sub>	0.82 <sup>+0.32</sup> <sub>-0.20</sub>	0.92 <sup>+0.20</sup> <sub>-0.21</sub>	-14.67	35/23	—	—
		001	(1)	1.29±0.10	—	—	-14.03	102/78	0.285±0.006	-0.03±0.02
19	ESO 301-G13	002	(1)	1.35±0.06	—	—	-14.07	125/102	0.257±0.005	-0.06±0.02
		001	(1)	1.19±0.09	—	—	-14.21	60/48	0.221±0.006	+0.04±0.03
		002	(1)	1.10±0.24	—	—	-14.08	10/9	0.241±0.016	+0.07±0.06
		003	(1)	1.31±0.07	—	—	-14.11	105/75	0.238±0.006	+0.00±0.02
20	VCV 0331-37	001	(1)	1.04 <sup>+0.20</sup> <sub>-0.19</sub>	—	—	-14.40	11/10	0.143±0.009	+0.08±0.06
		002	(—)	—	—	—	—	—	0.169±0.020	-0.05±0.12
		003	(1)	1.07±0.07	—	—	-14.42	60/58	0.144±0.004	+0.07±0.03
		004	(1)	1.24±0.08	—	—	-14.32	60/54	0.158±0.004	-0.01±0.03
21	RX J0349.1-4711	005	(1)	1.19±0.06	—	—	-14.30	105/81	0.174±0.004	+0.02±0.02
		001	(1)	1.62 <sup>+0.18</sup> <sub>-0.17</sub>	—	—	-14.68	15/14	0.046±0.003	-0.21±0.05
		003	(1)	1.35 <sup>+0.21</sup> <sub>-0.20</sub>	—	—	-14.70	19/12	0.059±0.003	-0.18±0.06
		001	(1)	1.42±0.20	—	—	-13.85	14/5	0.368±0.028	-0.08±0.08
22	Fairall 1116	002	(2)	3.32 <sup>+4.09</sup> <sub>-1.56</sub>	0.71 <sup>+0.65</sup> <sub>-0.23</sub>	0.72 <sup>+0.55</sup> <sub>-0.91</sub>	-13.51	4/3	—	—
		002	(1)	1.05±0.13	—	—	-13.91	30/19	0.375±0.018	+0.02±0.05
		003	(1)	1.33±0.05	—	—	-13.96	50/49	0.306±0.006	-0.04±0.02
		002	(2)	1.56 <sup>+0.43</sup> <sub>-0.13</sub>	0.92 <sup>+0.38</sup> <sub>-0.38</sub>	1.19 <sup>+0.10</sup> <sub>-0.09</sub>	-13.93	39/47	—	—
23	Fairall 1119	004	(1)	1.35±0.14	—	—	-14.15	15/16	0.193±0.010	-0.04±0.05
		005	(1)	1.07±0.12	—	—	-14.00	24/25	0.326±0.014	+0.13±0.04
		001	(1)	0.72±0.10	—	—	-14.56	25/26	0.126±0.005	+0.31±0.04

TABLE 4—Continued

#	Object	segment(s)	Model <sup>1</sup>	$\alpha_{X,\text{soft}}$	$E_{\text{break}}^2$	$\alpha_{X,\text{hard}}$	$\log F_{0.2-2.0\text{keV}}^3$	$\chi^2/\nu$	CR <sup>4</sup>	HR <sup>5</sup>
24	RX J0412.7–4712	002	(1)	0.60±0.14	—	—	-14.70	13/17	0.099±0.005	+0.34±0.04
		001	(1)	1.02±0.05	—	—	-14.19	98/104	0.254±0.005	+0.07±0.02
		002	(1)	1.09±0.07	—	—	-13.97	55/64	0.394±0.010	+0.01±0.03
25	1H0419–577	001	(1)	1.22±0.04	—	—	-13.47	207/156	1.189±0.011	+0.06±0.01
			(2)	2.01 <sup>+0.38</sup> <sub>-0.24</sub>	0.65±0.09	1.08±0.06	-13.35	159/154		
26	Fairall 303	002	(1)	1.07±0.09	—	—	-13.74	38/39	0.633±0.015	+0.13±0.02
		001	(1)	1.11±0.10	—	—	-14.32	30/29	0.210±0.008	+0.02±0.04
		002	(1)	1.32±0.10	—	—	-14.13	54/39	0.245±0.008	-0.08±0.03
		003	(1)	1.17±0.10	—	—	-14.36	20/32	0.146±0.005	-0.01±0.04
27	RX J0437.4–4711	001	(1)	1.20±0.05	—	—	-13.99	175/123	0.361±0.006	-0.04±0.02
			(2)	1.32 <sup>+0.11</sup> <sub>-0.07</sub>	1.92 <sup>+0.63</sup> <sub>-0.87</sub>	0.87 <sup>+0.20</sup> <sub>-0.18</sub>	-13.98	158/121		
28	RX J0439.6–5311	002	(1)	1.17±0.06	—	—	-13.85	87/74	0.496±0.012	-0.04±0.02
		001	(1)	2.16±0.09	—	—	-13.84	45/43	0.202±0.006	-0.54±0.03
		003	(1)	2.12 <sup>+0.13</sup> <sub>-0.12</sub>	—	—	-13.89	20/28	0.180±0.007	-0.52±0.03
		004	(1)	2.05±0.10	—	—	-13.79	33/35	0.255±0.008	-0.50±0.03
		005	(1)	2.07 <sup>+0.12</sup> <sub>-0.11</sub>	—	—	-13.84	41/29	0.239±0.009	-0.55±0.03
29	RX J0859.0+4846	001	(1)	0.91±0.06	—	—	-14.29	69/71	0.205±0.005	+0.12±0.02
		002	(1)	0.98±0.13	—	—	-14.28	19/14	0.208±0.012	+0.16±0.06
		003	(1)	1.14±0.09	—	—	-14.21	47/44	0.200±0.006	-0.02±0.03
30	RX J0902.5–0700	001	(1)	1.23 <sup>+0.40</sup> <sub>-0.37</sub>	—	—	-14.97	3/3	0.027±0.003	+0.16±0.09
		002	(1)	1.24 <sup>+0.19</sup> <sub>-0.18</sub>	—	—	-14.79	7/9	0.048±0.003	+0.09±0.06
		003	(1)	1.61 <sup>+0.18</sup> <sub>-0.17</sub>	—	—	-14.60	11/11	0.055±0.003	-0.02±0.06
31	Mkn 110	001	(1)	0.98±0.05	—	—	-13.29	181/125	1.991±0.017	+0.13±0.01
		002	(1)	1.02±0.07	—	—	-13.28	55/49	2.064±0.031	+0.12±0.02
32	PG 0953+414	001	(1)	1.28±0.09	—	—	-13.94	20/33	0.350±0.013	-0.10±0.04
33	RX J1005.7+4332	001	(1)	1.80 <sup>+0.29</sup> <sub>-0.27</sub>	—	—	-14.46	8/7	0.079±0.006	-0.47±0.07
		002	—	—	—	—	—	0.029±0.004	-0.35±0.11	
		003	—	—	—	—	—	0.010±0.001	-0.49±0.13	
34	RX J1007.1+2203	001	(1)	1.50 <sup>+0.27</sup> <sub>-0.26</sub>	—	—	-14.52	4/8	0.071±0.005	-0.11±0.08
		002	(1)	1.53±0.14	—	—	-14.79	32/19	0.041±0.002	-0.25±0.05
35	CBS 126	001	(1)	1.40±0.10	—	—	-14.33	71/29	0.145±0.006	-0.16±0.04
			(2)	2.11 <sup>+0.27</sup> <sub>-0.23</sub>	0.98 <sup>+0.17</sup> <sub>-0.18</sub>	0.80±0.18	-14.22	31/27		
		002	(1)	1.39±0.11	—	—	-14.15	41/32	0.222±0.008	-0.15±0.04
36	Mkn 141		(2)	1.88 <sup>+0.22</sup> <sub>-0.24</sub>	0.92 <sup>+0.24</sup> <sub>-0.14</sub>	1.04±0.16	-14..	23/30		
		001	(1)	0.76±0.08	—	—	-14.61	38/35	0.115±0.004	+0.20±0.03
		002	(1)	0.36±0.20	—	—	-15.33	11/5	0.031±0.003	+0.31±0.09
37	Mkn 142		(2)	1.25 <sup>+0.75</sup> <sub>-0.53</sub>	1.53 <sup>+0.97</sup> <sub>-0.59</sub>	-0.32 <sup>+0.48</sup> <sub>-0.73</sub>	-15.19	1/3		
		003	—	—	—	—	—	0.043±0.006	+0.19±0.13	
		001	(1)	1.38±0.06	—	—	-14.26	66/64	0.151±0.004	-0.20±0.02
38	RX J1117.1+6522	002	(1)	1.72±0.13	—	—	-13.82	27/24	0.259±0.011	-0.36±0.03
		001	(1)	1.93 <sup>+0.16</sup> <sub>-0.15</sub>	—	—	-14.40	20/18	0.070±0.003	-0.45±0.04
		002	(1)	1.05±0.25	—	—	-15.44	10/4	0.015±0.002	+0.02±0.10
		003	(1)	2.09 <sup>+0.21</sup> <sub>-0.20</sub>	—	—	-14.09	11/11	0.131±0.008	-0.55±0.05
39	Ton 1388	004	(1)	1.91±0.20	—	—	-14.79	20/9	0.036±0.002	-0.32±0.06
			(2)	2.65 <sup>+0.57</sup> <sub>-0.45</sub>	0.87 <sup>+0.30</sup> <sub>-0.19</sub>	0.83 <sup>+0.53</sup> <sub>-0.66</sub>	-14.62	7/7		
		001	(1)	1.26±0.08	—	—	-14.05	37/38	0.274±0.009	-0.07±0.03
40	EXO 1128+6908	002	(1)	1.43±0.22	—	—	-13.97	8/11	0.307±0.019	-0.14±0.06
		002	(1)	1.41±0.25	—	—	-13.96	9/4	0.311±0.025	-0.13±0.08
41	B2 1128+31	001	(1)	1.24±0.05	—	—	-13.93	147/117	0.387±0.007	-0.01±0.02
		002	(1)	1.05±0.13	—	—	-14.46	18/22	0.114±0.005	+0.09±0.04
		003	(1)	0.99±0.15	—	—	-14.43	13/18	0.142±0.007	+0.17±0.05
42	SBS 1136+579	001	(1)	1.14±0.15	—	—	-14.49	27/20	0.107±0.005	+0.03±0.05
		002	(1)	1.26±0.09	—	—	-14.61	40/34	0.093±0.003	-0.12±0.04
		002	(1)	0.98 <sup>+0.16</sup> <sub>-0.15</sub>	—	—	-14.68	5/12	0.070±0.004	+0.08±0.06
43	CASG 855	003	(1)	1.32 <sup>+0.34</sup> <sub>-0.31</sub>	—	—	-14.98	6/6	0.030±0.003	-0.08±0.09
		001	—	—	—	—	—	0.078±0.014	+0.42±0.16	
		002	(1)	0.62±0.15	—	—	-15.06	12/13	0.049±0.003	+0.38±0.06
		003	(1)	0.66±0.12	—	—	-14.98	22/17	0.051±0.003	+0.33±0.05
44	NGC 4051	004	(1)	0.54±0.14	—	—	-14.95	13/15	0.053±0.003	+0.30±0.05
		001	(1)	0.83 <sup>+0.33</sup> <sub>-0.32</sub>	—	—	-14.61	2/5	0.103±0.009	+0.23±0.09
		001	(1)	1.59±0.16	—	—	-12.85	33/23	4.093±0.183	-0.21±0.04
45	GQ Comae	002	(1)	1.37±0.06	—	—	-13.18	157/104	2.258±0.021	-0.03±0.01
			(2)	1.57±0.08	1.12 <sup>+0.25</sup> <sub>-0.20</sub>	0.75 <sup>+0.15</sup> <sub>-0.16</sub>	-13.15	109/102		
		001	(1)	1.10±0.06	—	—	-14.11	79/79	0.287±0.007	+0.08±0.02
46	RX J1209.8+6908	002	(1)	1.01±0.05	—	—	-14.13	93/88	0.288±0.005	+0.14±0.02
		001	—	—	—	—	—	0.008±0.001	-0.12±0.15	
		002	—	—	—	—	—	0.019±0.004	-0.51±0.17	
		004	(1)	1.86 <sup>+0.51</sup> <sub>-0.45</sub>	—	—	-14.95	6/5	0.023±0.003	-0.29±0.12
		005	—	—	—	—	—	—	0.007±0.002	-0.80±0.20
		006	(1)	3.07±0.17	—	—	-14.72	37/11	0.016±0.001	-0.62±0.005
47	PG 1211+143		(2)	3.22 <sup>+0.28</sup> <sub>-0.26</sub>	1.45 <sup>+0.36</sup> <sub>-0.26</sub>	0.05 <sup>+0.61</sup> <sub>-0.66</sub>	-14.70	15/9		
		014	(1)	1.89±0.12	—	—	-14.38	69/17	0.171±0.008	-0.22±0.05
48	Mkn 766		(2)	2.50 <sup>+0.30</sup> <sub>-0.31</sub>	1.20 <sup>+0.39</sup> <sub>-0.18</sub>	0.13 <sup>+0.37</sup> <sub>-0.60</sub>	-14.00	16/15		
		001	(1)	1.05±0.08	—	—	-13.78	76/49	0.603±0.013	+0.07±0.02
49	3C 273		(2)	1.80 <sup>+0.51</sup> <sub>-0.34</sub>	0.74 <sup>+0.19</sup> <sub>-0.15</sub>	0.87±0.10	-13.67	55/47		
		021	(1)	0.72±0.04	—	—	-13.10	172/149	4.389±0.072	+0.21±0.02
50	RX J1231.6+7044	039	(1)	0.74±0.04	—	—	-13.12	193/140	4.091±0.070	+0.21±0.02
		001	(1)	0.60 <sup>+0.38</sup> <sub>-0.40</sub>	—	—	-14.36	2/3	0.218±0.019	+0.15±0.09
		002	(1)	0.82 <sup>+0.13</sup> <sub>-0.12</sub>	—	—	-14.28	9/18	0.196±0.009	+0.17±0.05
		003	(1)	0.85±0.07	—	—	-14.30	40/47	0.200±0.006	+0.20±0.03
51	MCG+08-23-006	004	(1)	0.87±0.08	—	—	-14.30	33/41	0.207±0.007	+0.13±0.03
		001	(1)	0.82±0.15	—	—	-14.84	11/11	0.063±0.004	+0.19±0.06
52	NGC 4593	001	(1)	0.69±0.06	—	—	-13.72	65/72	0.934±0.015	+0.36±0.02
		002	(1)	1.97 <sup>+0.18</sup> <sub>-0.17</sub>	—	—	-14.61	24/18	0.044±0.002	-0.40±0.04
53	RX J1304.2+0205	002	(2)	2.19 <sup>+0.25</sup> <sub>-0.21</sub>	1.25 <sup>+0.69</sup> <sub>-0.65</sub>	1.07 <sup>+0.53</sup> <sub>-0.5</sub>	-14.55	16/16		

TABLE 4—Continued

#	Object	segment(s)	Model <sup>1</sup>	$\alpha_{X,soft}$	$E_{break}^2$	$\alpha_{X,hard}$	$\log F_{0.2-2.0keV}^3$	$\chi^2/\nu$	CR <sup>4</sup>	HR <sup>5</sup>		
54	PG 1307+085	003	(1)	$2.17^{+0.21}_{-0.20}$	—	—	-14.28	9/9	$0.071\pm 0.005$	$-0.50\pm 0.06$		
		001	(1)	$1.16\pm 0.07$	—	—	-14.25	57/60	$0.177\pm 0.005$	$+0.03\pm 0.03$		
		002	(1)	$1.26\pm 0.09$	—	—	-14.20	54/44	$0.209\pm 0.007$	$+0.02\pm 0.03$		
55	RX J1319.9+5235	001	(1)	$1.87\pm 0.12$	—	—	-14.41	38/26	$0.084\pm 0.003$	$-0.49\pm 0.04$		
		002	(1)	$1.86\pm 0.10$	—	—	-14.34	54/29	$0.101\pm 0.004$	$-0.46\pm 0.03$		
		003	(1)	$1.64\pm 0.13$	—	—	-14.28	25/20	$0.130\pm 0.006$	$-0.36\pm 0.04$		
56	IRAS1334+24	004	(3)	$1.93^{+0.09}_{-0.08}$	—	—	-14.20	48/44	$0.131\pm 0.04$	$-0.42\pm 0.03$		
		001	(1)	$1.61\pm 0.10$	—	—	-14.19	165/54	$0.177\pm 0.005$	$-0.23\pm 0.03$		
			(2)	$2.27^{+0.18}_{-0.17}$	$1.10^{+0.15}_{-0.12}$	$0.61^{+0.17}_{-0.18}$	-14.06	53/52	—	—		
		002	(1)	$1.60\pm 0.15$	—	—	-14.47	34/14	$0.095\pm 0.005$	$-0.21\pm 0.05$		
			(2)	$2.16^{+0.35}_{-0.33}$	$1.22^{+0.59}_{-0.26}$	$0.45^{+0.64}_{-0.40}$	-14.35	10/12	—	—		
		003	(1)	$1.76\pm 0.15$	—	—	-14.30	26/10	$0.124\pm 0.008$	$-0.24\pm 0.06$		
			(2)	$2.23^{+0.37}_{-0.32}$	$1.29^{+0.41}_{-0.28}$	$0.30^{+0.48}_{-0.59}$	-14.20	4/8	—	—		
		004	(1)	$1.06\pm 0.11$	—	—	-14.37	37/13	$0.176\pm 0.010$	$-0.13\pm 0.06$		
			(2)	$2.03^{+0.46}_{-0.40}$	$1.12^{+0.38}_{-0.22}$	$0.19^{+0.31}_{-0.41}$	-14.17	5/11	—	—		
		57	Ton 730	001	(1)	$1.41^{+0.18}_{-0.17}$	—	—	-14.18	8/10	$0.175\pm 0.011$	$-0.11\pm 0.06$
58	RX J1355.2+5612	001	(1)	$1.77^{+0.18}_{-0.17}$	—	—	-14.34	30/16	$0.100\pm 0.005$	$-0.35\pm 0.05$		
			(2)	$2.01\pm 0.27$	$1.50^{+2.51}_{-0.57}$	$0.76^{+0.57}_{-1.76}$	-14.45	19/14	—	—		
		002	(1)	$1.66\pm 0.30$	—	—	-14.06	9/6	$0.200\pm 0.014$	$-0.36\pm 0.07$		
		003	(1)	$1.61\pm 0.20$	—	—	-14.52	26/9	$0.078\pm 0.005$	$-0.30\pm 0.06$		
		004	(1)	$1.79\pm 0.13$	—	—	-14.25	25/19	$0.121\pm 0.006$	$-0.42\pm 0.04$		
		005	(1)	$2.09^{+0.47}_{-0.44}$	—	—	-14.19	2/3	$0.116\pm 0.011$	$-0.41\pm 0.08$		
		59	PG 1402+261	001	(1)	$1.35\pm 0.13$	—	—	-14.29	28/21	$0.140\pm 0.006$	$-0.16\pm 0.04$
		002	(1)	$1.46^{+0.16}_{-0.15}$	—	—	-14.23	15/13	$0.159\pm 0.009$	$-0.19\pm 0.06$		
		003	(1)	$1.39\pm 0.13$	—	—	-14.23	11/17	$0.156\pm 0.008$	$-0.17\pm 0.05$		
		60	RX J1413.6+7029	001	(1)	$0.64\pm 0.13$	—	—	-14.90	15/20	$0.057\pm 0.003$	$+0.27\pm 0.03$
002	(1)	$0.97\pm 0.06$	—	—	-14.42	85/77	$0.154\pm 0.004$	$+0.15\pm 0.02$				
61	NGC 5548	059	(1)	$0.41\pm 0.11$	—	—	-14.38	10/18	$0.213\pm 0.010$	$+0.43\pm 0.04$		
62	Mkn 813	002	(1)	$1.09\pm 0.08$	—	—	-14.06	44/42	$0.315\pm 0.010$	$+0.07\pm 0.03$		
			(2)	$1.62^{+0.98}_{-0.44}$	$0.64^{+0.44}_{-0.18}$	$1.00\pm 0.10$	-13.99	38/40	—	—		
		003	(1)	$1.00\pm 0.06$	—	—	-14.08	83/74	$0.296\pm 0.007$	$+0.13\pm 0.02$		
	(2)	$1.56^{+0.38}_{-0.26}$	$0.71^{+0.15}_{-0.13}$	$0.89\pm 0.07$	-14.01	66/72	—	—				
63	Mkn 684	001	(1)	$1.14^{+0.12}_{-0.11}$	—	—	-14.42	34/22	$0.125\pm 0.006$	$-0.04\pm 0.04$		
		006	(1)	$0.86\pm 0.06$	—	—	-14.50	90/48	$0.101\pm 0.003$	$+0.10\pm 0.03$		
		007	(1)	$1.15\pm 0.07$	—	—	-14.29	51/51	$0.171\pm 0.005$	$-0.01\pm 0.03$		
		008	(1)	$1.42^{+0.18}_{-0.17}$	—	—	-14.16	13/10	$0.190\pm 0.012$	$-0.09\pm 0.06$		
		009	(1)	$1.24\pm 0.07$	—	—	-14.11	55/56	$0.228\pm 0.006$	$-0.07\pm 0.03$		
64	Mkn 478	001	(1)	$1.41^{+0.22}_{-0.20}$	—	—	-14.38	17/10	$0.110\pm 0.007$	$-0.19\pm 0.06$		
			(2)	$1.94^{+0.79}_{-0.40}$	$1.03^{+2.84}_{-0.42}$	$0.86^{+0.41}_{-1.86}$	-14.29	9/8	—	—		
		002	(1)	$1.35\pm 0.11$	—	—	-14.17	29/31	$0.212\pm 0.008$	$-0.17\pm 0.04$		
			(2)	$2.13^{+1.66}_{-0.88}$	$0.60^{+0.84}_{-0.13}$	$1.20^{+0.15}_{-0.27}$	-14.07	23/29	—	—		
		003	(1)	$1.81\pm 0.15$	—	—	-13.98	33/14	$0.229\pm 0.013$	$-0.39\pm 0.05$		
	(2)	$2.01^{+0.28}_{-0.21}$	$1.77^{+1.30}_{-0.69}$	$0.49^{+0.74}_{-1.58}$	-13.95	21/12	—	—				
65	PG 1448+273	001	(1)	$1.64\pm 0.05$	—	—	-13.41	119/106	$0.860\pm 0.010$	$-0.23\pm 0.02$		
		003	(1)	$1.70^{+0.20}_{-0.19}$	—	—	-13.89	7/9	$0.277\pm 0.018$	$-0.27\pm 0.06$		
66	Mkn 841	002	(1)	$0.87\pm 0.04$	—	—	-13.96	148/156	$0.445\pm 0.007$	$+0.16\pm 0.02$		
		001	(1)	$0.96\pm 0.05$	—	—	-13.86	110/88	$0.532\pm 0.011$	$+0.12\pm 0.02$		
		001	(1)	$0.91\pm 0.06$	—	—	-13.99	86/81	$0.425\pm 0.010$	$+0.11\pm 0.02$		
		003	(1)	$1.05^{+0.15}_{-0.14}$	—	—	-13.82	17/16	$0.637\pm 0.028$	$+0.12\pm 0.04$		
67	Mkn 493	001	(1)	$1.29\pm 0.07$	—	—	-14.17	54/55	$0.204\pm 0.006$	$-0.09\pm 0.03$		
		002	(1)	$1.32\pm 0.07$	—	—	-14.04	65/61	$0.241\pm 0.006$	$-0.09\pm 0.03$		
		003	(1)	$1.24\pm 0.12$	—	—	-14.17	25/16	$0.208\pm 0.011$	$-0.05\pm 0.05$		
		004	(1)	$1.26\pm 0.08$	—	—	-14.28	32/43	$0.160\pm 0.005$	$-0.09\pm 0.03$		
		005	(1)	$1.34\pm 0.07$	—	—	-14.20	46/50	$0.206\pm 0.006$	$-0.16\pm 0.03$		
		006	(1)	$1.33\pm 0.05$	—	—	-14.13	87/84	$0.221\pm 0.005$	$-0.12\pm 0.02$		
68	Mkn 876	008	(1)	$1.12\pm 0.12$	—	—	-14.27	12/15	$0.176\pm 0.009$	$+0.07\pm 0.05$		
		001	(1)	$0.90\pm 0.06$	—	—	-14.23	83/75	$0.231\pm 0.005$	$+0.17\pm 0.02$		
			(2)	$1.37^{+0.77}_{-0.47}$	$0.89^{+0.36}_{-0.17}$	$0.73^{+0.08}_{-0.12}$	-14.14	63/73	—	—		
		002	(1)	$1.01^{+0.11}_{-0.10}$	—	—	-14.24	38/30	$0.197\pm 0.007$	$+0.10\pm 0.04$		
			(2)	$1.97^{+1.25}_{-0.44}$	$0.75^{+0.20}_{-0.21}$	$0.82^{+0.13}_{-0.12}$	-14.07	21/28	—	—		
		003	(1)	$0.82\pm 0.13$	—	—	-14.35	10/16	$0.176\pm 0.009$	$+0.23\pm 0.05$		
		004	(1)	$0.87\pm 0.13$	—	—	-14.31	20/20	$0.189\pm 0.009$	$+0.17\pm 0.05$		
		005	(1)	$0.93\pm 0.10$	—	—	-14.23	22/26	$0.216\pm 0.009$	$+0.16\pm 0.04$		
69	RX J1618.1+3619	006	(1)	$0.92\pm 0.08$	—	—	-14.25	60/53	$0.214\pm 0.006$	$+0.16\pm 0.03$		
		001	(1)	$1.53\pm 0.18$	—	—	-14.47	8/11	$0.092\pm 0.005$	$-0.21\pm 0.06$		
		002	(1)	$1.56^{+0.22}_{-0.20}$	—	—	-14.45	5/8	$0.079\pm 0.005$	$-0.20\pm 0.07$		
		003	(1)	$1.50^{+0.17}_{-0.16}$	—	—	-14.30	25/14	$0.154\pm 0.008$	$-0.20\pm 0.06$		
70	KUG 1618+410	001	(1)	$0.90^{+0.42}_{-0.41}$	—	—	-14.90	1/3	$0.047\pm 0.005$	$+0.11\pm 0.10$		
		002	(1)	$0.98\pm 0.11$	—	—	-14.82	10/20	$0.052\pm 0.002$	$+0.09\pm 0.05$		
71	PG 1626+554	001	(1)	$1.11\pm 0.07$	—	—	-14.24	37/44	$0.197\pm 0.006$	$+0.03\pm 0.03$		
		002	(1)	—	—	—	—	—	$0.196\pm 0.017$	$-0.13\pm 0.08$		
		003	(1)	$1.32\pm 0.06$	—	—	-14.19	59/70	$0.189\pm 0.005$	$-0.09\pm 0.02$		
72	EXO 1627+40	001	(1)	$1.15^{+0.25}_{-0.24}$	—	—	-14.68	4/5	$0.063\pm 0.005$	$-0.09\pm 0.08$		
		002	(1)	$1.06^{+0.13}_{-0.12}$	—	—	-14.68	23/22	$0.078\pm 0.003$	$+0.03\pm 0.04$		
		003	(1)	$1.41^{+0.15}_{-0.14}$	—	—	-14.70	14/14	$0.058\pm 0.003$	$-0.17\pm 0.05$		
		004	—	—	—	—	—	—	$0.042\pm 0.005$	$-0.13\pm 0.12$		
		007	—	—	—	—	—	—	$0.070\pm 0.008$	$-0.11\pm 0.11$		
73	RX J1702.5+3247	001	(1)	$1.73^{+0.31}_{-0.28}$	—	—	-14.19	3/4	$0.127\pm 0.011$	$-0.25\pm 0.08$		
		002	(1)	$1.79\pm 0.07$	—	—	-14.00	39/59	$0.205\pm 0.005$	$-0.33\pm 0.02$		
		003	(1)	$1.16\pm 0.32$	—	—	-14.66	2/5	$0.062\pm 0.005$	$-0.47\pm 0.08$		
		004	(1)	$1.67\pm 0.11$	—	—	-14.26	56/33	$0.125\pm 0.004$	$-0.32\pm 0.03$		
74	II ZW 136	003	(1)	$1.32\pm 0.17$	—	—	-13.73	17/16	$0.523\pm 0.026$	$-0.03\pm 0.05$		
		004	(1)	$1.38\pm 0.08$	—	—	-13.67	55/53	$0.547\pm 0.013$	$-0.02\pm 0.02$		
		005	(1)	$1.49\pm 0.13$	—	—	-13.88	48/28	$0.319\pm 0.012$	$-0.05\pm 0.04$		
		006	(1)	$1.24\pm 0.12$	—	—	-13.92	38/29	$0.353\pm 0.014$	$+0.07\pm 0.04$		
		001	—	—	—	—	—	—	$0.114\pm 0.019$	$+0.19\pm 0.16$		

TABLE 4—Continued

#	Object	segment(s)	Model <sup>1</sup>	$\alpha_{X,\text{soft}}$	$E_{\text{break}}^2$	$\alpha_{X,\text{hard}}$	$\log F_{0.2-2.0\text{keV}}^3$	$\chi^2/\nu$	CR <sup>4</sup>	HR <sup>5</sup>
		002	(1)	0.93±0.13	—	—	-14.31	27/21	0.191±0.009	+0.07±0.05
		003	(1)	1.04±0.25	—	—	-14.23	4/7	0.198±0.014	+0.11±0.07
		004	(1)	1.07±0.15	—	—	-14.28	19/16	0.188±0.010	+0.09±0.05
		005	(1)	0.97±0.07	—	—	-14.38	84/57	0.149±0.004	+0.14±0.03
76	RX J2216.8–4451	001	(1)	1.51±0.06	—	—	-14.31	112/88	0.128±0.003	-0.20±0.02
			(2)	2.62 <sup>+0.36</sup> <sub>-0.59</sub>	0.52 <sup>+0.10</sup> <sub>-0.05</sub>	1.39 <sup>+0.08</sup> <sub>-0.07</sub>	-14.14	93/86	—	—
		001	(1)	1.50±0.09	—	—	-14.29	32/36	0.136±0.005	-0.16±0.03
		002	(1)	1.69±0.13	—	—	-14.13	25/21	0.164±0.007	-0.30±0.04
		003	(1)	1.66 <sup>+0.11</sup> <sub>-0.17</sub>	—	—	-13.88	15/25	0.286±0.011	-0.26±0.04
		004	(1)	1.48±0.07	—	—	-13.98	50/58	0.272±0.007	-0.18±0.03
77	RX J2217.9–5941	001	—	—	—	—	—	—	0.022±0.003	-0.44±0.12
		002	(1)	2.01 <sup>+0.24</sup> <sub>-0.22</sub>	—	—	-14.75	14/11	0.029±0.002	-0.35±0.06
			(2)	2.23 <sup>+0.18</sup> <sub>-0.27</sub>	1.66 <sup>+2.68</sup> <sub>-0.74</sub>	0.73 <sup>+0.75</sup> <sub>-1.73</sub>	-14.70	6/9	—	—
		003	(1)	2.45 <sup>+0.44</sup> <sub>-0.40</sub>	—	—	-14.68	4/2	0.023±0.002	-0.65±0.08
		008-010	(1)	1.50±0.30	—	—	-15.62	9/4	0.006±0.001	-0.27±0.10
78	RX J2242.6–3845	001	(1)	1.68 <sup>+0.27</sup> <sub>-0.26</sub>	—	—	-14.69	7/6	0.045±0.003	-0.33±0.07
		002	(1)	1.60 <sup>+0.16</sup> <sub>-0.15</sub>	—	—	-14.42	7/12	0.080±0.005	-0.26±0.06
		003	—	—	—	—	—	—	0.044±0.005	-0.30±0.10
79	RX J2245.3–4652	003	(1)	1.16±0.10	—	—	-14.66	67/26	0.082±0.003	-0.03±0.04
			(2)	2.30 <sup>+0.49</sup> <sub>-0.37</sub>	0.85 <sup>+0.17</sup> <sub>-0.14</sub>	0.62±0.18	-14.41	23/24	—	—
		004	(1)	1.27±0.25	—	—	-14.72	10/5	0.056±0.005	-0.05±0.09
			(2)	3.03 <sup>+3.62</sup> <sub>-0.68</sub>	1.03 <sup>+0.53</sup> <sub>-0.57</sub>	0.17 <sup>+0.78</sup> <sub>-1.20</sub>	-14.57	—	—	—
80	RX J2248.6–5109	001	(1)	1.04±0.10	—	—	-14.05	20/29	0.368±0.014	+0.03±0.04
		002	(1)	1.09±0.06	—	—	-14.07	76/71	0.306±0.007	+0.02±0.03
		004	(1)	1.03±0.04	—	—	-14.20	160/169	0.228±0.003	+0.07±0.01
		005	(1)	0.88±0.13	—	—	-14.24	14/17	0.236±0.012	+0.12±0.05
81	MS 2254-36	001	(1)	1.19 <sup>+0.11</sup> <sub>-0.10</sub>	—	—	-14.19	18/26	0.223±0.009	-0.02±0.04
		002	(1)	1.14±0.08	—	—	-14.19	41/48	0.215±0.006	-0.04±0.03
		004	(1)	1.14±0.10	—	—	-14.35	19/29	0.150±0.006	-0.01±0.04
		005	(1)	1.18 <sup>+0.08</sup> <sub>-0.07</sub>	—	—	-14.22	40/48	0.201±0.006	-0.05±0.03
82	RX J2258.7–2609	001	(1)	0.71 <sup>+0.20</sup> <sub>-0.19</sub>	—	—	-14.40	4/6	0.196±0.015	+0.32±0.07
		002	(1)	0.98±0.07	—	—	-14.24	72/64	0.232±0.006	+0.16±0.03
		003	(1)	0.88±0.31	—	—	-14.51	8/7	0.142±0.014	+0.07±0.10
		004	(1)	0.91±0.05	—	—	-14.45	112/103	0.155±0.003	+0.18±0.02
83	RX J2301.6–5913	001	(1)	0.82 <sup>+0.17</sup> <sub>-0.16</sub>	—	—	-14.34	11/11	0.183±0.011	+0.22±0.06
		002	(1)	0.84±0.08	—	—	-14.31	47/53	0.217±0.006	+0.25±0.03
		004	(1)	0.77±0.08	—	—	-14.23	45/43	0.290±0.009	+0.32±0.03
		005	(1)	0.86±0.06	—	—	-14.23	68/70	0.231±0.006	+0.24±0.02
		006	(1)	0.83±0.14	—	—	-14.21	16/15	0.265±0.014	+0.22±0.05
84	RX J2301.8–5508	001	(1)	1.49 <sup>+0.23</sup> <sub>-0.21</sub>	—	—	-14.61	9/8	0.061±0.004	-0.20±0.07
		002	(1)	1.38±0.14	—	—	-14.54	24/19	0.084±0.004	-0.09±0.05
85	RX J2304.6–3501	001	(1)	1.06 <sup>+0.48</sup> <sub>-0.46</sub>	—	—	-14.82	4/6	0.052±0.008	-0.11±0.15
86	RX J2312.5–3404	001	(1)	0.67±0.11	—	—	-14.95	34/21	0.055±0.003	+0.27±0.04
		002	(1)	0.77±0.10	—	—	-14.72	19/27	0.087±0.004	+0.20±0.04
87	RX J2317.8–4422	001	(1)	2.58±0.15	—	—	-14.41	40/12	0.052±0.003	-0.64±0.06
		002	—	—	—	—	—	—	0.008±0.002	—
88	RX J2325.2–3236	001	(1)	1.08±0.09	—	—	-14.37	48/37	0.155±0.006	-0.00±0.04
		002	(1)	1.02 <sup>+0.09</sup> <sub>-0.08</sub>	—	—	-14.44	47/44	0.132±0.004	+0.03±0.03
		003	(1)	1.21±0.11	—	—	-14.38	25/23	0.140±0.006	-0.01±0.04
89	IRAS 23226–3843	001	(1)	0.83 <sup>+0.07</sup> <sub>-0.06</sub>	—	—	-14.20	38/52	0.274±0.008	+0.21±0.03
		002	(1)	0.87±0.07	—	—	-14.31	48/49	0.196±0.006	+0.18±0.03
		001	(1)	0.60±0.20	—	—	-14.27	2/7	0.231±0.016	+0.32±0.07
		002	(1)	0.94±0.04	—	—	-14.14	182/163	0.283±0.004	+0.14±0.02
90	MS 23409–1511	001	(1)	1.79 <sup>+0.15</sup> <sub>-0.14</sub>	—	—	-14.10	21/19	0.163±0.007	-0.32±0.04
		002	(1)	1.77 <sup>+0.08</sup> <sub>-0.07</sub>	—	—	-14.07	49/53	0.187±0.005	-0.35±0.03
		003	(1)	1.87±0.11	—	—	-14.02	46/34	0.192±0.007	-0.38±0.03
		004	(1)	1.78 <sup>+0.11</sup> <sub>-0.10</sub>	—	—	-14.12	30/34	0.166±0.006	-0.34±0.03
		005	(1)	1.91±0.20	—	—	-14.26	17/5	0.106±0.008	-0.40±0.07
91	RX J2349.4–3126	001	—	—	—	—	—	—	0.007±0.002	—
		003	(1)	1.03 <sup>+0.32</sup> <sub>-0.30</sub>	—	—	-14.76	8/5	0.061±0.005	+0.04±0.08
		006	(1)	1.03 <sup>+0.32</sup> <sub>-0.31</sub>	—	—	-14.75	8/5	0.023±0.003	-0.39±0.12
		007	(1)	1.03 <sup>+0.32</sup> <sub>-0.31</sub>	—	—	-14.75	8/5	0.031±0.002	+0.05±0.07
92	AM 2354–304	001	(1)	1.16±0.09	—	—	-14.27	60/43	0.197±0.006	+0.01±0.03
		003	(1)	1.21±0.07	—	—	-14.35	72/63	0.151±0.004	+0.01±0.03

<sup>1</sup>Spectral models used are: (1): absorbed power law, (2): absorbed broken power law, (3) absorbed blackbody plus power law<sup>2</sup>The break energy  $E_{\text{break}}$  is given in units of keV.<sup>3</sup>the unabsorbed rest-frame 0.2-2.0 X-ray flux  $\log F_{0.2-2.0\text{keV}}$  is given in units of  $\text{W m}^{-2}$ <sup>4</sup>CR is the XRT count rate given in units of counts  $\text{s}^{-1}$ .<sup>5</sup>The hardness ratio is defined as  $\text{HR}=(\text{H-S})/(\text{H+S})$  where S and H are the background subtracted numbers of counts in the 0.3-1 and 1-10 keV energy bands, respectively

TABLE 5  
PROPERTIES OF THE SPECTRAL ENERGY DISTRIBUTION

#	Object	segment(s)	$\alpha_X^1$	$\alpha_{UV}^2$	$\alpha_{ox}^4$	$\alpha_{UV-corr}^3$	$\alpha_{ox-corr}^5$	$\log L_X^6$	$\log L_{BBB}^6$	$L/L_{Edd}$	$\log L_{BBB}^{6,7}$	$\log 5100^6$	$\log L_{BBB-corr}^6$	$L/L_{Edd-corr}$
1	Mkn 335	003	1.30±0.09	+0.58±0.08	1.26	+0.78±0.12	1.34	36.75	37.72	0.51	37.53	36.73	38.07	1.32
2	ESO 242-G008	001+002	0.74±0.18	+1.48±0.16	1.36	+0.12±0.21	1.67	35.78	36.78	0.03	36.81	36.70	38.16	0.60
		003	1.17±0.10	+0.98±0.15	1.29	+0.40±0.19	1.66	36.44	37.24	0.07	37.22	36.73	38.59	2.14
3	Ton S 180	005	1.48±0.08	+0.25±0.07	1.42	+0.25±0.07	1.42	37.18	38.77	6.30	38.31	37.48	38.77	6.30
4	QSO 0056-36	003	1.13±0.07	-0.03±0.14	1.43	-0.12±0.14	1.43	37.48	39.19	0.29	38.58	37.72	39.19	0.29
5	RX J0100.4-5113	001	1.08±0.10	+0.69±0.08	1.39	+0.77±0.10	1.25	36.56	37.85	0.30	37.60	37.00	37.91	0.25
6	RX J0105.6-1416	001	0.92±0.20	+0.77±0.10	1.25	+0.77±0.10	1.25	36.86	37.91	0.25	37.70	37.09	37.58	0.30
7	RX J0117.5-3826	001	1.73±0.29	+0.93±0.09	1.39	+0.93±0.09	1.39	37.46	38.25	0.30	38.22	37.58	38.25	0.30
8	MS 0117-28	002	2.12±0.40	-0.21±0.07	1.67	—	—	37.80	39.48	2.75	38.91	38.11	—	—
9	RX J0128.1-1848	001	0.92±0.08	+0.89±0.04	1.26	+0.89±0.04	1.26	36.70	37.67	0.70	37.52	37.01	37.67	0.70
10	RX J0134.2-4258	001	1.29±0.26	+0.08±0.10	1.52	—	—	37.40	39.29	10.0	38.75	37.91	—	—
11	RX J0136.9-3510	001	1.87±0.20	+0.12±0.09	1.36	—	—	38.03	38.69	4.00	38.60	37.70	—	—
12	RX J0148.3-2758	008	1.57±0.16	+0.75±0.09	1.41	+0.75±0.09	1.41	37.55	38.47	2.40	38.33	37.57	38.47	2.40
13	RX J0152.4-2319	003	1.23±0.04	+0.45±0.09	1.35	+0.45±0.09	1.35	37.28	38.55	0.43	38.26	37.53	38.55	0.43
14	Mkn 1044	001	1.46±0.08	+0.74±0.05	1.31	+0.74±0.05	1.31	36.25	37.15	0.59	37.00	36.30	37.15	0.59
15	Mkn 1048	005	0.78±0.05	+0.49±0.10	1.33	+0.27±0.12	1.33	36.22	38.07	0.09	37.66	37.05	38.29	0.14
16	RX J0311.3-2046	001	0.83±0.05	+0.72±0.14	1.22	+0.38±0.10	1.30	36.82	37.76	0.06	37.57	36.90	38.10	0.13
17	RX J0319.8-2627	001	1.08±0.07	+0.60±0.12	1.35	-0.12±0.22	1.46	36.66	37.94	0.08	37.57	36.95	38.49	0.63
18	RX J0323.2-4931	002	1.08±0.23	+2.40±0.09	1.16	+1.72±0.13	1.30	36.30	36.80	0.09	36.90	36.81	36.93	0.12
19	ESO 301-G13	002	1.35±0.06	+0.70±0.10	1.30	+0.65±0.11	1.30	36.78	37.80	0.34	37.60	36.85	37.80	0.34
20	VCV 0331-37	001	1.04±0.20	+0.62±0.09	1.30	+0.38±0.10	1.34	36.52	37.55	0.40	37.34	36.72	37.75	0.62
21	RX J0349.1-4711	001	1.62±0.18	+0.43±0.12	1.46	—	—	37.68	38.91	1.51	38.51	37.69	—	—
22	Fairall 1116	003	1.33±0.05	+0.42±0.10	1.39	—	—	36.94	38.20	0.20	37.85	37.08	—	—
23	Fairall 1119	001	0.72±0.10	+2.32±0.19	1.05	+2.14±0.19	1.06	36.22	36.71	0.002	36.77	36.66	36.71	0.002
24	RX J0412.7-4712	001	1.02±0.05	+0.69±0.07	1.28	-0.64±0.22	1.59	37.33	38.42	0.16	38.23	37.61	39.47	1.60
25	1H 0419-577	001	2.01±0.40	+0.69±0.09	1.24	-0.65±0.21	1.50	38.01	38.69	0.25	38.55	37.87	39.68	7.76
26	Fairall 303	002	2.32±0.10	+0.75±0.06	1.24	+0.35±0.08	1.32	36.37	37.20	0.54	37.01	36.35	37.64	1.35
27	RX J0437.4-4711	001	1.32±0.10	+0.84±0.05	1.32	+0.79±0.05	1.32	36.75	37.71	0.08	37.62	36.97	37.71	0.08
28	RX J0439.6-5311	001	2.16±0.09	+0.16±0.05	1.24	+0.08±0.07	1.24	38.43	38.82	12.9	38.61	37.34	38.82	12.9
29	RX J0859.0+4846	001	0.91±0.06	+0.70±0.11	1.31	+0.03±0.10	1.44	36.87	38.00	0.21	37.82	37.17	38.56	0.85
30	RX J0902.7-0700	002	1.24±0.19	+0.60±0.10	1.36	+0.60±0.10	1.36	36.43	37.57	0.53	37.34	36.60	37.57	0.53
31	Mkn 110	001	0.98±0.05	+0.25±0.11	1.15	-0.95±0.25	1.44	37.10	37.96	0.87	37.75	36.78	39.33	20.4
32	PG 0953+414	001	1.28±0.09	-0.12±0.33	1.44	-0.02±0.60	1.47	38.19	39.54	1.12	39.19	38.26	39.98	3.63
33	RX J1005.7+4332	001	1.80±0.28	+0.12±0.05	1.52	+0.12±0.05	1.51	37.40	38.85	0.90	38.35	37.46	38.85	0.90
34	RX J1007.1+2203	002	1.53±0.14	+0.78±0.08	1.43	+0.78±0.08	1.43	36.63	37.63	0.90	37.50	36.58	37.63	0.90
35	CBS 126	001	2.11±0.25	+0.55±0.13	1.42	+0.17±0.11	1.49	36.89	38.19	0.22	37.89	37.04	38.64	0.60
36	Mkn 141	001	0.76±0.08	+1.73±0.16	1.28	+1.73±0.16	1.28	35.94	36.77	0.02	36.84	36.72	36.77	0.02
37	Mkn 142	002	1.72±0.13	+0.60±0.08	1.34	+0.60±0.08	1.34	36.79	37.64	0.76	37.52	36.60	37.64	0.76
38	RX J1117.1+6522	001	1.93±0.16	+1.11±0.12	1.47	—	—	37.28	38.09	0.40	38.07	37.51	—	—
39	Ton 1388	001	1.26±0.08	+0.18±0.12	1.56	—	—	37.80	39.65	1.58	39.10	38.32	—	—
40	EXO 1128+63	001	1.24±0.05	+0.91±0.12	1.23	+0.91±0.12	1.23	36.68	37.55	0.27	37.43	36.63	37.55	0.27
41	B2 1128+31	001	1.05±0.13	+0.11±0.16	1.45	-0.13±0.18	1.50	37.86	39.44	1.23	38.86	38.06	39.72	2.34
42	SBS 1136+579	002	0.98±0.16	+1.15±0.10	1.35	-0.05±0.15	1.59	37.00	37.67	0.23	37.75	37.35	38.80	3.00
43	CASG 855	001	0.83±0.33	+2.46±0.19	1.11	+2.36±0.18	1.13	35.90	36.36	0.01	36.44	36.22	36.39	0.01
44	NGC 4051	001	1.59±0.16	+1.57±0.09	1.10	+0.82±0.28	1.27	35.04	35.36	0.18	35.45	34.75	35.82	0.52
45	GQ Comae	002	1.01±0.05	+0.19±0.11	1.23	-0.10±0.11	1.29	37.66	38.77	0.36	38.39	37.51	39.16	0.91
46	RX J1209.7+3217	006	3.22±0.27	+0.77±0.07	1.71	-0.33±0.24	1.90	36.97	37.98	1.45	37.85	37.08	38.87	10.0
47	PG 1211+143	014	2.50±0.30	+0.41±0.11	1.66	+0.41±0.11	1.66	37.15	38.59	0.89	38.40	37.72	38.59	0.89
48	Mkn 766	001	1.80±0.34	+2.85±0.15	1.00	-0.31±0.47	1.67	35.73	36.08	0.04	36.11	35.84	38.08	5.00
49	3C 273	039	0.74±0.04	+0.34±0.11	1.34	—	—	38.63	40.02	1.12	39.62	38.93	—	—
50	RX J1231.6+7044	003	0.85±0.07	+0.33±0.14	1.23	—	—	37.71	38.82	0.63	38.48	37.73	—	—
51	MCG+08-23-067	001	0.82±0.15	+2.15±0.17	1.11	+1.84±0.16	1.15	35.41	35.92	0.17	36.07	35.90	35.96	0.22
52	NGC 4593	001	0.69±0.06	+1.97±0.07	1.15	-0.99±0.57	1.74	35.48	36.05	0.01	36.12	35.92	38.36	2.00
53	RX J1304.2+0205	002	2.19±0.23	+0.50±0.04	1.46	+0.50±0.04	1.46	37.55	38.50	1.78	38.24	37.43	38.50	1.78
54	PG 1307+085	001	1.16±0.07	+0.21±0.11	1.41	+0.22±0.11	1.41	37.48	39.18	0.76	38.53	37.72	39.18	0.76
55	RX J1319.9+5235	001	1.87±0.12	+1.97±0.14	1.15	+0.42±0.19	1.55	37.18	37.35	0.89	37.40	36.67	37.35	0.89
56	IRAS 1334+24	001	2.27±0.17	+2.75±0.15	1.35	-0.63±0.60	2.06	37.34	38.05	0.06	38.05	38.02	40.37	20.0
57	Ton 730	001	1.44±0.18	-0.29±0.09	1.37	-0.29±0.09	1.37	37.02	38.38	0.51	36.96	37.89	38.38	0.51
58	RX J1355.2+5612	001	2.01±0.27	+0.84±0.10	1.35	+0.48±0.12	1.43	37.17	38.00	1.48	37.92	37.11	38.25	3.00
59	PG 1402+261	001	1.35±0.13	+0.16±0.12	1.51	+0.16±0.12	1.51	37.49	39.2	3.00	38.85	37.90	39.12	3.00
60	RX J1413.6+7029	001	0.64±0.13	+2.13±0.33	1.05	—	—	36.49	36.90	0.02	36.90	36.89	—	—
61	NGC 5548	059	0.41±0.11	+1.88±0.13	1.24	+1.09±0.15	1.44	35.37	36.26	0.00	36.26	36.17	36.75	0.01
62	Mkn 813	003	1.56±0.34	+0.10±0.11	1.39	-1.57±0.17	1.75	37.41	38.99	0.29	38.47	37.69	40.69	9.50
63	Mkn 684	009	1.24±0.07	+0.63±0.04	1.45	+0.63±0.04	1.45	36.52	37.99	1.25	37.62	37.00	37.99	1.25
64	Mkn 478	002	2.13±1.00	+0.39±0.07	1.52	-0.06±0.06	1.61	36.92	38.53	0.15	38.22	37.48	38.95	3.00

TABLE 5—*Continued*

#	Object	segment(s)	$\alpha_X^1$	$\alpha_{UV}^2$	$\alpha_{ox}^4$	$\alpha_{UV-corr}^3$	$\alpha_{ox-corr}^5$	$\log L_X^6$	$\log L_{BBB}^6$	$L/L_{Edd}$	$\log L_{BBB}^{6,7}$	$\log 5100^6$	$\log L_{BBB-corr}^6$	$L/L_{Edd-corr}$
66	Mkn 841	002	0.87±0.04	+0.41±0.10	1.34	+0.41±0.10	1.34	36.56	37.82	0.08	37.47	36.77	37.82	0.08
67	Mkn 493	001	1.29±0.07	+0.75±0.04	1.41	+0.75±0.04	1.59	36.21	37.22	0.66	37.12	36.51	37.22	0.66
68	Mkn 876	001	0.90±0.06	+0.30±0.14	1.49	—	—	37.33	39.01	0.11	38.63	37.90	—	—
69	RX J1618.1+3619	001	1.53±0.18	+2.43±0.18	1.08	+2.07±0.20	1.21	35.89	36.20	0.22	36.38	36.08	36.30	0.28
70	KUG 1618+410	001	0.98±0.11	+1.71±0.20	1.27	+0.63±0.32	1.55	35.56	36.37	0.08	36.40	36.26	37.18	0.51
71	PG 1626+554	001	1.11±0.07	+0.30±0.10	1.36	+0.16±0.12	1.40	37.34	38.63	0.25	38.30	37.51	38.85	0.40
72	EXO 1627+40	002	1.06±0.12	+0.40±0.05	1.15	+0.33±0.06	1.15	37.58	38.32	0.81	38.15	37.29	38.32	0.81
73	RX J1702.5+3247	002	1.79±0.07	+0.73±0.13	1.42	+0.68±0.15	1.42	37.78	38.66	1.86	38.55	37.84	38.66	1.86
74	II Zw 136	004	1.38±0.08	+0.48±0.11	1.40	+0.48±0.11	1.40	37.27	38.52	1.00	38.21	37.49	38.52	1.00
75	RX J2146.6–3051	002	1.69±0.13	+0.52±0.13	1.27	–0.13±0.40	1.39	36.76	38.14	0.35	37.78	36.81	38.40	0.71
76	RX J2216.8–4451	001	1.50±0.09	+0.28±0.08	1.47	+0.28±0.08	1.47	37.32	38.57	1.78	38.28	37.51	38.57	1.78
77	RX J2217.9–5941	002	2.23±0.18	+0.51±0.06	1.57	+0.51±0.06	1.57	37.06	38.20	1.02	38.01	37.17	38.20	1.02
78	RX J2242.6–3845	002	1.60±0.16	+0.56±0.07	1.36	—	—	37.64	38.45	1.38	38.31	37.47	—	—
79	RX J2245.3–4652	003	2.30±0.44	+0.61±0.10	1.51	—	—	37.56	38.95	1.15	38.74	38.14	—	—
81	MS 2254–36	002	1.14±0.09	+1.13±0.07	1.21	+0.51±0.15	1.38	36.29	37.07	0.24	37.05	36.52	37.40	0.51
82	RX J2258.7–2609	002	0.98±0.07	+0.89±0.15	1.15	–0.47±0.28	1.45	36.84	37.50	0.19	37.54	36.92	38.56	2.08
83	RX J2301.6–5913	002	0.84±0.08	+0.71±0.15	1.11	—	—	37.38	38.13	0.02	38.00	37.27	—	—
84	RX J2301.8–5508	002	1.38±0.14	+0.84±0.07	1.48	+0.84±0.07	1.48	37.10	38.32	0.58	38.18	37.66	—	—
85	RX J2304.6–3501	001	1.06±0.47	+1.13±0.41	1.28	+1.13±0.41	1.28	36.14	36.47	0.08	36.50	36.11	36.47	0.08
86	RX J2312.5–3404	001	0.67±0.11	+0.61±0.14	1.34	+0.38±0.14	1.41	37.03	38.47	0.13	38.21	37.59	38.7	0.20
87	RX J2317.8–4422	001	2.58±0.15	+0.65±0.09	1.46	+0.65±0.09	1.46	37.18	38.00	2.34	37.98	37.05	38.00	2.34
88	RX J2325.2–3236	002	1.08±0.09	–0.06±0.15	1.30	—	—	37.60	39.00	1.00	38.51	37.67	—	—
89	IRAS 23226–3943	001	0.60±0.20	+1.98±0.15	1.20	+1.98±0.15	1.21	36.15	36.96	0.01	36.96	36.87	36.85	0.01
90	MS 2340–1511	002	1.77±0.08	+0.58±0.09	1.43	+0.58±0.09	1.43	37.52	38.53	0.22	38.40	37.58	38.53	0.22
91	RX J2349.4–3126	003	1.03±0.31	+1.36±0.24	1.22	+0.42±0.27	1.32	36.84	37.50	0.34	37.56	35.99	38.34	2.30
92	AM 2354–304	001	1.16±0.09	+1.13±0.09	1.33	+1.13±0.09	1.33	36.07	37.00	0.10	37.00	36.60	37.00	0.10

<sup>1</sup>X-ray slope in the 0.2–2.0 keV energy range<sup>2</sup>Optical/UV slope corrected for Galactic reddening<sup>3</sup>Optical/UV slope corrected for Galactic and intrinsic reddening<sup>4</sup>UV-to-X-ray spectra slope  $\alpha_{ox}$ , as defined by Tananbaum et al. (1979)<sup>5</sup>UV-to-X-ray spectra slope  $\alpha_{ox}$ , as defined by Tananbaum et al. (1979) corrected for Galactic and intrinsic reddening<sup>6</sup>uminosities are given in units of W.<sup>7</sup>Using the broken power law model as shown in Figure 1.

TABLE 6  
MEAN, STANDARD DEVIATION, AND MEDIAN OF THE PARAMETERS OF THE WHOLE SAMPLE, NLS1s (43)  
AND BLS1s(49)

Property	all			NLS1s			BLS1s		
	mean	sd <sup>1</sup>	median	mean	sd <sup>1</sup>	median	mean	sd <sup>1</sup>	median
$\alpha_X$	+1.38	0.55	+1.26	+1.68	0.51	+1.59	+1.11	0.42	+1.03
$\alpha_{UV}$	+0.81	0.65	+0.65	+0.85	0.66	+0.65	+0.79	0.67	+0.61
$\alpha_{ox}$	+1.34	0.14	+1.35	+1.36	0.16	+1.39	+1.32	0.11	+1.33
$\alpha_{UV-corr}$	+0.44	0.67	+0.42	+0.61	0.51	+0.60	+0.28	0.78	+0.17
$\alpha_{ox-corr}$	+1.42	0.17	+1.41	+1.42	0.15	+1.42	+1.42	0.18	+1.40
$\log L_X$ [W]	36.94	0.73	37.00	36.93	0.75	37.10	36.96	0.71	36.89
$\log L_{BBB-expo}^2$ [W]	38.00	0.96	38.07	37.86	0.99	38.01	38.11	0.92	38.07
$\log L_{BBB-bknp}^3$ [W]	37.80	0.80	37.92	37.72	0.986	38.07	37.89	0.75	37.82
$\log L_{5100}$ [W]	37.14	0.67	37.11	37.01	0.71	37.11	37.27	0.62	37.09
$L/L_{Edd}$	1.04	2.10	0.39	1.79	2.87	0.81	0.37	0.40	0.23
$L/L_{Edd-bknp}$	0.55	1.02	0.24	1.01	1.36	0.57	0.15	0.14	0.11
$\log L_{BBB-corr}$ [W]	38.32	0.97	38.60	38.12	0.85	38.10	38.53	1.07	38.50
$\log L_{5100-corr}$ [W]	37.13	0.64	37.09	36.98	0.63	37.05	37.30	0.61	37.09
$L/L_{Edd-corr}$ [W]	1.87	3.26	0.76	1.95	2.75	0.89	1.79	3.72	0.60
XRT CR ratio	2.51	3.11	1.55	3.13	4.11	1.82	1.95	1.64	1.36
RASS-XRT flux-ratio	2.34	3.85	1.26	2.69	5.06	1.20	2.04	2.35	1.26
$\Delta UVW2$ [mag]	0.24	0.32	0.21	0.23	0.31	0.13	0.25	0.33	0.16
$z$	0.112	0.077	0.089	0.119	0.090	0.086	0.105	0.063	0.087

<sup>1</sup>Standard deviation of the sample mean

TABLE 7  
CORRELATION ANALYSIS<sup>1</sup>

	$\alpha_X$	$\alpha_{UV}$	$\alpha_{ox}$	$\alpha_{UV-corr}$	$\alpha_{ox-corr}$	$\log L_X$	$\log L_{BBB}$	$L/L_{Edd}$	$\log 5100$	
$\alpha_X$	$r_1$ (#)	-0.15 (87)	+0.47 (87)	-0.24 (71)	+0.43 (71)	+0.34 (90)	+0.23 (87)	0.51 (86)	0.28 (87)	
	P	0.1606	<0.0001	0.0408	0.0002	0.0009	0.0301	<0.0001	0.0079	
$\alpha_{UV}$	$r_s, T_s$ (#)	$r_s, T_s$ (#)	-0.63 (87)	—	+0.03 (71)	-0.67 (87)	-0.82 (87)	-0.63 (86)	-0.77 (87)	
	P	P	<0.0001	—	0.8011	<0.0001	<0.0001	<0.0001	<0.0001	
$\alpha_{ox}$	+0.48, +5.0 (87)	-0.57, -6.3 (87)	1	-0.27 (71)	—	+0.46 (87)	+0.64 (87)	+0.55 (86)	+0.64 (87)	
	<0.0001	<0.0001	1	0.0235	—	<0.0001	<0.0001	<0.0001	<0.0001	
$\alpha_{UV-corr}$	-0.14, -1.2 (71)	—	-0.21, -1.8 (71)	1	-0.68 (67)	-0.43 (71)	-0.48 (71)	-0.20 (70)	-0.45 (71)	
	0.2419	—	0.0844	1	<0.0001	0.0001	<0.0001	0.0898	<0.0001	
$\alpha_{ox-corr}$	+0.34, +3.0 (71)	-0.16, -1.3 (71)	—	-0.60, -6.3 (71)	1	+0.16 (71)	+0.20 (71)	+0.07 (70)	+0.24 (71)	
	0.0037	0.1813	—	<0.0001	1	0.1763	0.0875	0.5590	0.0408	
$\log L_X$	+0.37, +3.7 (90)	-0.70, -9.1 (87)	+0.46, +4.8 (87)	-0.45, -4.2 (71)	+0.27, +2.3 (71)	—	+0.93 (87)	+0.61 (86)	+0.95 (87)	
	0.0004	<0.0001	<0.0001	>0.0001	0.0244	1	<0.0001	<0.0001	<0.0001	
$\log L_{BBB}$	+0.28, +2.7 (87)	-0.88, -16.6 (87)	+0.64, +7.7 (87)	-0.50, -4.8 (71)	+0.30, +2.6 (71)	+0.91, +19.9 (87)	1	+0.61 (86)	+0.99 (87)	
	0.0083	<0.0001	<0.0001	<0.0001	0.0113	<0.0001	1	<0.0001	<0.0001	
$L/L_{Edd}$	+0.55, +6.1 (86)	-0.57, -6.3 (86)	+0.57, +6.3 (86)	-0.06, -0.5 (70)	+0.16, +1.3 (70)	+0.63, 7.4 (86)	+0.61, +7.1 (86)	—	+0.61 (86)	
	<0.0001	<0.0001	<0.0001	0.6186	0.1979	<0.0001	<0.0001	1	<0.0001	
$\log 5100$	+0.32, +3.1 (87)	-0.80, -12.3 (87)	+0.64, +7.6 (87)	-0.51, -4.9 (71)	+0.33, +3.0 (71)	+0.94, +25.2 (87)	+0.98, +46.2 (87)	+0.63, +7.5 (86)	1	
	0.0026	<0.0001	<0.0001	<0.0001	0.0037	<0.0001	<0.0001	<0.0001	<0.0001	
$\log L_{BBB-corr}$	+0.24, +2.0 (71)	-0.66, -7.3 (71)	+0.51, +4.9 (71)	-0.81, -11.4 (71)	+0.54, +5.4 (71)	+0.81, +11.3 (71)	—	+0.31, +2.7 (70)	+0.88, +15.0 (71)	
	0.0493	<0.0001	<0.0001	<0.0001	<0.0001	<0.0001	—	0.0087	<0.0001	
$L/L_{Edd-corr}$	+0.53, +5.3 (71)	-0.31, -2.7 (71)	+0.34, +3.0 (71)	-0.64, -6.9 (71)	+0.59, +6.0 (71)	+0.53, +5.1 (71)	+0.45, +4.2 (71)	—	+0.50, +4.9 (71)	
	<0.0001	0.0087	0.0037	<0.0001	<0.0001	<0.0001	<0.0001	—	<0.0001	
$\log L_{5100-corr}$	+0.26, +2.2 (71)	-0.59, -6.1 (71)	+0.58, +5.8 (71)	-0.50, -4.8 (71)	+0.43, +3.8 (67)	+0.86, +13.9 (71)	+0.88, +15.3 (71)	+0.33, +2.9 (70)	—	
	0.0311	<0.0001	<0.0001	<0.0001	<0.0001	<0.0001	<0.0001	0.0050	—	
FWHM( $H\beta$ )	-0.65, -7.9 (90)	-0.11, -1.0 (87)	-0.17, -1.7 (87)	-0.27, -2.3 (71)	-0.01, -0.1 (71)	-0.05, -0.5 (90)	+0.09, +0.8 (87)	-0.50, -5.3 (86)	+0.04, +0.4 (87)	
	<0.0001	0.3201	0.0927	0.0244	0.9523	0.6813	0.4259	<0.0001	0.6901	

<sup>1</sup>The part above the diagonal in the gives the linear correlation coefficient  $r_1$  and the corresponding probability P and number of sources involved. The lower part of the table lists  $R_S, T_S$ , number of sources, and



## A. Spectral Energy Distribution Plots

Here we display the SEDs for each AGN with the power law model with exponential cutoff (Model A) for the reddening uncorrected and corrected UVOT data and the double broken power law model (Model B). Note that the SEDs with intrinsic reddening corrected UVOT data are only shown for those AGN for which the Balmer decrement was measured.

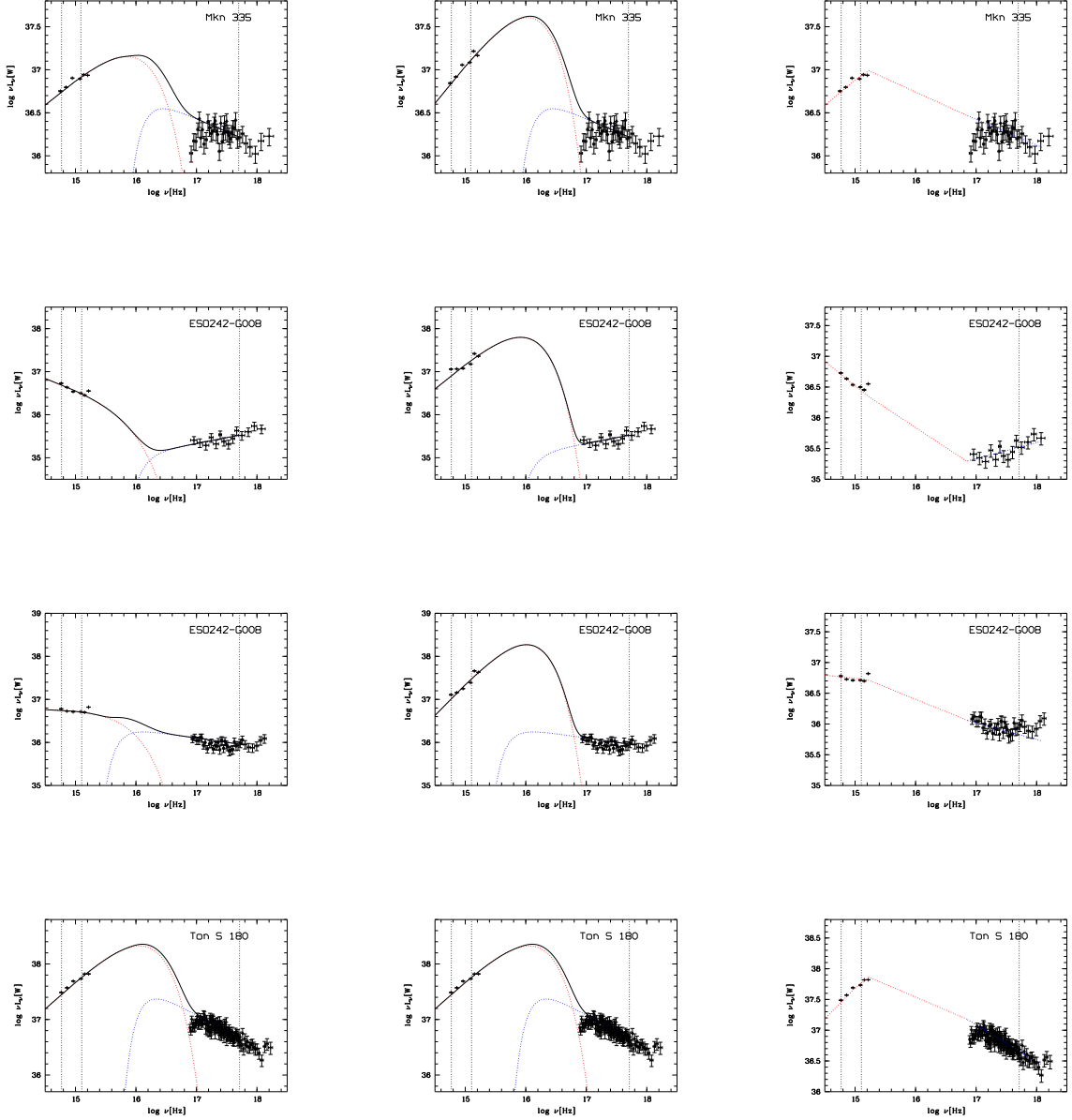


Fig. 25.— Spectral Energy Distributions of the AGN of our sample. The first column shows the UVOT and XRT data fitted by an power law with exponential cut off and an absorbed power law (Model A) to the intrinsic reddening uncorrected UVOT data, the second column displays the same model to the reddening corrected UVOT data, and the third column shows the data fitted by a double broken power law (Model B).

